



DYNAMIC MODELLING OF A BOLTED DISC ROTOR ASSEMBLY

by

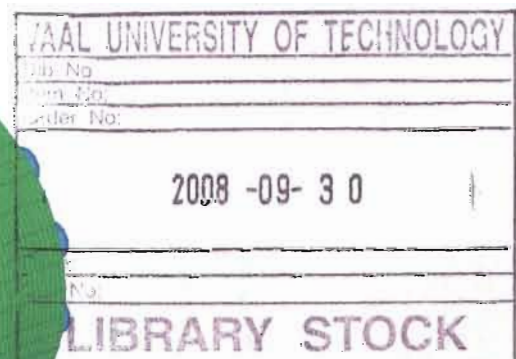
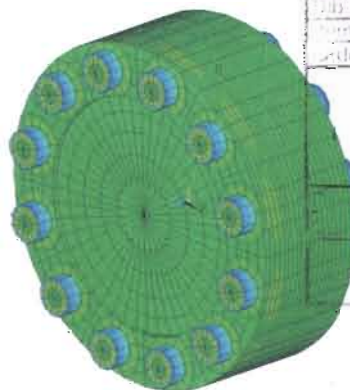
Gert Blignaut

A Dissertation

Submitted to the Faculty of Engineering and Technology  
in Fulfilment of the Requirements for the  
Degree of Magister Technologiae in Mechanical Engineering

Department of Mechanical Engineering

Study leader: Johan Roberts (North – West University)



# VAAL UNIVERSITY OF TECHNOLOGY

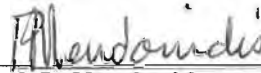
## FACULTY OF ENGINEERING AND TECHNOLOGY

The undersigned certify that they have read, and recommended to the Faculty of Engineering and Technology for acceptance, a Dissertation entitled “DYNAMIC MODELLING OF A BOLTED DISC ROTOR ASSEMBLY” submitted by G. J. Blignaut in fulfillment of the requirements for the degree of ***Magister Technologiae*** in Mechanical Engineering.



**Chairman, Mr. J. G. Drotsky**

Department of Mechanical Engineering



**Prof. P. Mendonidis**

Faculty Engineering and Technology



**Prof. D. Dicks**

Faculty Engineering and Technology

## **Abstract**

A project investigating the behaviour of an assembled preloaded rotor was performed for an M-Tech qualification in the Mechanical Engineering Department.

Pre-stressing of mechanical structures is widely applied to improve their performance, and in this project the behaviour of an assembled preloaded rotor was investigated.

An Impact Test was done on the structure to see if induced stresses originated by a set of bolts which keep the discs system together, would influence the natural dynamic response of the rotor. Tendencies in the natural response were investigated.

Analytical models like the Finite Element Beam model and the Solid Finite Element model were studied in order to find a representative description of this particular structure's dynamic behaviour after pre-tension. From the experimental results it was apparent that the slenderness of the pre-tensioned sector influences the natural frequency. The solid finite element model appears to be the most applicable model to present the assembled rotor-disk system as a continuous shaft. Furthermore, modelling and predictions for a typical rotor and similar assembled structures can be generated from the findings.

# Acknowledgements

The following people and Institutions contribute to this project.

- J. Roberts, Study leader.
- The Mechanical Workshop of the Mechanical Engineering Department.
- J. Drotsky, Head of Mechanical Engineering Department.
- J. Enslin, Principle Lecture of Mechanical Engineering Department.
- Tom Edwards.
- National Research Foundation.

Thank You

## ***Nomenclature***

<b>Symbol</b>	<b>Meaning</b>	<b>Units</b>
A	Area	m <sup>2</sup>
d	Diameter	m
D	Diameter	m
E	Young's Modulus	N/m <sup>2</sup>
G	Shear modulus	N/m <sup>2</sup>
H( $\omega$ )	Amplification factor	
F	Force	N
$F_n$	Field transfer matrix	
F( $\omega$ )	Fourier transform of excitation	
I	Inertia	m <sup>4</sup>
G <sub>i</sub>	Shape function matrix	
k, K	Stiffness, stiffness Matrix	N/m
K <sub>s</sub> , K <sub>sf</sub>	Constant, shear factor	unit less
L, l	Length	m
M	Moments, Mass Matrix	N.m ,kg
P	Force, Point matrix	N, unit less
P <sub>cr</sub>	Critical force	N
R, r	Radius, ratio	m, unit less
u	Displacement	m
V	Shear force	N
$v_n, v_0$	State vectors	
X( $\omega$ )	Fourier transform of response	
y	Displacement	m
$\beta$	Beta, shear angle	rad
$\delta$	Delta, log decrement	
$\phi$	Shear factor	
$\psi$	slope, gradient	rad
$\theta$	Theta, slope	rad
$\zeta$	Damping ratio	
$\omega$	Natural frequency	rad/s
$\omega_d$	Damped natural frequency	rad/s
S <sub>i</sub>	Geometric stiffness	N.m
$\gamma$	Density	kg/m <sup>3</sup>
$\lambda$	Lamda, eigenvalues	( rad/s) <sup>2</sup>
$\varsigma$	Stiffness factor	unit less
$\varepsilon$	Strain	
$\sigma$	Stress	N/m <sup>2</sup>
$\tau$	Shear stress	N/m <sup>2</sup>

## List of Figures

<b>Figure</b>	<b>Description</b>	<b>Page</b>
Fig.1.1	The Assembled Rotor System.....	1
Fig.2.1	View of Tapered and Stepped Cross-Section Shaft-Disc System. (Sabuncu,1990)	8
Fig.2.2	Hardening and Softening Nonlinear load deflections Characteristics.(Rivin,1999...	9
Fig. 2.3	Pre-Tensioned Beam Seen from Top, (Kerr, 1976) .....	11
Fig.2.4	Double Member Cantilever Beam. Constraint on the Left Side. (Tomski, 1994) ....	12
Fig. 2.5	Enhancement of Bending Stiffness by Internal Axial Load. (Rivin,1999).....	12
Fig. 2.6	Pressure Cone.....	15
Fig.2.7	Shear Deformation of a Shaft Element during Bending (Yamamoto, 1991).....	18
Fig.3.1	Photograph of the Force Washer, Hardened Washer, Accelerometer and Impulse Hammer with Copper Tip used in the Tests.....	28
Fig.3.2	Sketch Defining Sections of Shaft . .....	30
Fig.3.3	Rotor supported by ropes, locations of input and output measuring positions.....	30
Fig.3.4	Tensioned Bolt and Force Transducer between two Hardened Washers.....	31
Fig. 3.5	Plot of Coherence of Accelerance vs Frequency Data of a Test on a Six Disc, 12 Bolt Rotor System .....	31
Fig. 3.6.	Plot of the Phase of Accelerance vs Frequency Data for a Six Disc, 12 Bolt Rotor System.....	33
Fig. 3.7	Plot of the Phase of Accelerance vs Frequency Data for an Eight Disc, 12 Bolts Rotor System.....	34
Fig. 3.8	Plot of Logarithmic Magnitude of Accelerance and Phase vs Frequency Data for Six Discs, 6,8,12 Bolts, 23500N Preload in Bolts.....	36
Fig. 3.9	Plot of Logarithmic Magnitude of Accelerance and Phase vs Frequency Data for Six Discs, 6,8,12 Bolts, 30300N Preload in Bolts.....	37
Fig. 3.10	Waterfall plot of Mode shapes using Four Disks, 12 Bolts. Imaginary Component of the Accelerance plotted vs Frequency. ....	39
Fig.4.1	Cross-Sectional Area of Preload Region. ....	43
Fig.4.2	Cross-Section Area of Rotor(Eight discs) .....	43
Fig.4.3	Five Numbered Selected Elements in Critical Areas. ....	45
Fig.4.4	Close-up of a 3-Dimensional Solid Model revolved 360°(Eight discs) .....	46
Fig.4.6a	Meshed Solid Model, Transverse Mode shape One , Six Discs. ....	49
Fig.4.6b	Meshed Solid Model, Transverse Mode shape Two , Six Discs. ....	49

Fig.4.6c	Meshed Solid Model, Transverse Mode shape Three, Six Discs. ....	50
Fig.4.7	Cross-Sectional Cut of the Elastic Strain Plot along the Axial - direction.....	51
Fig.4.8	Cross-Sectional Cut of the Elastic Strain Plot along the Axial - direction.....	52
Fig.4.9	Cross-Sectional Cut of the Elastic Strain Plot along the Axial - direction.....	52
Fig. 5.1	Cross-Section Area of Disc.....	55
Fig.5.2	Hardening and Softening Nonlinear Load Deflections Characteristics. ....	56
Fig.5.3	Axi-Symmetric Cut of Bolt, Disc and Washer. ....	58
Fig.5.4	Axi-Symmetric Von Misses Stress Plot .....	58
Fig.5.5	Axi-Symmetric Area Contact Pressure plot. ....	59
Fig.5.6	Cross-section Cut of Disc.....	63
Fig. 5.7	Cross-Section of Component .....	63
Fig.5.8	A Cross-Sectional Cut of Disc-Volume, Main Stresses in z-direction Plot, Stress in Bolts: $522.4 \times 10^6$ Pa.....	68
Fig.5.9.	Bar Graphs comparing Different Number of Bolts for each Mode Shapes, for Two Disc Assembly. ....	70
Fig.5.10	Bar Graphs comparing Different Number of Bolts for each Mode Shapes, for Four Disc Assembly.....	71
Fig.5.11	Bar Graphs comparing Different Number of Bolts for each Mode Shapes, for Six Disc Assembly.....	71
Fig.5.12	Bar Graphs comparing Different Number of Bolts for each Mode Shapes, for Eight Disc Assembly.....	72
Fig. 5.13	Frequency results FE model vs Frequency results Experimental model for 23500 N preload on a Two Disc Rotor.....	73
Fig. 5.14	Frequency results FE model vs Frequency results Experimental model for 30300 N preload on a Two Disc Rotor.....	74
Fig. 5.15	Frequency results FE model vs Frequency results Experimental model for 23500 N preload on a Four Discs Rotor.....	74
Fig.5.16	Frequency results FE model vs Frequency results Experimental model for 30300 N preload on a Four Disc Rotor.....	75
Fig.5.17	Frequency Results FE model vs Frequency results Experimental model for 23500 N preload on a Six Disc Rotor.....	75
Fig.5.18	Frequency results FE model vs Frequency results Experimental model for 30300 N Preload on a Six Disc Rotor.....	76

Fig.5.19	Frequency results FE model vs Frequency results Experimental model for 23500 N Preload on a Eight Disc Rotor.....	76
Fig.5.20	Frequency Results FE Model vs Frequency Results Experimental Model for 30300 N Preload on a Eight Disc Rotor.....	77



## *List of Tables*

<b>Table</b>	<b>Description</b>	<b>Page</b>
Table 3.1	Natural frequencies (Hz) for assemblies with two Discs, 6,8,12 Bolts, 70% and 90% Preload.....	34
Table 3.2	Natural frequencies (Hz) for assemblies with Four Discs, 6,8,12 Bolts, 70% and 90% Preload.....	35
Table 3.3	Natural frequencies (Hz) for assemblies with Six Discs, 6,8,12 Bolts, 70% and 90% Preload.....	37
Table 3.4	Natural frequencies (Hz) for assemblies with Eight Discs, 6,8,12 Bolts, 70% and 90% Preload.....	38
Table 4.1	Element Dimensions of Five Selected Elements from Fig.4.3.....	44
Table 4.2	Shape Checking Tests of Five Selected Elements.....	45
Table 4.3	Number of elements for different disc configurations.....	47
Table 4.4	Results of Natural frequencies of FE Solid Model for different number of discs.....	48
Table 5.1	Natural Frequencies from Equation (5.3) illustrating the affect of slenderness, when $\rho = 7800$ ; $E = 200 \times 10^9$ ; $n=1$ .....	61
Table 5.2	Natural Frequencies of Compound Component Fig. 5.6, Free-Free support.....	64
Table 5.3	Stiffening effect $\zeta$ per bolt for each disc-volume configuration.....	66
Table 5.4	Y- Displacement.....	69
Table 5.5	Natural frequencies(Hz), Two Discs, 12 Bolts, 70% and 90% preload.....	77
Table 5.6	Natural frequencies(Hz) Four Discs, 12 Bolts, 70% and 90% Preload.....	78
Table 5.7	Natural frequencies(Hz), Six Discs, 12 Bolts, 70% and 90% Preload.....	78
Table 5.8	Natural frequencies(Hz) Eight discs, 12 bolts, 70% and 90% preload.....	78
Table 5.9	Differences between the two models.....	78
Table. 5.10	Mass differences between Experimental (12 bolts) and FEM.....	79

# Table of Contents

<b>Contents</b>	<b>Page</b>
<b>Approval Page</b>	<b>i</b>
<b>Abstract</b>	<b>ii</b>
<b>Acknowledgements</b>	<b>iii</b>
<b>Nomenclature</b>	<b>iv</b>
<b>List of Figures</b>	<b>v</b>
<b>List of Tables</b>	<b>viii</b>
<b>Table of Contents</b>	<b>ix</b>
<b>1 INTRODUCTION</b>	
1.1 Background.....	1
1.2 Scope of work.....	2
1.3 Layout of the dissertation.....	3
1.4 Main Research Question.....	3
1.5 Delimitations.....	3
1.6 Assumptions.....	4
<b>2 LITERATURE STUDY</b>	
2.1 Introduction.....	5
2.2 Research Topics.....	6
2.2.1 Stiffness.....	6
2.2.2 Damping.....	7
2.2.3 The Effect of Slenderness.....	8
2.2.4 Stress Stiffening.....	8
2.2.5 The Effect of Pre-Tension on Structures.....	10
2.2.6 Contact Stiffness and Damping.....	13
2.2.7 Bolt and Flange Interaction.....	14
2.2.8 Non-Linear Measurements.....	15
2.2.9 Analytical Model.....	16
2.2.10 Finite Element Method (FEM) .....	19
2.2.11 Non-linearity-Finite Element Method.....	19
2.2.12 Modal Analysis.....	20
2.2.13 Synthesis.....	20
2.3 Technical Background.....	21
2.3.1 Stiffness Concepts.....	21
2.3.2 Modal Analysis and Testing.....	22

2.3.2.1	Modal Analysis.....	22
2.3.2.2	Real and Complex Modes .....	22
2.3.2.3	Resonance and Anti-Resonance.....	23
2.3.2.4	Excitation.....	23
2.3.2.5	Coherence Function.....	25
2.3.2.6	Phase Plots.....	25
2.3.2.7	Analytical Modal Models.....	25
<b>3</b>	<b>EXPERIMENTAL PROCEDURES AND RESULTS</b>	
3.1	Introduction.....	27
3.2	Test Equipment.....	27
3.3	Experimental Procedure.....	28
3.3.1	Bolt Stresses during preload.....	28
3.3.2	Procedure.....	29
3.3.2	Setup of Analyser.....	29
3.4	The Quality of Measured Data.....	31
3.4.1	Signal Quality.....	31
3.4.2	Signal Fidelity.....	32
3.4.3	Measurement Repeatability.....	32
3.4.4	Measured Data Consistency.....	32
3.5	Preliminary Checks on Frequency Response Function Data.....	32
3.5.1	Low Frequency Asymptotes.....	32
3.5.2	Incidence of Anti-Resonance.....	32
3.6	Identifications of Resonance Frequencies.....	33
3.7	Results.....	33
3.8	Experimental Discussion.....	39
3.9	Synthesis.....	40
<b>4</b>	<b>NATURAL FREQUENCIES: SOLID FINITE ELEMENT MODEL</b>	
4.1	Background.....	41
4.2	The Objective of the Analysis.....	41
4.3	Accuracy.....	41
4.4	Simplifications.....	42
4.5	Modelling of The Rotor.....	42
4.6	Important Frequencies in the Structure.....	47
4.7	Natural Frequency Results.....	47
4.8	Discussion of Mode shapes.....	49
4.9	Synthesis.....	52

<b>5 DISCUSSION</b>	
5.1	Background..... 54
5.2	Stiffness Characterisation..... 55
5.3	Analysis of Preload Region..... 57
5.4	Effect of Axial Force..... 60
5.4.1	Cross-Sectional Moment of Inertia..... 61
5.4.2	Geometric Stiffening..... 64
5.4.3	The stress-stiffening affect of an assembled disc-volume after pretension..... 67
5.4.4	Synthesis..... 69
5.5	Slenderness of Structure..... 70
5.6	Verification of Models ..... 72
5.6.1	Comparison and Correlation Between Prediction and Experimental Results..... 72
5.6.2	Localisation..... 78
5.6.3	Reconciliation..... 79
5.6.4	Conclusion..... 79
5.7	Synthesis..... 80
<b>6 CONCLUSIONS AND RECOMMENDATIONS</b>	
6.1	Analytical Models..... 81
6.2	Reconciliation Between Literature, Test Results and Analytical Model..... 81
6.3	Methodology for Designing an Assembled Rotor-Disk System..... 82
6.3.1	Concepts of modelling..... 82
6.3.2	Preliminary design..... 82
6.3.3	Important key factors for an assembled structure..... 83
6.4	Final Conclusion..... 83
6.5	Recommendations..... 84
<b>Appendix A: Formulas</b>	85
<b>Appendix B: Drawings</b>	87
<b>Appendix C: Frequency Response Function Graphs</b>	90
<b>Appendix D: Equipment</b>	97
<b>Appendix E: Finite Element Information</b>	99
<b>Appendix F: Tensile Test: Bolt</b>	101
<b>Bibliography</b>	103

## INTRODUCTION

### 1.1 Background

The proposal to investigate the dynamic behaviour of composite rotors is derived from the original Design Proposal of the Pebble Bed Modular Reactor (PBMR) DP1. The School of Mechanical Engineering of the Potchefstroom campus of the North West University is involved with simulation, design and optimization of the PBMR Power station of Eskom (Electricity supplier). High-speed rotating rotors often consist of bolted rotor-disc assemblies. The DP1 Power Turbine from the PBMR is an example of such a composite rotor system.

It is normal practice in industry to bolt discs together to construct a rotor. Small steam and gas turbines make use of this configuration. Results obtained from this research may be used not only in the PBMR project, but also in other industries. In fact, all applications requiring solid couplings between rotors would benefit from this research.

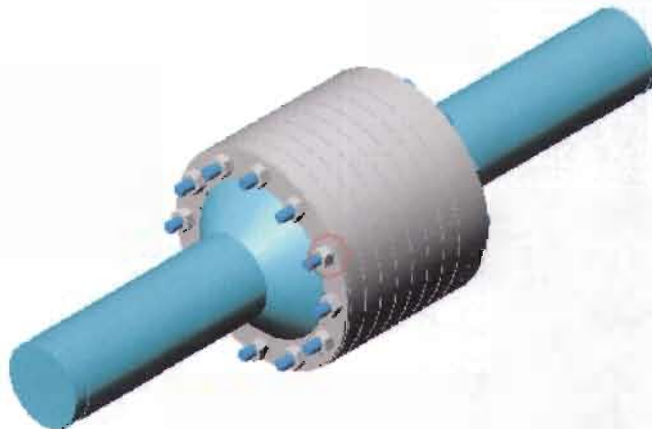


*Fig.1.1*

*The Assembled Rotor System.*

*(The circle indicates the zone under investigation.)*

Pre-stressing of mechanical structures is widely applied to improve their performance. Pre-stressing of the bolts of a rotor bolted disc rotor assembly is imperative because the rotor is deemed to have failed when the contact between adjacent discs is lost.

Induced stresses in the assembled rotor-disc system (*Figure 1.1*) may influence the dynamic response of the rotor during operation. The bolts which keep the discs together are under tensile stress, whereas the

discs themselves are under compressive stress. It is worthwhile finding out how the number of bolts and the pre-stressing of the bolts influence the natural vibration frequency of a compound rotor-system.

For simulation, the composite rotor-disc system is modelled as an equivalent solid shaft because of the constraints of currently available rotor dynamic software.

This project will examine the natural dynamic behaviour of the composite rotor-disc-system under different conditions of pre-load. Since modes of vibration which lie within the frequency range of the operating conditions always present potential problems, the primary goal of the modal study is to ensure that the system under investigation does not have a resonant frequency near the operating frequency or the range of operating frequencies when subjected to a preload.

Stiffness is the capacity of a mechanical system to sustain loads without excessive changes of its geometry (deformations). It is one of the most important design criteria for mechanical components and systems. Although strength is considered the most important design criterion, there are many cases where stresses in components and their connections are significantly below the allowable levels where the dimensions as well as performance characteristics of mechanical systems are determined by stiffness requirements. The stiffness criterion is gaining in importance due to the increased use of high strength materials resulting in reduced cross-sections. The importance of dynamic characteristics of machines is highlighted by their increased speed and power, which combined with lighter structures, may result in severe resonances and the development of self excited vibrations. Thus the dimensions and performance characteristics are not only determined by considering the strength, but also the stiffness requirements.

Stress is proportional to strain according to Hooke's law. For all practical purposes most materials will exhibit a change in stiffness before inelastic or plastic behaviour is encountered. Although a bolted disc rotor assembly is a structure which may show signs of nonlinear behaviour, this study will be restricted to linear approximation of stress-strain behavior.

## **1.2 Scope of Work**

The change in magnitude of natural frequencies of a down-scaled assembled rotor disc system preloaded with bolts will be the focus of this investigation. The experimental procedure will involve testing different configurations of the assembled rotor system to determine which factors influence the dynamic behaviour.

The different configurations will consist of parameters such as:

- Number of bolts.
- Number of discs.
- Magnitude of the preloads of the bolts.



An Analytical model will be generated to represent the rotor-system during preload. Different mathematical approaches will be used to see if simple models exist to describe the complex geometry of this specific rotor-system.

Damping is considered to be less vital for this research.

### **1.3 Layout of the Dissertation**

In Chapter 2, the literature study, the following topics are assessed: Stiffness and damping, the effect of slenderness, stress stiffening, bolt and flange interaction and a short discussion about the possible analytical models. The experimental procedure and natural frequency results of the assembled rotor-disc system are set out in Chapter 3. The selection and discussion of the finite element model and the generated natural frequencies that were used are given in Chapter 4. In Chapter 5, the differences and similarities between the experimental results and the valid analytical model are discussed and evaluated, as are certain crucial arguments.

Final conclusions and guidelines for modeling an assembled rotor-system when considering preload and natural frequencies will be presented in Chapter 6.

### **1.4 Main Research Question**

In Exploring the relationship between natural frequencies, number of bolts and preload applied, the main research question is:

Can a bolted disc rotor assembly be modelled as an integral, continuous shaft? If so, to what extent does the number of bolts, number of discs and preloading of the bolts influence this model?

### **1.5 Delimitations**

In order to simplify the simulation, the following delimitations will be assumed to apply:

- Only the linear response of the system will be considered.
- Investigation of the rotor will be done without any external damping influences like
- Bearings, seals, external forces.
- Excitation will be applied at a single point at a time.
- Only free-free support of the rotor assembly will be investigated.
- Only lateral natural frequencies will be investigated.
- Only one scaled model will be investigated.

## 1.6 Assumptions

The following assumptions are made:

- Inherent dynamic characteristics will not be affected by the measurements.
- Material properties remain in the linear regime.
- Disc (rotor) material properties can be assumed isotropic and homogeneous.
- Stresses induced by the bolts will not affect or change the material properties of the discs.
- No vibration occurs before excitation.
- Vibrations die out when the excitation source is removed.
- Material damping will be assumed constant across all frequencies under investigation.
- Time-invariance. The dynamic characteristics will not change during the measurements.
- The magnitude and orientation of loading remain constant throughout the deformations.
- The response is always linearly proportional to the excitation.
- The modal frequencies are determined simply by observing the maximum magnitudes on the Frequency Response Function (FRF).
- No slippage occurs between interfacing components, it will be assumed solid during Finite Element Model Analysis (FEA) when determining the natural frequencies.
- No separation between discs exist during dynamic movement of the rotor.
- The lateral deflection of the rotor is small.
- Geometric simplification is applied whenever feasible.



# LITERATURE STUDY

## 2.1 Introduction

It must be stated in the beginning that there exists very limited literature concerning assembled rotors .

In modelling the dynamic characteristic of a dynamic rotor system, a number of steps is essential in the development of the equation of motion. Fundamental verification of model validity is made by comparison with experimental results, which leads to additional refinements, as required. The computation of the critical speeds with respect to the operating conditions of the machine is an important (key) design factor in the preliminary design stage.

Ehrich (1992) described that transverse vibrations of rotors are more complex than that of torsional or longitudinal vibrations. The reason for this is the deformation of the rotor due to a combination of bending and shearing, which is inherently more complicated than simple twisting or stretching. Bending is normally not restricted to a single plane, two orthogonal planes must be considered. It is necessary to characterise the motion of each point by two independent coordinates: a transverse displacement and an angular displacement.

When the rotor is spinning, the motions in the two orthogonal planes are coupled by gyroscopic and asymmetric effects.

Rotating machines are classified according to their characteristics as follows:

- If the deformation of the rotating shaft is negligible in the operating speed range, it is called a rigid rotor.
- If the shaft deforms appreciably at some rotational speed in the operating range, it is called a flexible rotor.

The deformation of a rotor becomes highest in the vicinity of the critical speed (Yamamoto, 2001).

The existing literature on the following topics was reviewed:

- Stiffness and Damping.
- The effect of slenderness.
- The effect of pre-tension on structures.
- Stress stiffening.
- Contact stiffness and damping.

- Bolt and flange interaction.
- Contact surfaces.
- Non-linear measurements.
- Analytical models.
- Modal analysis.

## 2.2 Research Topics

### 2.2.1 Stiffness

Stiffness is a complex parameter. There are generally different values of stiffness  $K_x$ ,  $K_y$ ,  $K_z$  in the three orthogonal directions. Variable stiffness (orientation dependent) in shafts may cause quasi-harmonic vibrations. Rivin (1999) presented an extremely thorough overview of stiffness and damping in his book 'Stiffness and Damping in Mechanical Design'. He outlines the stiffness being the capacity of a mechanical system to sustain loads without excessive changes of its geometry. Although strength is considered as the most important design criterion, stiffness is also an important design measure for mechanical components and systems. The strength of structural materials can be significantly improved by the proper selection of materials (or alloys) or heat treatment procedures. In contrast, the Modulus of Elasticity ( $E$ ) is not very sensitive to alloying and heat treatment. Rivin (1999) proved that whether a system is in bending, tension or compression circumstance, the natural frequency is dependent on the ratio  $E/\gamma$ , where  $\gamma$  is density. The higher this value, the higher the natural frequency.

A significant statement by Rivin (1999) is that stiffness adjustment or tuning would not be possible for very inflexible components by preloading.

Although non-linear systems are characterized by stiffness varying with the loading conditions, in some mechanical systems stiffness can only be modified (enhanced) by the geometry of the component, or interaction with other components.

Stiffness effects on the performance of mechanical systems are due to the influence of deformations on static and fatigue strength, accuracy, and dynamic stability. Currently the importance of the stiffness criteria is increasing due to:

- Increasing accuracy requirements due to increasing speeds of machines.
- Better analytical techniques, resulting in smaller safety factors, which result in the reduced cross-sections and increasing deformations.
- Use of high strength materials also resulting as well in reduced cross sections.

- Increasing importance of dynamic characteristics of machines since their increased speed and power may result in intense resonances and the development of self-excited vibrations.
- Structural stiffness, in most structures, depends on the following:
  - Elastic moduli.
  - Geometry.
  - Character of support.
  - Load conditions and joint connections.

### 2.2.2 Damping

Even though damping is not a focal point in this project, it is necessary to point out the consequence and the nature of damping. Adams (1998) explained that damping represents inefficiencies of the material due to energy loss at a molecular level or energy loss of the system due to component interaction. Higher damping factors cause the oscillation amplitude to decrease. Damping has very little effect on natural frequencies at structural values. Damping affects the physical real response of the model when shaken or bumped.

Maia (1997) explained that, in practice, the damping ratio,  $\zeta$  is never zero, because there is always some degree of energy dissipation in real systems. Any dynamic model should include a damping mechanism, a non-zero value of  $c$ . It is important to note that damping is only effective near resonance. Away from resonance the response is hardly influenced by damping where all the response curves coincide.

Furthermore, according to Adams (1998), damping values will not be found in a general reference, but must be determined through testing or from industry or product specific literature, and if the results of the dynamic analysis are critical, damping must be determined from testing.

Cook (2001) revealed by that structural damping is usually small, typically  $\zeta < 0.15$ , so that  $\omega_d \approx \omega$ . Therefore, because of damping in structural problems and its effect on the structural response is small, it is modelled well enough by regarding it as viscous damping when considering finite element analysis, Cook (2001).

Ewins (2000) had a different opinion from Cook. He argued that viscous damping is not very representative when applied to multi-degree-of-freedom (MDOF) systems. He made it clear that there is a frequency dependence which is not described by the standard viscous dashpot model. Therefore, a damper whose rate varies with frequency is needed in such cases.



### 2.2.3 The Effect of Slenderness

Sabuncu and Kaçar (1990) studied the combination of a linearly tapered stepped and uniform cross-section continuous shaft disc systems (*Figure 2.1*). In their article they confirm Rivin's (1999) statement about the geometry. They used the Euler-Bernoulli beam theory in their analysis and consider the effects of various tapers on the frequencies of vibration.

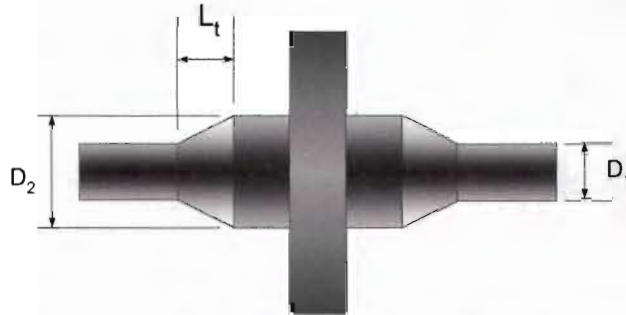


*Fig.2.1 View of Tapered and Stepped Cross-Section Shaft-Disc System (Sabuncu,1990)*

Sabuncu and Kaçar (1990) came to the conclusion, that if the diameter  $D_2$  increases, the lumped mass in the middle of the shaft increases, leading to a decrease in critical speed. An increase in the tapered section,  $L_1$ , makes the system more flexible, which results in a lower critical speed.

Yamamoto (2001) looked into the effect of slenderness using mathematical models. He stated that the critical speed of a rotor changes as a function of slenderness. He refers to slenderness as the ratio of  $R/(2L)$ . (Please note that some authors present slenderness in a different terminology). He also noticed the Euler-Bernoulli beam formulation is not suitable for short stubby beams because the critical speeds of a rotor represented by the Bernoulli-Euler beam does not depend on the slenderness ratio, which has a constant value. More ever, Rivin (1990) found the effect of a tensile force on the stiffness of a slender work piece quickly increases with increasing the slenderness ratio ( $L/D$ ). He also found that the maximum stiffening effect depends on the allowable tensile strength.

### 2.2.4 Stress Stiffening

As a general rule, stiffness increases as strain rate increases, Rivin (1999). The linear load-deflection plot (characteristic) allows one to determine stiffness as a function of force, though most of the load deflection characteristics of mechanical systems are non-linear. The degree of non-linearity is not very significant and for this reason the system is considered as linear for the sake of simplicity. Significant nonlinearity must be taken into consideration, especially in the analysis of dynamic processes in which nonlinearity may cause

undesirable effects. Rivin (1999) described two basic types of nonlinear load-deflection (*Figure 2.2*), both of which allow for varying the actual stiffness by moving the working point along the characteristic.

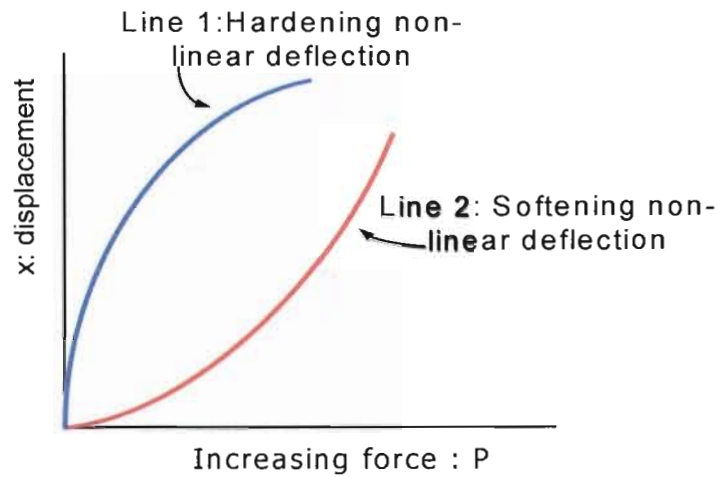


*Fig.2.2 Hardening and Softening Nonlinear load deflections Characteristics (Rivin, 1999).*

Very importantly, Rivin (1999) pointed out that the stiffness modification can be reached by preloading the components responsible for the stiffness parameters of the system. Preloading involves intentional application of internal forces to respective components. An appropriate preload increases the stiffness but it may reduce strength due to the application of the additional forces. This means that some portion of the overall strength is transformed into stiffness. Hence, two components would behave as a solid if they were pressed together with high contact forces Rivin (1999).

The authors of the notes for the ANSYS (Finite Element) Software state that stress stiffening (also called geometric stiffening, incremental stiffening, initial stress stiffening by other authors) is the stiffening (or weakening) of a structure due to its stress state. In the model, the effect of stress stiffening is accounted for by generating an additional stiffness matrix, called the "Stress Stiffness Matrix" which is added to the regular stiffness matrix to give the total stiffness.

Computation of the stress stiffness matrix is based on the stress state of the previous equilibrium iteration. Thus, at least two iterations are normally required to generate a valid stress-stiffened problem. The first iteration is used to determine the stress state that will be used to generate the stress stiffness matrix of the second iteration. If this additional stiffness affects the stresses, more iterations need to be done to obtain a converged solution.

Rivin (1990) presents a formula quantifying the effect of stress stiffening for a member under a tensile stress that is lower than the Euler Force  $P_{cr}$  for a cylindrical member:

$$\varsigma = 4 \left( \frac{L}{D} \right) \sqrt{\epsilon_T}$$

where

$\varsigma$  : Stiffening effect.

$\epsilon_T$  : The relative elongation from the tensile force.

L : Length of member.

D : Diameter of member.

From this equation, the effect of the tensile force on the stiffness is raised when the "slenderness ratio"  $\frac{L}{D}$  increases. The maximum stiffening effect also depends on the allowable tensile strength of the material.

### 2.2.5 The Effect of Pre-Tension on Structures

Van Nostrand (1952) described stress from a metallurgical point of view. When a force is applied to deform a single crystal of a metal, there is a deformation of the lattice structure. If the force is applied in one direction, the distances between the atoms will be decreased in the force direction, and vice versa. The atoms then exert a resisting force which tends to restore them to normal positions. These internally distributed forces which tend to resist deformation may be defined as stress. The relationship between the stress and strain is controlled by the intensity of the atomic bond, and the differences in moduli are actually associated with the bond characteristics of the different elements.

Kerr (1976) studied experimentally and analytically the dynamic response of a pre-stressed beam. He constructed a beam with two horizontal steel strips which are interconnected by aluminium cross bars (*Figure 2.3*). The beam was mounted on a shaker table during the experiment. A circular rod is used to apply tension on the free end of the beam with a negligibly small inertia effect. All the pre-stressing load steps  $P$ , applied during the experiment, were below  $P_{critical}$ . The observation which Kerr made was that the measured natural frequencies deviated by less than 1% from his analytical model. According to Kerr (1976) this small deviation corroborates his analytical findings. The simple linear analysis (mathematical model) which Kerr presented is not able to determine the change in force in the cable and the cable eccentricity during vibration. No axial force actually enters the final formulation on the end. Therefore he comes to the conclusion that the dynamic (or static) lateral response of the pre-stressed beam is the same as if the pre-

stressing force  $P$  were absent. Kerr noticed that a resulting axial pre-stressing force which passes through the centroids of the beam cross-section had no effect on the bending response of the beam and no effect on the natural frequencies, no matter how large the magnitude of the force.

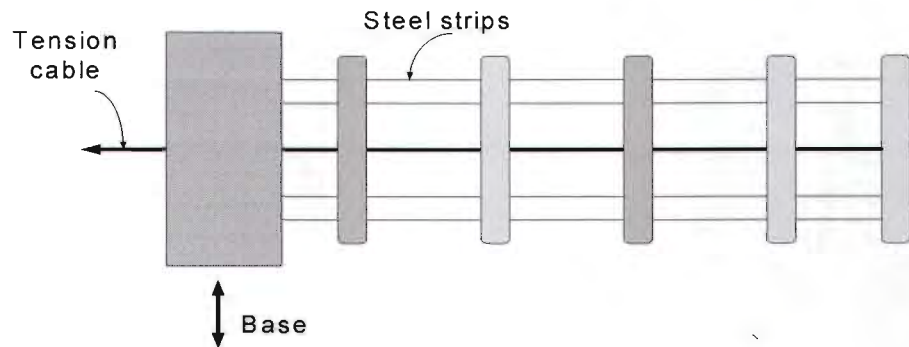


Fig. 2.3 Pre-Tensioned Beam seen from above (Kerr, 1976).

It must also be borne in mind that the equipment used at that time could not measure with the high resolution and accuracy of today's equipment.

A similar experiment was done by Tomski (1994), who approached the structure as a nonlinear system. He performed an experiment with a compound beam (Figure 2.4).

A preload is created in member one which results a reaction on member two. Tomski (1994) demonstrated that whether the stress in member one is tensile or compressive, the beam always vibrates with a lower natural frequency. He established tests with two sets of pre-stressed geometrically non-linear compound beams with different lengths. He found the preload has a significant effect upon the natural frequency of the beam with greater length. Sabuncu and Kaçar (1990) came to the same conclusion in their article, and refer to it as the effect of slenderness. Tomski (1994) did not specify in his article whether, Young's Modulus and the dimensions were the same for member one and member two.

Majid (1972) stated that, during the axial compressive loading of a structure the resulting axial load reduces the overall stiffness of the structure. He continued by saying that the effect of axial loading violates the yield criteria by making the bending moments at certain sections higher than the fully plastic moments of these cross-sections.



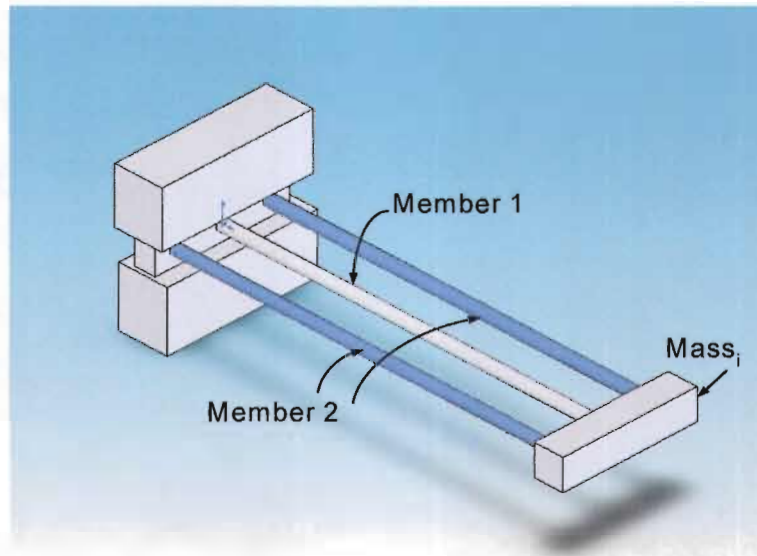


Fig.2.4 Double Member Cantilever Beam constraint on the Left Side (Tomski, 1994).

Hammed (2005) discussed the effect of the magnitude of the pre-stress force through the center of a beam, on the natural frequencies of pre-stressed beams. His description of the dynamic behaviour of such a beam, involves two substructures which are interconnected through equilibrium and compatibility requirements. When increasing the magnitude of the axial tensile force (preload) in the case of a compound beam, the natural frequency decreases. He refers to this phenomenon as “compression softening”.

Hammed (2005) made the important statement that, according to his knowledge, there is no rigorous mathematical model competent to properly define the effect of the pre-stress force on the natural frequencies of pre-stressed beams.

Rivin (1999) explained the “Reverse Buckling” concept in his book. Effective stiffness enhancement of structural components subjected to bending can be achieved by axial preloading in tension of the component, loaded in bending for reducing its bending deformations. Rivin (1999) made use of a self contained composite beam (Figure 2.5) which had an external tubular member and an internal core (Bolt) to illustrate the stiffening effect.

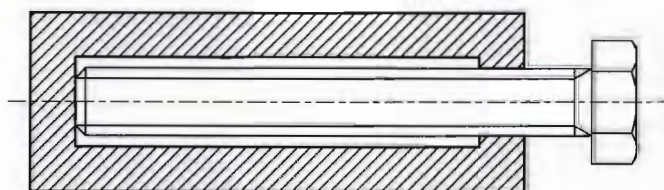


Fig. 2.5 Enhancement of Bending Stiffness by Internal Axial Preload (Rivin, 1999).



Since the cross-sectional moment of inertia of a round beam is proportional to the fourth power of its diameter, both strength and stiffness of the composite beam in bending, are determined by the external tubular member, whose stiffness is usually 85 - 90% of the total stiffness. The outside member is in tension due to the tightening bolt. The tensile force compensates for the equal compression force within the bolt. These forces cause stiffening in the external member and a reduction of stiffness in the internal core. Since the value of the buckling force for the external member  $P_{cr_e}$  is much higher than the value of  $P_{cr_i}$  for the internal core, the relative stiffness change is more pronounced for the internal core. Due to the insignificant initial contribution of the internal core to the overall stiffness (10 - 15%), a relatively small increase in stiffness of the external member will result in an improvement of the overall stiffness, even if the external core stiffness is reduced to a negligible value.

### 2.2.6 Contact Stiffness and Damping

Rivin (1999) explained that the actual contact area of flat contact surfaces is small because of the roughness and waviness of the contacting surfaces, since only the outstanding areas of surfaces asperities or waves are in contact. If the contact surfaces are perfectly flat (perfectly matched) the contact deformation is insignificant. Contact deformations between conforming surfaces influence vibration to a significant degree. Furthermore the contact stiffness is very sensitive to the method of surface finishing and that the contact stiffness for vibratory loads (dynamic stiffness) is the same as static stiffness if the joint is not lubricated (Rivin,1994:94). Moreover contact stiffness can also be enhanced by contact pressures, through increasing the load or reducing the surface area (Rivin,1999).

Rivin(1999) noted that preloading of structural joints such as interfaces may result in the reduction of damping, and that there are three major processes which contribute to the loss of energy in flat joints during the vibration process, these being:

- Material damping.
- Loss of energy in contact areas between fitting parts, and
- Losses due to lubrication.

Rivin (1999) claimed that if two contact surfaces are perfectly flat or match perfectly, then the contact deformation is insignificant. Hence the joint stiffness depends primarily on the joint area, which corresponds

with the conclusions of Little (1967). The contact pressure can be adjusted with the same preload. (This is relevant to this project with references to the interface areas between the discs).

The contact surfaces are characterized by non-linear hardening due to an increase of effective contact area with the increasing load. Therefore due to this nonlinearity of contact deformations, Fast Fourier Transformation (FFT) based dynamic experimental techniques for mechanical systems in which contact deformations play a substantial role, should be used with caution.

Results concerning contact surfaces from experimental findings are summarised as follows by Rivin (1999):

- Better surface finishing results in higher contact stiffness and damping decreases with improved surface finish.
- Joints with the same surface finish ( $R_a$ ) exhibit practically the same damping.
- Damping slightly increases when the width of the contact area is increased.
- The log decrement  $\delta = 0.3 - 0.37$  for damping with tangential vibration. This applies to joints with preload  $\sigma_m = 50 - 80$  MPa, without any lubrication.
- In non-lubricated joints, damping does not depend on the pressure in the joint range when the pressure is in the order of 1 - 2 MPa (Rivin, 1999:158).

### 2.2.7 Bolt and Flange Interaction

Little (1967) studied bolt and flange interaction. He confirmed that estimating clamping stiffness is problematical unless the joint geometry of the clamping area is clearly defined. It is necessary to discuss this occurrence, because this is the focal zone in the rotor and it may affect the results. Little (1976) stated that in bolted joints clamping-stiffness depends on the stress flow around the bolt or stud. The stress flow lines spread out and generate a conical volume that defines the clamping-pressure cone (Figure 2.6).

Little (1976) illustrated that there has been an overestimation of clamping stiffness ( $K_c$ ) in the past. The slope of the clamping pressure cone depends on the flange geometry and only a small part of the flange experiences excessive clamping pressure.

Stiffness of the clamping pressure cone can be computed directly from  $K_c = \beta E d$ , where the

- $\beta$ -values are obtained from the graphs, Little (1976).
- E: Young's Modulus.
- d: nominal diameter of bolt (Figure 2.6).

A reasonable range of 15-20 degrees is adequate for  $\Phi$ . He further stated that, the stiffness  $K_c$  of the clamped flanges depends mainly on the ratio  $D/d$ , and changing this ratio is the most effective way to increase  $K_c$ .

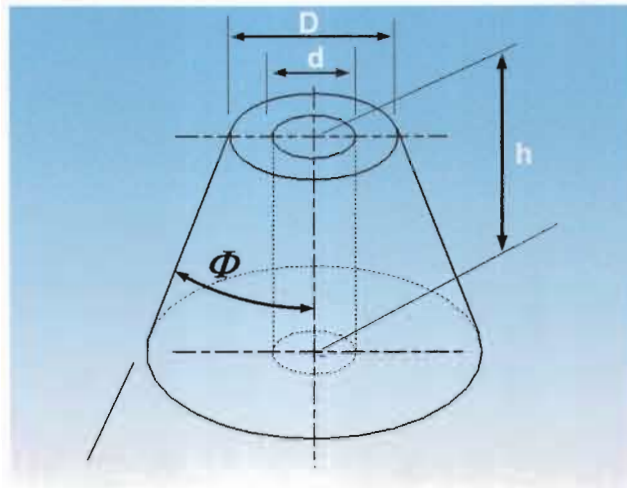


*Fig. 2.6 Pressure Cone Little (1976).*

Ito et al. (1979) investigated the interface pressure distribution of the bolt-flange assembly. He observed that the pressure distribution depends largely upon the flange material and especially upon the quality of finishing of the joint surface and to some extent, the flange thickness. He also noticed the measured pressure distribution differs greatly from the theoretical prediction.

The book by Cook et al. (2001) provide a thorough survey on structural dynamics and vibration from a Finite Element perspective. They indicated that stress concentrations are local effects that have little influence on overall displacement modes. In view of the Rayleigh quotient, the stress concentrations have little influence on vibration frequencies.

Adams (1998) affirmed the same point in that extremely localised behaviour will most likely not cause gross yielding if the local area is supported by regions of lower stress on all sides.

## **2.2.8 Non-Linear Measurements**

In practice, most engineering structures have a certain degree of non-linearity due to the non-linear dynamic characteristics of joints, material properties etc. For practical purposes, in many cases, they may be regarded as linear structures if the degree of non-linearity is insignificant in the response range of

interest. Therefore Linear modal analysis methods can be applied to analyse their dynamic characteristics. However a distinction between a non-linear excitation method and a non-linear structure has to be made. Maia et al (1997) addressed non-linear modal analysis in the book Theoretical and Experimental Modal Analysis. He held that most of the theories upon which structural dynamic analysis is founded, rely a great deal on the assumption that the dynamic behaviour of the structure is linear. This means that if a given loading is doubled, the resulting deflections are doubled or the deflection due to two or more simultaneously applied loads is equal to the sum of the deflections caused when the loads are applied one at a time.

An expectation of non-linear behaviour in the considered rotor-structure raises the question: "Do we want to describe the non-linear behaviour, or do we want to make a linear approximation?"

Modal analysis assumes linear systems and uses linear models. If we deal with a structure which exhibits some nonlinear behaviour, we will attempt to make the best linear approximation. Sinusoidal excitation with maximum amplitude control is commonly used to study nonlinearities.

Maia et al (1997) proposed that the high crest factor of transient excitation makes it possible for the identification of non-linear behaviour, but they add that there is not much evidence to support the advantages of using transient excitation.

## 2.2.9 Analytical Model

**Mathematical models** are important for a number of reasons, namely:

- To understand and communicate how structures behave under dynamic loads.
- To simulate or predict the response caused by external forces.
- To simulate changing dynamic characteristics due to external physical modifications.

There exist three errors that an analytical model deals with in describing the dynamics of a structure. These are:

- Parameter,
- Discretisation, and
- Structural errors.

The parameter errors can be corrected. The structural errors are flexibilities that exist at joints or interfaces between components for which information is usually not available.



Ehrich (1992) provides a comprehensive survey of analytical models for rotor systems. He holds that the Direct Stiffness Method (DSM) and the Transfer Matrix Method (TMM) are the most regularly used procedures for the analysis of free and forced vibrations of rotor dynamic-systems. The major advantage of the TMM over the DSM is that it does not require the large amount of computer storage and the manipulation of large system arrays.

The TMM method makes use of a marching procedure, which starts with the boundary condition at one side of the structure, and marches successively along the equation of the structure to the other side.

$$\{v_n\}^R = [P_n][F_n][P_{n-1}][F_{n-1}] \cdots [P_1][F_1]\{v_0\}^L$$

Where  $\{v_n\}^R, \{v_0\}^L$  : {Displacement, Slope, Moment, Shear force} vector

$[P_n]$  : Point matrix

$[F_n]$  : Field matrix

This method is particularly appropriate for chainlike structures such as rotors. It offers procedures for the use of this method for almost all aspects of rotor dynamics analysis. Ehrich (1992) declared that with a few refinements, this TMM is a reliable analytical procedure widely used by rotor dynamics experts throughout the world.

The Transfer Matrix equation used by Ehrich (1992) differs from the original equation which was derived by Myklestad (method). The whirl to spin ratio  $\rho$  is included in the point matrix. The equation (method) Ehrich (1992) utilized in determining the critical speeds and modes, is for an undamped rotor with isotropic supports, where the rotation rate is equal to whirl speed .

Li (2000) concluded that it is very difficult to get exact solutions from differential equations for free vibrations of bars with variable cross-sections under the action of various axial loads, including concentrated and variable distributed axial loads.

It is known that when the wavelength of a vibration mode relative to the beam thickness becomes small, the effect of the inertia of rotation, called rotary inertia, and that of the deformation due to shearing forces, called shear deformation appears (Yamamoto,1991).

Fertis (1995) described that transverse shear and rotary inertia can have a considerable effect on higher modes during dynamic analysis. This is supported by Rivin (1992) in that the stiffness of a structural material is characterised by its elastic (Young's) modulus E for tension and compression, but in many cases the Modulus of Elasticity values are not enough; another important material parameter which must be taken into consideration is the shear modulus G,

for most metals being:

$$G \approx 0.4 \times E.$$

The state of every section of a beam of length  $L$  is completely specified if we specify

position ( $y$ ), slope ( $\frac{\partial y}{\partial x}$ ), moment  $EI \frac{\partial^2 y}{\partial x^2}$ , and shear  $EI \frac{\partial^3 y}{\partial x^3}$ .

Yamamoto (1991) explains beam theory necessary for a thick rotor in his book. Analysis of continuous rotors is based on the theory of lateral beam vibrations. The most fundamental theory is the Bernoulli-Euler beam theory, which assumes that the cross section remains a flat plane perpendicular to the centreline during vibration. This means that the bending moment at an arbitrary position of the shaft is proportional to the inverse of the radius of curvature of the centreline of the shaft. These equations are representative of the motion of the rotor if it is slender. In the case of relatively thick shafts, the cross section does not remain flat during bending, due to shear. Shear deformation means the deformation of a shaft element due to transverse shear forces as shown in Figure 2.7. Since the element that has the shape shown by the dashed lines deforms to the one shown with solid lines due to shearing forces, the normal line of the cross section shifts with gradient,  $\Psi$ , from the centreline of the rotor (with gradient  $\frac{\partial u}{\partial s}$ ) by an amount,  $\beta$ . This

angle  $\beta (= \frac{\partial u}{\partial s} - \Psi)$  is called the shear angle, where the shear force  $F_x$  and shear angle  $\beta$  has the

relationship  $\beta = \frac{F_x}{kAG}$ , where

- $A$  is the area of the cross section.
- $G$  is the shear modulus.
- $k$  is a constant.

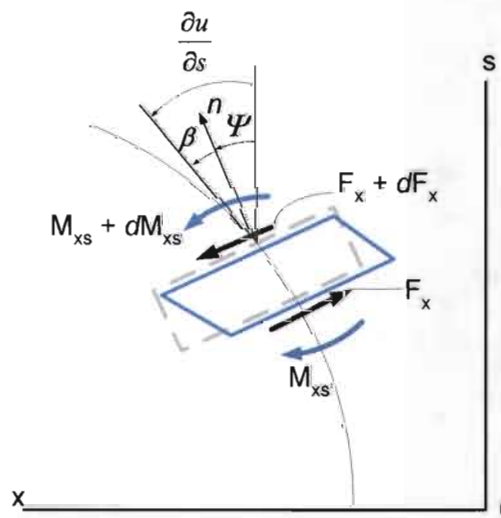


Fig. 2.7 Shear Deformation of a Shaft Element during Bending (Yamamoto, 1991)

### **2.2.10 Finite Element Method (FEM)**

In the book Engineering Vibration, Inman (1996) summarised the finite element method as a powerful technique for modelling and solving boundary value problems. This method is extremely useful for complicated systems such as abnormal geometric shapes. Analytical mathematical models like Finite Elements (FE) are based on mass and stiffness distributions and constraints with specific boundary conditions. The finite element method approximates a structure in two distinct ways. The first is to divide the structure into a number of smaller parts, called discretisation. The vibration equation for each individual part or an element is then determined and solved, resulting in a global stiffness and mass matrix. A complete derivation of the finite element is available in any Finite Element Analysis textbook.

Kumar (1995) makes the following informative statement about the beam element: Typical rotors are usually modelled by a series of beam elements, formulated from the classical Timoshenko beam theory. But beam elements cannot model the flexibility of discs mounted on solid shafts. In the formulation of beam elements the assumption is made, that plane sections remain plane, making it impossible for the element to take into account the distortion effects that occur due to large changes in diameter, nor the inability of beam elements to model the distortion effects that occur in a hollow conical section. These limitations restrain the use of beam elements as discs with flexibility.

### **2.2.11 Non-linear-Finite Element Method**

There comes a point when one has to question many of the simplifications and approximations made during model development. Nearly everything in the world is non-linear. The degree of non-linearity, or the variance between a non-linear and a linear approximation will determine how valid the linear results are. The fact is that even a non-linear solution can be attained by solving many small linear steps iteratively.

The book by Cook et al. (2001) provides an assessment of non-linear behaviour using finite elements. Cook stated that when material properties are stress-dependant, the problem is non-linear. Non-linearity encompasses a wide variety of phenomena as well as possible interaction with one another etc. Cook et al. (2001) share the same opinion as Maia (1997) in the affirmation that Linear Models will provide satisfactory approximations for many problems of practical interest.

In structural mechanics, the types of non-linearity include the following :

- Material non-linearity in which material properties are functions of the state of stress or strain like non-linear elasticity.
- Contact in gaps between adjacent parts which open and close.



- Geometric non-linearity: large deformations where equilibrium equations must be written with respect to the deformed structural geometry.

These categories are all non-linear because the stiffness and loads become functions of displacement or deformation.

### 2.2.12 Modal Analysis

Modal analysis is an efficient tool for describing, understanding and modelling structural behaviour. Basically, modal analysis is the study of the natural characteristics of a structure.

The natural frequencies of a structure are the frequencies at which the structure naturally tends to vibrate if it is subjected to a disturbance. Natural frequencies and mode shapes are functions of the structural properties and boundary conditions. If the structural properties change, the natural frequencies change, but the mode shape may not necessarily change (Brael & Kjaer, 1999).

Maia (1997) explains the difference between 'structure' and 'system'. It is inevitable that the terms 'structure' and 'system' will be found in texts on modal analysis. Often these two terms are intended to mean the same. A system is the idealisation of a structure where mathematical models can be readily established and explored. When referring to a structure, it is often implied that its idealisation exists. Alternatively, the term 'structural system' is also used.

### 2.2.13 Synthesis

Some studies concurred that pre-stressing tends to decrease the natural frequencies of pre-stressed beams, whereas others report that pre-stressing has negligible or no effect on the natural frequencies.

Little (1967) stated that the clamping-stiffness of bolted joints depends on the stress flow around the bolt. Ito et al. (1979) explained that the pressure distribution depends largely upon the flange material and especially upon the quality of finish of the joint surface and flange thickness.

Rivin (1999) and Rivin et al. (1990) point out that stiffness can be enhanced using axial pre-tension, but it is subjected to the slenderness and rigidity of the structure. It also appears that small localised stress regions will not affect the behaviour of the rest of a structure significantly.

The information in the articles of Tomski et al. (1994) and Sabuncu and Kaçar (1990) is very appropriate because of the structural similarities between the bolted rotor-disc-system and their structures. Sabuncu and Kaçar (1990) and Yamamoto (2001) have the same opinion: Slenderness is a function of critical speeds or natural frequency. Similar results were derived by Tomski et al. (1994) who found that pre-



tension has an increasingly significant effect upon the natural frequency with increasing the length of the structure.

The Transfer Matrix Method (TMM) is a very popular method according to Ehrich (1992). On the other hand, The Finite Element Method (FEM) is especially appropriate for complicated systems with irregular geometries. According to Kumar and Sujatha (1995), the beam finite element does not take into account the distortion effects that occur due to large changes in diameter in the axial direction. According to Hammad (2005) there is no mathematical model that is able to properly define the effect of pre-stress on the natural frequencies of a pre-stressed beam. The rotor under investigation consists of relatively thick and short sectors. Taking the above into consideration it is necessary to search for a reliable method which will include shear effects.

## 2.3 Technical Background

### 2.3.1 Stiffness Concepts

Stiffness is a complex parameter at a point in a system. That can be characterized by values in the three orthogonal directions in a coordinate frame. Ratios of the stiffness values in these orthogonal directions determine the dynamic stability of the system.

It is necessary to explain definitions related to stiffness:

- *Structural stiffness* is due to deformation of a part or component.
- *Contact stiffness* is due to deformation in a connection between two components.
- *Static stiffness*,  $k_{st}$ , is stiffness measured during a very slow loading process.
- *Dynamic stiffness*,  $k_{dyn}$ , is stiffness measured under conditions above 0.5 Hz.
- *Proof load*: The maximum load that a bolt can withstand without acquiring a permanent set.
- *Proof strength* : The quotient of the proof load and the tensile area.
- *Material non-linearity*: Material properties are functions of the state of stress or strain.
- *Geometric non-linearity*: Where the deformation is so large that equilibrium equations may be written with respect to the deformed structural geometry.

## **2.3.2 Modal Analysis And Testing**

### **2.3.2.1 Modal Analysis**

Modal analysis is the study of the natural characteristics of a structure (Bruel & Kjaer, 1999).

Modal testing (System Analysis) is the exposure of the inherent properties of a system obtained by exciting a system with measurable forces and studying the Response/Force ratio. In linear systems this ratio is independent; indicating that the inherent properties remain the same during excitation. The properties of the transmission path between the source and receiver represent the inherent dynamic characteristics of the combined system. The modal parameters are, modal frequency, modal damping and mode shape.

The modal parameters of all the modes within the frequency range of interest represent a complete dynamic description of the inherent properties of the structure.

The modal parameters are the important parameters for formulating an analytical dynamic model. This process of formulating a model may be fulfilled through analytical or experimental techniques.

Analytical models using Finite Elements are based on mass and stiffness distributions with specific boundary conditions.

### **2.3.2.2 Real and Complex Modes**

Ewins (2000) presented a thorough overview of the difference between real and complex modes. A complex mode is one in which each part of the structure has not only its own amplitude of vibration but also its own phase. This means each part of the structure which is vibrating in a complex mode will reach its own deflection peak at a different moment compared to the vibration cycle of its neighbours which all have different phases. A real mode is one in which the phase angles are all identical from  $0^\circ$  or  $180^\circ$ . This means that all parts of the structure reach their own maxima at the same time (instant) in the vibration cycle, or pass through their zero deflection position at the same moment. This is in contrast with complex modes where the maxima or the zero positions are attained at different times. This is the same with the zero position.

Complex modes occur in practice for a variety of reasons and it is important to know the necessary conditions for them to exist. Ewins (2000:115) stated further that normal modes of regular linear structures can be complex only if the damping is distributed in a non-proportional way. He made the important statement that this situation can arise quite readily in practice because the internal (hysteretic) damping of most structures is distributed in proportion to the stiffness distribution but that the majority of damping in real structures is generally found to be concentrated at the joints between components of a structure assembly, and this does not result in proportional distribution.

Another factor that will generate complex modes is the close proximity of two or more modes. This means that these natural frequencies are separated by an amount which is less than the established damping in either or both modes. Another factor is repeated roots (structures with a **double symmetry**), where two or more modes have identical natural frequencies for example in structures with double symmetry.

### 2.3.2.3 Resonance and Anti-Resonance

If two consecutive modes have the same sign for modal constants, then there will be an anti resonance at some frequency between the natural frequencies of those two modes. If they have opposite signs, there will not be an anti-resonance but only a minimum. The important feature of anti-resonance is the fact that there is a phase change associated with it as well as a very low magnitude.

Anti-resonances decrease with growth of the separation between excitation and response points and progressive increase in the phase angle of the FRF as the frequency gets higher. Therefore, there is a positive increase in degrees if the corresponding anti-resonance is at a minimum. That means the phase loses  $180^\circ$  as it passes over a resonance and gains  $180^\circ$  of phase as it passes over an anti-resonance (Avitabile, 2001). If damping is integrated, the resonance and anti-resonance are blunted and the phase angles are no longer exactly between  $0^\circ$  or  $180^\circ$ .

### 2.3.2.4 Excitation

There are three types of excitation: Burst, rapid sine sweep and the impact from a hammer blow. The first two require an attached shaker. The burst random and sine chirp are two common excitation signals widely used today. The principle underlying these signals is that the excitation and the consequent response are completely contained within the single sample of measurement at which it is made. It is common practice to repeat the transient event more than once and to average the results to get the final result. The Frequency Response Function (FRF) is very simply the ratio of the output response of a structure due to an applied force (Avitabile, 2001).

The FRF is derived from the ratio: 
$$H(\omega) = \frac{X(\omega)}{F(\omega)}$$

The FRF describes the dynamic properties of a system independent of the signal type used for the measurement. The FRF is therefore equally applicable to harmonic, transient and random excitation.

The FRF is a complex function (i.e. one with both magnitude and phase) that is frequently used to define the relationship between the input to a system (either mechanical or electrical) and its corresponding

output. For this reason, the FRF is sometimes referred to a 'transfer function'. In such cases, the input to the system is connected to channel one and the output to channel two of an analyzer (DI, 2003).

The most popular excitation technique used for modal analysis is impact, or hammer excitation. The waveform produced by an impact is a transient (short duration) energy transfer event. The spectrum is continuous, with a maximum amplitude at 0 Hz and decaying amplitude with increasing frequency. The spectrum has a periodic structure with zero force at frequencies at  $n/T$  intervals, where  $n$  is an integer and  $T$  is the effective duration of the transient. The useful frequency range is from 0 Hz to a frequency  $F$ , at which point the spectrum magnitude has decayed by 10 to 20 dB. The duration, and thus the shape of the spectrum, of an impact is determined by the mass and stiffness of both the impactor and the structure. For a relatively small hammer used on a hard structure, the tip hardness of the hammer tip determines the spectrum. The hammer tip acts as a mechanical filter. This means it determines the frequency of the available energy. Selection of the correct tip stiffness enables the cut-off frequency to be chosen.

Disadvantages of the impact excitation method are:

- High crest factor makes the technique unsuitable for testing a system with non-linear properties since the non-linear behaviour will be induced (provoked).
- High peak energy is required to apply sufficient energy to a large structure.
- The signal is highly deterministic. This means no linear approximation can be made for non-linear systems.
- Due to the deterministic nature of the signal, the coherence function cannot show neither leakage nor non-linear behaviour.

The advantages of hammer testing are:

- Speed : only a few averages are needed.
- No elaborate fixtures are required.
- It is portable.
- It is relatively inexpensive (Briel & Kjaer, 1999).

H Storck and H Sumali (1999) the authors executed experiments on rubber mountings which were extremely non-linear, and advised that the impact force has to be as small as possible to remain within the linear range.



## 2.3.2.5 Coherence Function

The Coherence Function provides us with a means of assessing the degree of linearity between the input and output signals. The interpretation of the Coherence Function is that for each frequency it shows the degree of linear relationship between the measured input and output signals. Avitabile (2001) explains that the coherence function is used as a data quality assessment tool which identifies how much of the output signal is related to the measured input signal. A common application of the Coherence Function is a check on the validity of Frequency Response Function measurements.

A high coherence value indicates that there is a linear relationship between the input and output signals, suggesting that the FRF measurement is valid at that frequency range (although it is not guaranteed to be so), whereas a low coherence value practically guarantees a poor FRF measurement at that frequency (Diagnostic Instrument user manual, 2002).

The deterministic character of impact excitation limits the use of the Coherence Function. The Coherence Function will show a value of one unless:

- There is an anti-resonance, i.e. where the signal to noise ratio is rather poor. No particular attention needs to be paid to this because by taking a number of averages the
- FRF curve is smoothed out for noise.
- If the impact point is close to a node point the Coherence may be extremely low ( $\approx 0,1$ ).
- However, this is acceptable, since the modal strength at this point is weak and not important for the analysis.

## 2.3.2.6 Phase Plots

Anti-resonances decrease as the separation between excitation and response points grow and there is a progressive increase in the phase angle of the FRF as the frequency gets higher. Therefore, there is a positive increase in degrees if the corresponding anti-resonance is a minimum. That means the phase loses  $180^\circ$  as it passes over a resonance and gains  $180^\circ$  of phase as it passes over an anti-resonance (Avitabile, 2001). If damping is integrated, the resonance and anti-resonance are blunted and the phase angles are no longer exactly between  $0^\circ$  or  $180^\circ$ .

## 2.3.2.7 Analytical Modal Models

Analytical models are desired or necessary for a number of reasons:

- To understand and communicate how structures behave under dynamic loads,
- To use in data reduction and smoothing techniques (curve fitting),
- To simulate or predict the response to assumed external forces,

- To simulate changing dynamic characteristics, due to physical modifications.

A Mathematical model is generally not a model of the structure itself. Rather it is a model of the structure's dynamic behaviour, constrained by a set of assumptions and boundary conditions .

The next chapter discuss and explain test equipment, experimental procedures and results



## EXPERIMENTAL PROCEDURE AND RESULTS

This chapter sets out to find experimental values, using Modal Analysis, of the assembled rotor system of the first three transverse modes for a range of configurations.

### 3.1 Introduction

The experimental procedure, specification and description of equipment used and reliability of obtained the data will be presented and discussed.

Modal analysis is the study of the natural characteristics of a structure. System analysis (Modal Testing) is used to determine the inherent properties of the system by exciting the system with measurable forces and studying the response/force ratio. The advantages and disadvantages of the Impact method have already been discussed in Chapter Two.

Tests were done on the full rotor system (*Figure 3.3*), the parameters which were altered before each impact test were the number of discs, number of bolts, and the preload in the bolts.

### 3.2 Test Equipment.

Specifications related to equipment used

- Mass of disc: 2.99 kg (*Figure 3.2*).
- Mass of one hub: 13.38 kg (*Figure 3.2*).
- Mass of one hardened washer: 17.6 gram
- Mass of three lengths of 10 mm threaded bar used respectively for:
  - Two to four discs: 58.4 gram.
  - Six discs : 81.5 gram.
  - Eight discs : 107.8 gram.
- Mass of one nut: 10.2 gram.
- The maximum frequency range used during experimental analysis was 5000 Hz (*5000 Hz is quite high if the frequency is converted to rotational Speed, but this is necessary in order to intercept the first three transverse mode shapes*).
- Analyser: DI 2200, two channel.
- Transducer: PCB , 107.1 mV/g, accelerometer (*Figure 3.1*).
- Impact hammer: PCB (*Figure 3.1*).



- Force transducer: HBM, KMR 100 kN, 3 mV, 50 gram (*Figure 3.1*).
- Data acquisition system: 2 X 8 channel Catman-spider system, HBM.



*Fig.3.1 Photograph of the Force Washer, Hardened Washer, Accelerometer and Impulse Hammer with Copper Tip used in the Tests.*

*(The photo gives an indication of the size of the equipment used during the test)*

### 3.3 Experimental Procedure

Before the impact test the bolts were pre-tensioned to the required loads, 23500 N and 30300 N respectively. (These values are consistent with previous test-run experiments in the laboratory)

#### 3.3.1 Bolt Stresses during preload:

Nominal stress area for 10 mm bolt = 58 mm<sup>2</sup> (5,8 x10<sup>-5</sup> m<sup>2</sup>)

Yield stress = 660x10<sup>6</sup> Pa,

Ultimate tensile = 905x 10<sup>6</sup> Pa, see Appendix for certificate.

The maximum stresses induced in the bolts for the duration of these experiments were:

$$\begin{aligned}
 \sigma_{90\%} &= \frac{F}{A_{\text{nominal}}} \\
 &= \frac{30300}{5.8 \times 10^{-5}} \\
 &= 522.4 \text{ MPa}
 \end{aligned}$$

$$\begin{aligned}\sigma_{70\%} &= \frac{F}{A_{nominal}} \\ &= \frac{23500}{5.8 \times 10^{-5}} \\ &= 405.1 \text{ MPa}\end{aligned}$$

These stress values are still in the linear region as can be seen from the stress-strain graph in Appendix F.

### 3.3.2 Procedure

Force transducers connected to the Catman-spider system were utilized to characterize the load in each bolt. The bolts were gradually tensioned to ensure uniform tension until the required load was reached. The rotor was supported with two ropes, using two short M10 bolts on the sides, presenting a free-free condition during impact testing. A small impact hammer with a brass tip was applied to excite the structure in the vertical direction. The first three lateral modes with a frequency range of 0 - 5000 Hz were investigated.

The impact was done on five different locations in the same directional line as the mounted response transducer. The response was measured at only one location through the entire experiment (Figure 3.3). The response transducer was glued onto the structure. The impact location was at location no. 5 for all the presented plots below, unless otherwise specified. Figure 3.2 shows a cross-section cut illustrating the location of the disc-volume zone.

Flat Force Washers were included between the washers and the disc material (Figure 3.4). These special hardened washers were included on both sides of the force transducer during testing to ensure equal distribution of pressure on the force transducer and to prevent possible permanent strain in the discs. Bolts of the same material (High tensile) were used during the entire experiment. The contact surfaces of the discs have a high surface finishing. No lubrication was used between discs. Pre-twist on the bolts caused by the applied torque was ignored.

### 3.3.2 Setup of Analyser

Input Channel 1: Hammer.

Input Channel 2: Response Transducer (accelerometer).

Delay: 0.

Bandwidth: 5 kHz.

Samples/Line: 2048/800. ( $\Delta F = 5000/800 = 6.25$  Hz).

Averaging: Linear.

Process averages for each impact location: 6.

Window type: Force/Exp. (Force Exponential Window) primarily for frequency response function measurements using impact techniques.

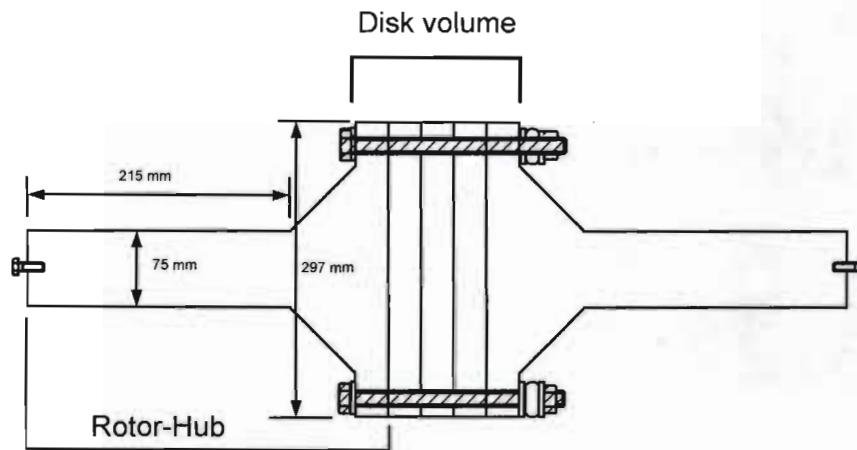


*Fig.3.2 Sketch Defining Sections of Shaft .*

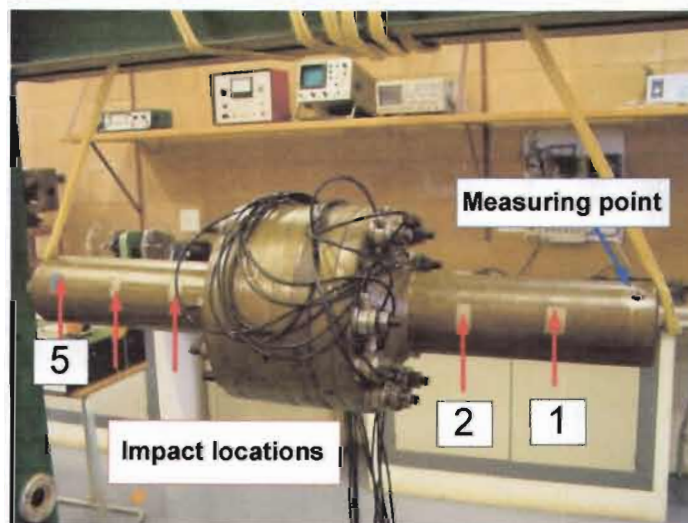


*Fig.3.3 Rotor supported by ropes, locations of input and output measuring positions.  
(Impact was done in a direct-line with response position).*

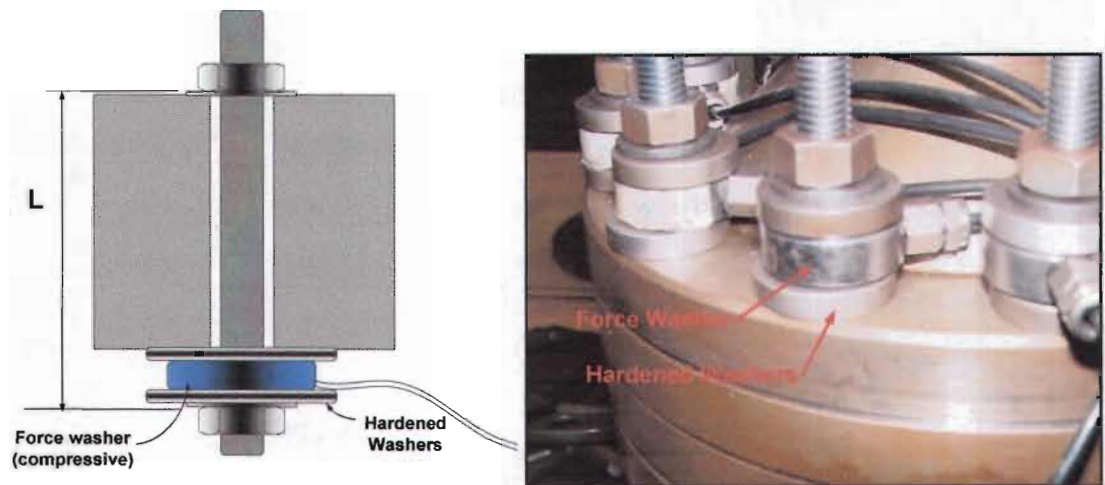


Fig.3.4 Tensioned Bolt and Force Transducer between two Hardened Washers.

### 3.4. The Quality of Measured Data

#### 3.4.1 Signal Quality

The coherence is a measurement of the noise signal. A typical Coherence vs Frequency plot, Figure 3.5, is a descriptive example of the reliability of the frequency response function measurement. The relatively high value above 0.98 indicates sufficient strength and clear measured signals. It is not practical to include all the relevant plots.

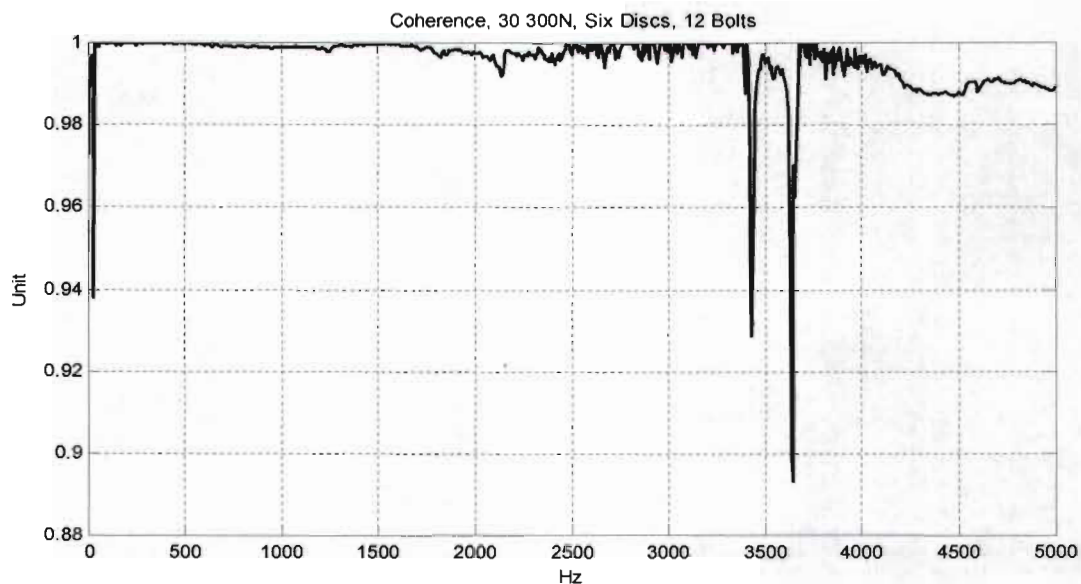


Fig. 3.5 Plot of Coherence of Accelerance vs Frequency Data of a Test on a Six Disc, 12 Bolt Rotor System. The graph gives an indication of how accurate the measurement process is over a given frequency range.

### **3.4.2 Signal Fidelity**

The excitation and response positions are all well separated during the experiment. A structure under test does not always react purely in the vertical direction, and this was found to happen during these experiments. In some instances double peaks developed at resonance, mostly during mode two, which could be misinterpreted as complex modes, but this was not the case here. It turned out that the impact direction was not always in line with the response transducer in the vertical direction, as the varying stiffness in certain radial directions caused by the bolt positions also contaminated the response transducer in the perpendicular direction.

### **3.4.3 Measurement Repeatability**

Measurements were repeated between certain time periods, after dismantling and assembling the structure. The results were always consistent.

### **3.4.4 Measurement Reliability**

A larger impact hammer, but with a softer tip was used for a different excitation signal, however this produced the same results, but the small impact hammer with a copper tip (*Figure 3.1*) generated more noticeable peaks.

### **3.4.5 Measured Data Consistency**

The same set of bolts was used during the entire experiment. During every cycle of the experiment the bolts were systematically tensioned gradually in two steps to loads of 23 500 N and 30 300 N respectively. This duplication of excessive cyclic loads could possibly caused hardening on certain components.

## **3.5. Preliminary Checks of the Frequency Response Function Data**

### **3.5.1 Low Frequency Asymptotes**

The structure used in this project was freely supported (*Figure 3.3*). The mass-like asymptotic trend is interrupted by what appears to be a rigid body mode at a low frequency, lower than the first flexural mode (*Figure 3.8*).

### **3.5.2 Incidence of Anti-Resonance**

Clear resonance and anti-resonance characteristics are visible on certain plots. Not all the impact locations responses were plotted.



### 3.6. Identification of Resonance Frequencies

Distinct resonance peaks were confirmed by examining the phase plot. The phase loses 180 degrees when passing over resonance and gains 180 degrees when passing over anti-resonance.

The necessary phase plots from the experiments in addition with the FEM results of Chapter Four, verify the dominant modes in the transverse direction. A phase plot was obtained for each measurement location. It is not practical to insert all the plots in the thesis. Two examples of the phase- Frequency Response Function (FRF) of six and eight discs are shown below to confirm the resonance frequencies (*Figure 3.6 and 3.7*).

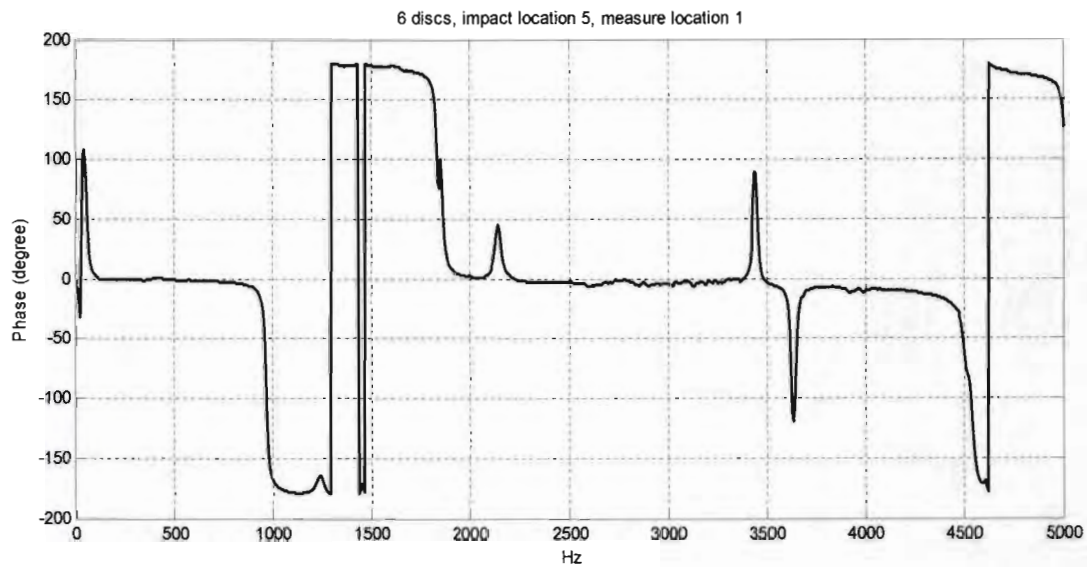


*Fig. 3.6 Plot of the Phase of Accelerance vs Frequency Data for a Six Disc, 12 Bolt Rotor System.*

*Clear phase changes( $180^{\circ}$ ) are visible at each resonance peak for transverse vibration.*

### 3.7 Results

Tables 3.1 and 3.2 list the natural frequency results of different configurations. Not only changes in magnitude, but also tendencies are highlighted. The related plots of the data below are given in Appendix C.

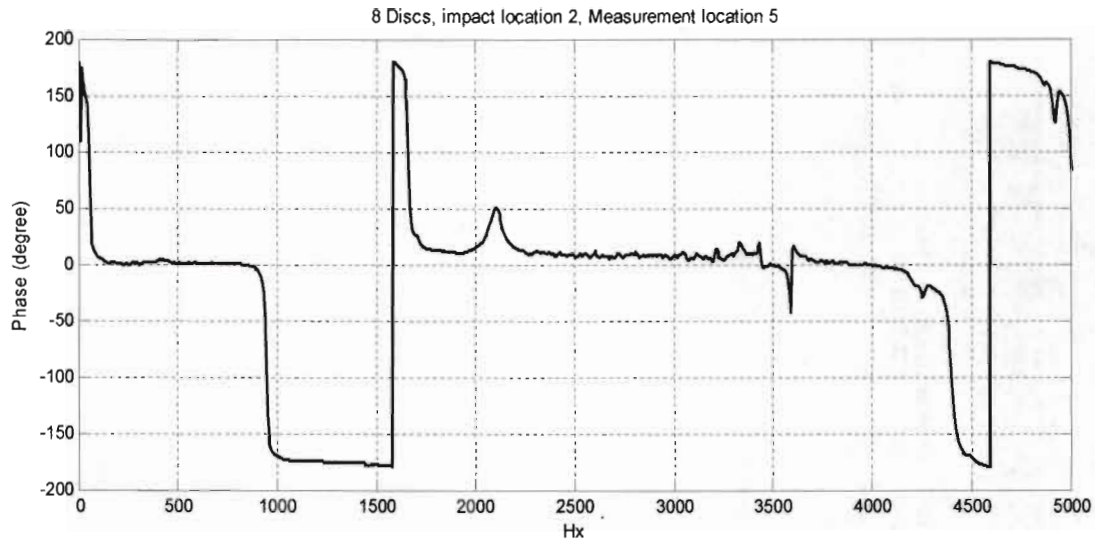


Fig. 3.7 Plot of the Phase of Accelerance vs Frequency Data for an Eight Disc, 12 Bolts Rotor System.  
Clear phase changes( $180^\circ$ ) are visible at each resonance peak for transverse vibration.

**Table 3.1:** Natural frequencies (Hz) for assemblies with two Discs, 6,8,12 Bolts, 70% and 90% Preload. Mass includes the mass of the transducers, hardened washers, studs and nuts.

Preload	2 discs	12 bolts	8 bolts	6 bolts
23 500 N	mode 1	1075	1075	1081
	mode 2	2438	2456	2481
	mode 3	4838	4863	4875
30 300 N	mode 1	1075	1075	1081
	mode 2	2438	2456	2481
	mode 3	4844	4869	4881
Mass (kg)		28.051	27.465	27.172

#### Observations Two Disc assembly:

- There is no significant difference in frequency for similar modes even with different parameters.
- There is a small increase in natural frequency under mode two and three for rotor system with fewer bolts.

**Table 3.2:** Natural frequencies (Hz) for assemblies with Four Discs, 6,8,12 Bolts, 70% and 90% Preload. Mass includes the mass of the transducers, hardened washers, studs and nuts.

Preload	4 discs	12 bolts	8 bolts	6 bolts
23 500 N	mode 1	1013	1013	1013
	mode 2	2125	2138	2150
	mode 3	4669	4681	4688
30 300 N	mode 1	1013	1013	1013
	mode 2	2131	2144	2150
	mode 3	4706	4700	4694
Mass (kg)		34.045	33.459	33.166

**Observations Four Disc assembly:**

- The number of bolts and preload do not influence the natural frequencies in the first mode.
- The natural frequency increases slightly under mode two with fewer bolts .
- The natural frequency increases slightly under mode two and three with increasing preload.

Frequency Response Graphs (Figure 3.8 and 3.9) of six disc system are shown for 6, 8, 12 bolt configuration subjected to 23 500N and 30 300N respectively.

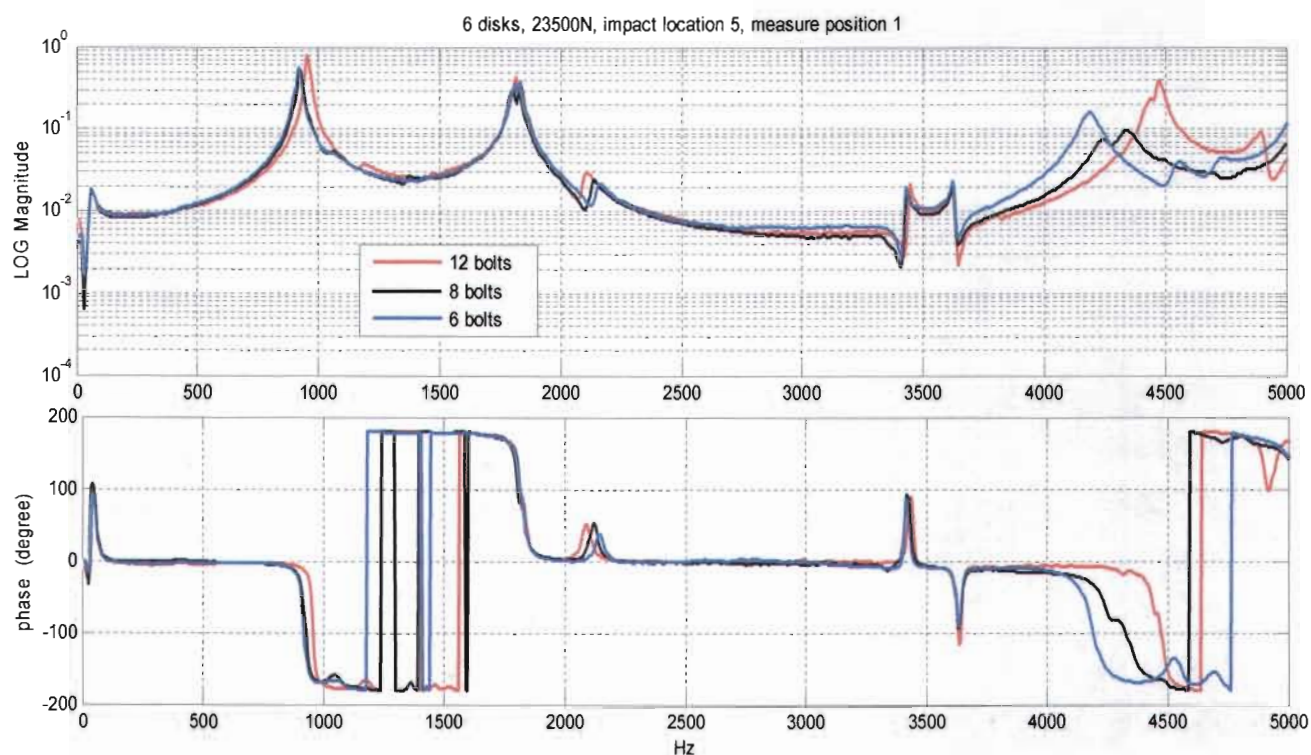


Fig. 3.8 Plot of Logarithmic Magnitude of Accelerance and Phase vs Frequency Data for Six Discs, 6,8,12 Bolts, 23500N Preload in Bolts.



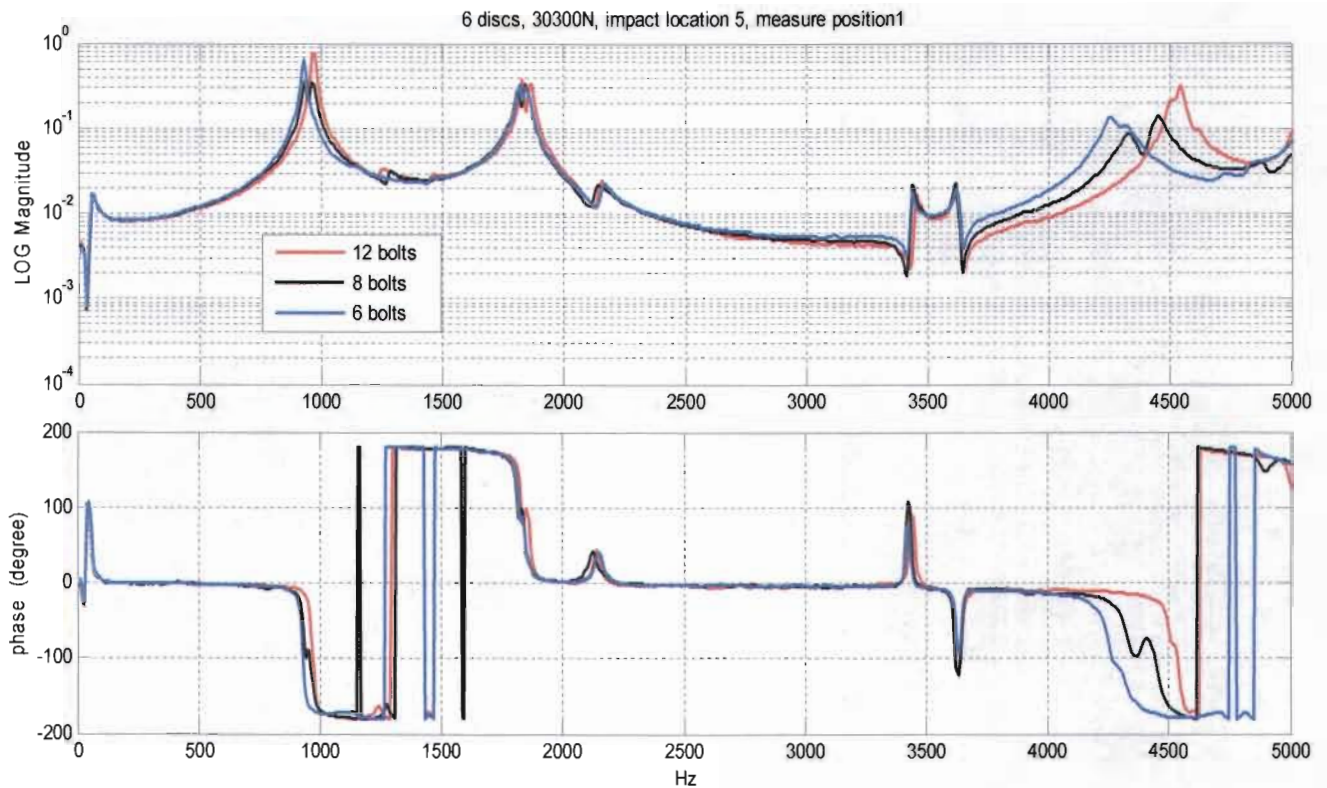


Fig. 3.9 Plot of Logarithmic Magnitude of Accelerance and Phase vs Frequency Data for Six Discs, 6,8,12 Bolts, 30300N Preload in Bolts.

**Table 3.3:** Natural frequencies (Hz) for assemblies with Six Discs, 6,8,12 Bolts, 70% and 90% Preload. Mass includes the mass of the transducers, hardened washers, studs and nuts.

Preload	6 discs	12 bolts	8 bolts	6 bolts
23 500 N	mode 1	950	925	912
	mode 2	1813	1800	1806
	mode 3	4475	4344	4188
30 300 N	mode 1	962	931	925
	mode 2	1825	1813	1816
	mode 3	4538	4450	4250
Mass (kg)		40.316	39.638	39.299

#### Observations Six Disc assembly:

- The natural frequency increases slightly under mode one and three as the preload increases.
- For similar modes there is a systematic decrease in natural frequency as the number of bolts decreases.



**Table 3.4:** Natural frequencies (Hz) for assemblies with Eight Discs, 6,8,12 Bolts, 70% and 90% Preload. Mass includes the mass of the transducers, hardened washers, studs and nuts.

Preload	8 discs	12 bolts	8 bolts	6 bolts
23 500 N	mode 1	925	912	893
	mode 2	1656	1650	1631
	mode 3	4294	4256	4113
30 300 N	mode 1	943	931	912
	mode 2	1663	1656	1650
	mode 3	4494	4350	4213
Mass (kg)		46.625	45.842	45.251

#### Observations Eight Disc assembly:

- There is a systematic increase in natural frequency with an increase in preload for each number of bolts.
- For similar modes there is a systematic decrease in natural frequency as the number of bolts decreases.

#### Mode shapes

A waterfall plot (Figure 3.10) shows the first three mode shapes constructed by the imaginary part of the FRF. The erroneous shape of mode three on the graph is caused by the impact location at node number four, which was a node during mode three.

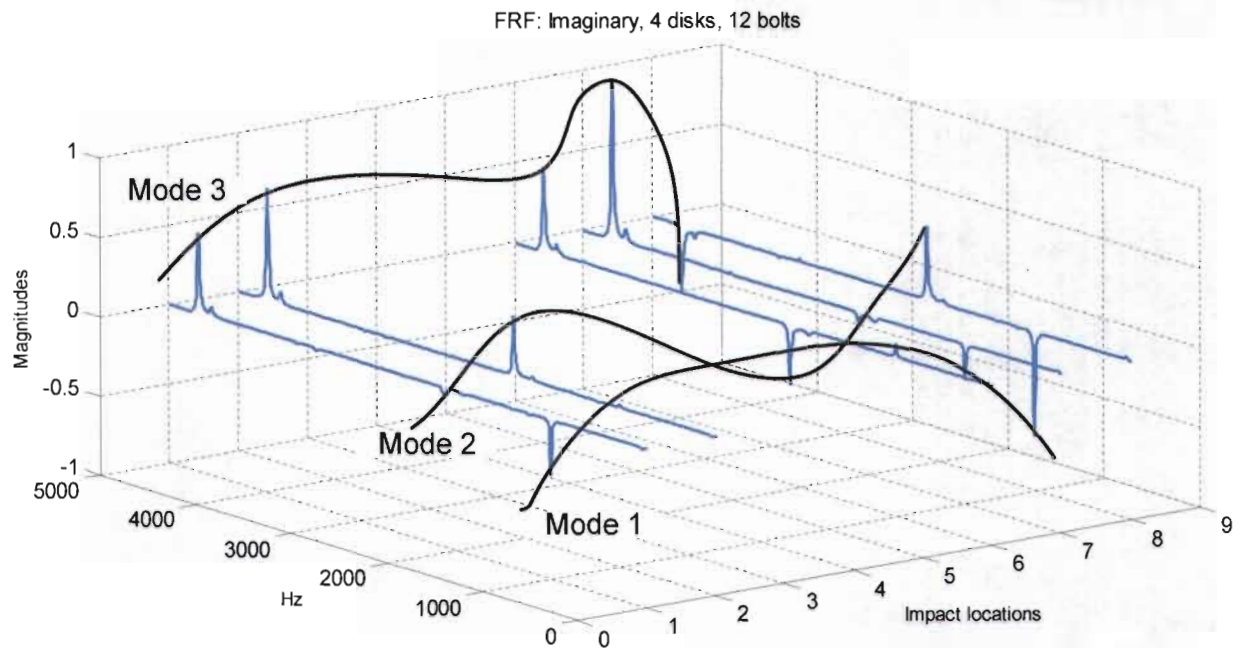


Fig. 3.10 Waterfall plot of Mode shapes using Four Disks, 12 Bolts.  
Imaginary Component of the Accelerance plotted vs Frequency.

### 3.8 Experimental Discussion

- All the Coherence plots are, in essence, the same. The peaks of interest for the transverse modes are close to a value of one on the Coherence Graphs which is an indication of a clear signal received from the transducers.
- The frequency resolution (Samples/Line) used, could hide small deviations during measurements.
- Natural frequencies obtained from the FRF graphs are confirmed by the phase-plots where there is a  $180^\circ$  phase change at resonance.
- Because of the equal spacing of the six and eight bolt configurations i.e. the position of bolts, the stiffness was not the same in all radial directions, which may have contributed to the complex mode phenomena (Split peaks).
- From the FRF plots there is no significant indication of which parameter, mass or stiffness, dominated certain peaks.
- As the spectra are averaged, the non-linear terms should cancel out, resulting in the best linear estimate.

- For a rotor with fewer than four discs, the natural frequency increases as the number of bolts decrease. More bolts imply more mass and rigidity, which forces the structure to oscillate slower. The opposite occurs when the disc-volume becomes slender, where upon the frequency decreases as the number of bolts decreases, which is an indication that stiffness becomes more dominant as the slenderness increases.

### 3.9 Synthesis

Mass (rigidity) dominates when the rotor is short and stubby, while stiffness dominates when the rotor becomes slender.

In Chapter 5, the effect of the pre-tension, stiffness and slenderness will be examined and discussed before verifying the analytical model. A more visual presentation will be given of the location of possible nonlinear behaviour caused by pre-tension. In the next Chapter the finite element model will be set out.

# FINITE ELEMENT ANALYSIS MODEL AND RESULTS

## 4.1 Background

Modal analysis is the basic building block of dynamic analysis. There are a few ways to model the rotor, some of them time consuming. Moreover since assembly models may become complex it is best to choose the most efficient approach and the best element type for that specific part. Only linear behaviour is valid in modal analysis software. If one specifies nonlinear elements, they are treated as linear. For example, if you include contact elements, their stiffness is calculated, based on their initial status and never changed.

Therefore, the question that arises is: Will the outcome of a straightforward approach generate acceptable results?

## 4.2 The Objective of the Analysis

The aim, in this chapter, is to find a straightforward procedure to represent the bolted rotor, with solid finite elements (brick elements) to determine the natural frequencies with acceptable accuracy using acceptable simplification and without complicated refinement.

Since the experimental results indicate small deviations between similar configurations, it is realistic to start with an ordinary FE model.

## 4.3 Accuracy

Accuracy is important. The maximum frequency range during the experimental analysis was 5000 Hz. The relative shift in natural frequency during pre-tension, obtained from the experimental tests, was relatively small.

Finite element meshes need to be tailored to the physics of the given problem; i.e., fine in the direction of rapidly changing field gradients and relatively coarse in directions with less rapidly changing fields.

When the end results of a modal analysis are the natural frequencies of a structure, the mesh can be somewhat coarser than that be required for a detailed stress analysis. As the number of elements increases, the modal analysis results should converge, as in any other structural study. During this analysis, the optimum number of elements allowable for acceptable computing time was chosen.

## 4.4 Simplifications

Rivin (1999) claimed that two components will behave as a solid if they are forced together with high contact pressure. Moreover if two contact surfaces are perfectly flat or match perfectly, the contact deformation is irrelevant. Based on this, the contact surfaces between the discs were assumed to be solid during the analysis.

When considering the 90% preload of 30300N the following hold:

Total Force applied to disc contact surface = (Force in one bolt)(number of bolts) (4.1)

$$\begin{aligned} F &= (30300)(12) \\ &= 363600 \text{ N} \end{aligned}$$

Contact area of disc face :  $A = \pi(R_2^2 - R_1^2) - \pi(\frac{d}{2})^2(12holes)$  (4.2)

(Refer to disc dimensions Appendix B)

$$\begin{aligned} A &= \pi(0.0975^2 - 0.0675^2) - \pi(\frac{0.0105}{2})^2(12) \\ A &= 0.0142 \text{ m}^2 \end{aligned}$$

Pressure on contact areas of disc:  $\sigma = \frac{F}{A}$  (4.3)

90% preload  $\sigma = 25.59 \text{ MPa}$

70% preload  $\sigma = 19.859 \text{ MPa}$

It is also ineffective to model the friction between the disc contact surfaces during modal analysis. The ANSYS software which was utilised, makes use of a linear approach during modal analysis. Therefore, any nonlinearities such as plasticity and contact (gap) elements were ignored even when defined.

The mass of the force transducer and nuts was neglected due to their relatively small mass relative to the total mass of the structure, and also due to their location on the rigid discs (Figure 3.4). It was decided to start with a solid model representing a structure with an optimum number of 12 bolts without any bolt pre-tension.

Small detail like the shoulders in the internal openings were not modelled as they were not critical areas (Figure 4.1). However the large openings were modelled (Figure 4.5).

The most noticeable area where possible yielding could take place is in the interaction between bolt, washer and disc. However this occurrence was not taken into consideration during FE (Finite Element) analysis when searching for the natural frequencies because such small stress locations should not



influence the overall structure significantly (see next chapter). Damping was also not included in the analysis.

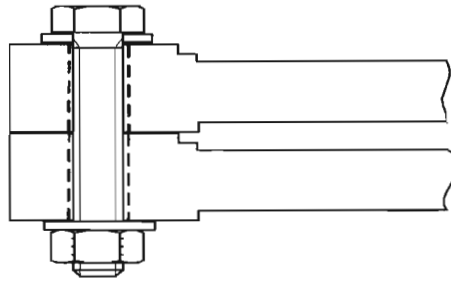


*Fig.4.1 Cross-Sectional Area of Preload Region.*

## 4.5 Modelling of The Rotor

### Discussion of the geometry and physical properties

**Model:** The contact surfaces were modelled as a solid. No provision was made for the bolts. Solid modelling was used to generate a 2 - D model of half of the cross-section of the rotor on the x-axis (*Figure 4.2*). A reasonable mesh was revolved  $360^\circ$  into a 3 - D solid model which was automatically meshed (*Figure 4.5*).

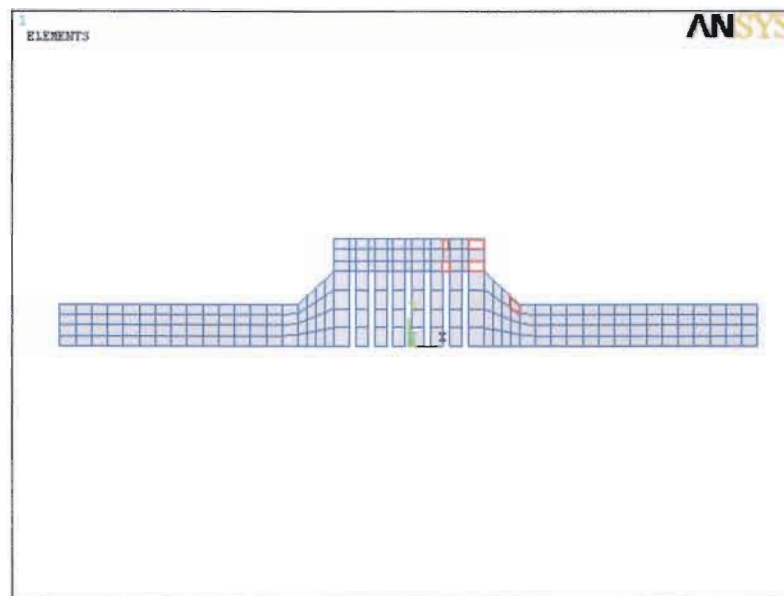


*Fig.4.2 Cross-Section Area of Rotor (Eight discs).*

Elements in the axial centre of the shaft have a poor aspect ratio. The solid model starts with a prism element in the centre of the shaft which transmits to cubic elements further from the centre to the outside where the aspect ratio improves in the critical zone. The mesh used in this analysis was fairly coarse for the element types used due to computer limitations. The aspect ratio of the surface elements is shown in Figure 4.4.

Five elements were examined in critical areas (Figure 4.3). This was performed by computing shape parameters (functions of geometry) then comparing them to element shape default values (Table 4.2). Some shape testing of 3 - Dimensional solid elements was performed indirectly. Aspect ratio, parallel deviation, and maximum corner angle were computed for 3- Dimensional solid elements using the following steps:

1. Each of these three quantities was computed, as applicable, for each face of the element as though it were a quadrilateral or triangle in 3- Dimensional space.
2. Because some types of 3 - Dimensional solid element distortion cannot be revealed by examination of the faces, cross-sections through the solid were constructed. Then, each of the 3 quantities was computed, as applicable, for each cross-section as though it were a quadrilateral or triangle in 3 - Dimensional space.
3. The metric for the element was assigned as the worst value computed for any face or cross-section.

A brick element which was used, has six quadrilateral faces and three quadrilateral cross-sections and the cross-sections are connected to mid-side nodes. The shape checking test results (Table 4.2) show that all the elements were in good shape. The dimensions of five selected elements in critical area from Figure 4.2 and 4.3. are shown in Table 4.1.

**Table 4.1 : Element Dimensions of Five Selected Elements from Figure 4.3.**

Element	L (meter)	t (meter)	h (meter)
3272	0.014	0.033	0.00975
3232	0.014	0.02137	0.00975
3260	0.006	0.03712	0.00975
3220	0.006	0.02937	0.00975
2404	0.008	0.01717	0.0081

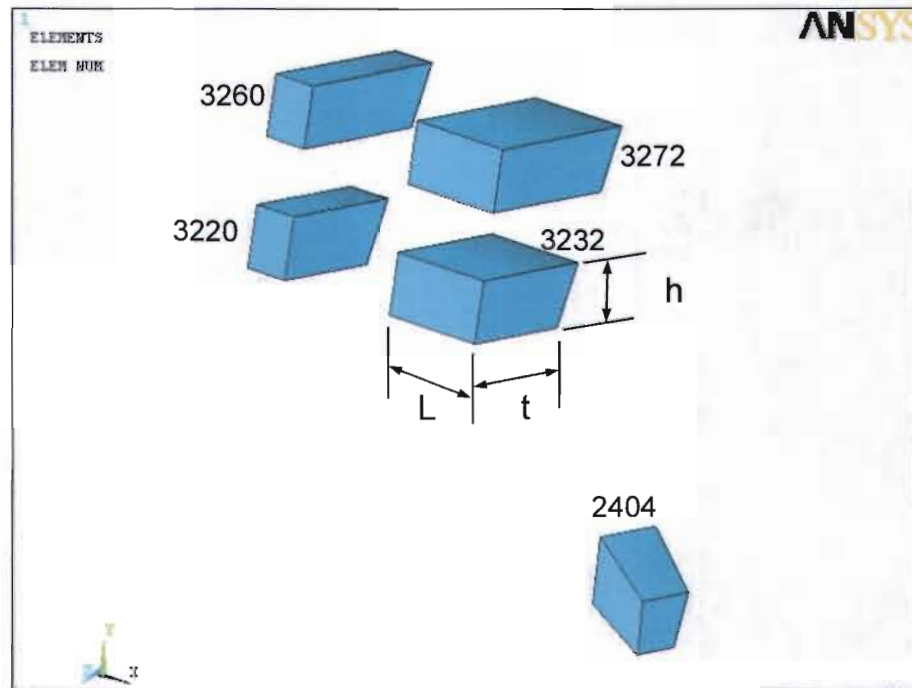


Fig.4.3 Five Numbered Selected Elements in Critical Areas.

**Table 4.2 : Shape Checking Tests of Five Selected Elements**

Test	Warning count	Error count	default	Warning+ Error %
Aspect ratio	0	0	20	0.00 %
Parallel Deviation	0	0	100°	0.00 %
Maximum Angle	0	0	165°	0.00 %
Jacobian Ratio	0	0	30	0.00 %
Warping Factor	0	0	0.2*	0.00 %

### Constraints

No constraints were assumed during modal analysis. Free – free support were assumed.

\* 22.5° rotation of top face of element.

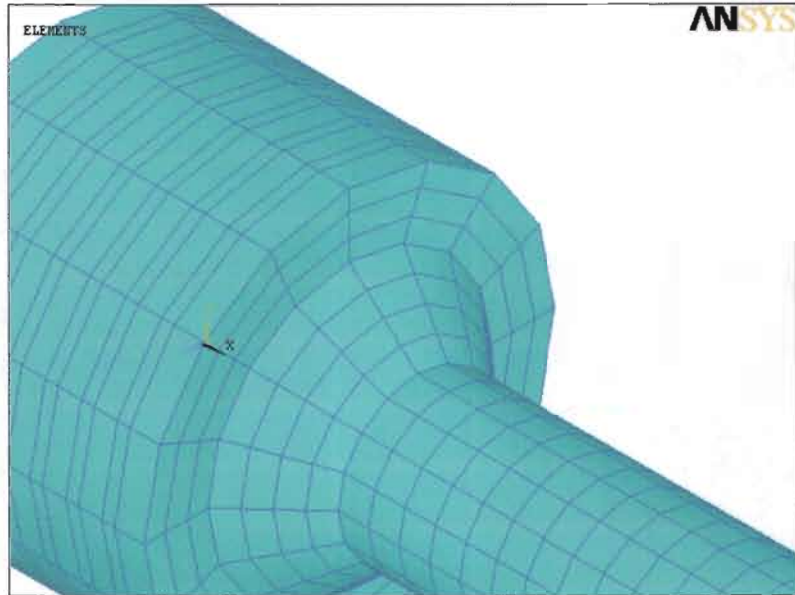


*Fig.4.4 Close-up of a 3 - Dimensional Solid Model revolved 360° (Eight discs).*

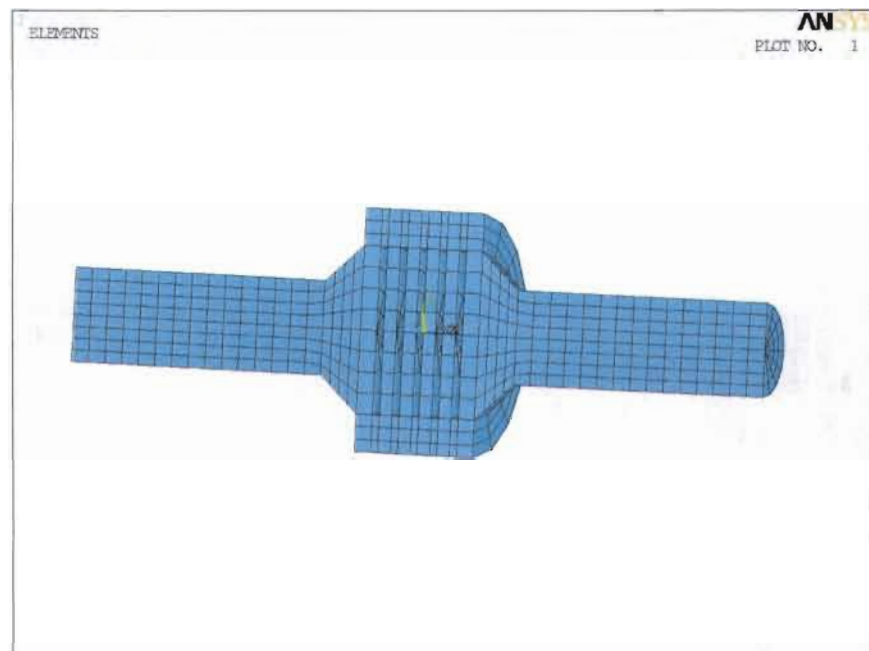


*Fig. 4.5 Cross - Sectional area of Rotor with of Six Discs meshed with Brick Elements during Modal Analysis illustrating the openings of Discs.*

**Element type : Solid95 (ANSYS)**

This is a higher order solid element which can tolerate irregular shapes without great loss of accuracy. The element has compatible displacement shapes and is well suited to model curved boundaries.

The element is defined by 20 nodes having three degrees of freedom per node: translated in the nodal x, y, and z directions. The element may have spatial orientation. It also has plasticity, creep, stress stiffening, large deflection, and large strain capabilities.

**Table 4.3:** *Number of elements for different disc configurations.*

<b>Rotor Configuration</b>	<b>Number of Elements</b>
Two discs	2704
Four discs	3024
Six discs	3344
Eight discs	3664

**Mechanical Properties:**  $E = 200e9 \text{ Pa}$  ;

$\rho = 7800 \text{ kg/m}^3$ ;

$\nu = 0.3$

Mild Steel Yield Stress = 310 MPa (Rotor-Disc Material) (Thornton, 1985)

Shear modulus is determined by the software using  $E$  and  $\nu$  .

#### **Algorithm used during Modal analysis :** Block Lanczos

The Block Lanczos method is used for large symmetric eigenvalue problems which internally uses a QL algorithm and uses the sparse matrix solver. This method is recommended when the model consists of poorly shaped solid elements. It achieves a faster convergence rate than other similar methods. It is especially powerful when searching for eigen-frequencies in a given part of the eigenvalue spectrum.

This method allows inputs for the beginning (lower end), and the ending (upper end), of the frequency range of interest. Multiple shift points are used. The lower input end represents the first shift point for the eigen-value iterations and increase in magnitude. A block shifted Lanczos algorithm is the theoretical basis of the eigen solver. The method used by the modal analysis employs an automated shift strategy, combined with Sturm sequence checks, to extract the number of eigen-values requested. The Sturm sequence check also ensures that the requested number of eigen frequencies beyond the user supplied shift frequency are found without missing any modes.



This method requires a significant amount of computer memory for solving large models (100,000 Degrees of freedom, for example) with many constraint equations. The Lagrange Multiplier approach is implemented to treat constraint equations in the Block Lanczos eigensolver. This method's algorithm is a variation of the classical Lanczos algorithm.

The sparse direct solver is based on a direct elimination of equations, as opposed to iterative solvers, where the solution is obtained through an iterative process that successively refines an initial guess to a solution that is within an acceptable tolerance of the exact solution. Direct elimination requires the factorization of an initial very sparse linear system of equations into a lower triangular matrix followed by forward and backward substitution using these triangular systems. The lower triangular matrix factors are typically much larger than the initial assembled sparse matrix.

## 4.6 Important Frequencies in the Structure

The first three transverse modes are important frequencies in the structure.

## 4.7 Natural Frequency Results

The results of the solid finite element analysis for a different number of discs are specified in Table 4.4, together with the mass computed by software. The first three transverse mode shapes provided by the software are illustrated in Figure 4.6a, 6b and 6c below. Results of the FEM were compared with the corresponding experimental results in Chapter 5.

**Table 4.4:** Results of Natural frequencies of FE Solid Model for different number of discs.

No. of discs	FE Mass of Rotor (kg)	Mode 1 (Hz)	Mode 2 (Hz)	Mode 3 (Hz)
2	26.39	1084	2486	4835
4	32.91	1013	2117	4620
6	39.428	973	1869	4500
8	45.947	947	1689	4386

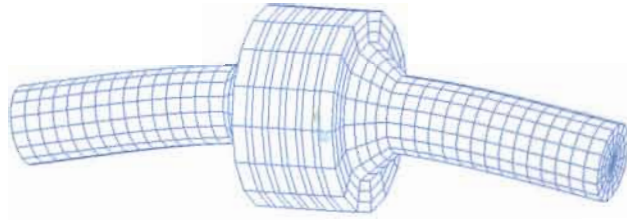


*Fig.4.6a Meshed Solid Model, Transverse Mode shape One , Six Discs.*

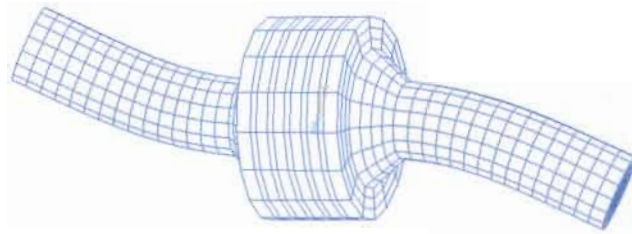


*Fig.4.6b Meshed Solid Model, Transverse Mode shape Two , Six Discs.*

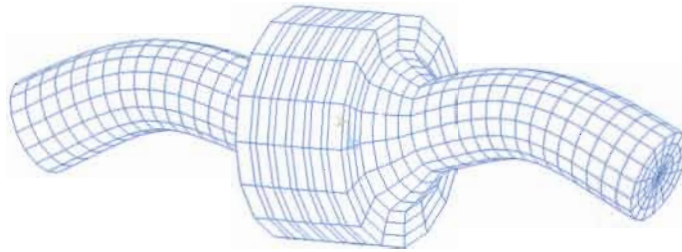


*Fig.4.6c Meshed Solid Model, Transverse Mode shape Three, Six Discs.*

## 4.8 Discussion of Mode Shapes

Due to the geometry of the rotor, it is necessary to examine the strain distribution during each mode. Each mode shape relates to its corresponding modal frequency through the weight and stiffness as constrained in an analysis. The more weight, or inertia, the harder it is to change directions when fluctuating. The natural frequency of a part will increase when adding more constraints, thus the location of the constraints is equally important. The appropriate combination of increased stiffness, weight, and redistributed weight is required to fine tune the natural frequencies of a structure. The frequency is, therefore, defined by two fundamental parameters, mass ( $m$ ) and rigidity ( $k$ ), or springback.

Another way of looking at this, is that the first mode shape is the shape with the least strain energy. The second and third mode shapes require more energy to generate and therefore obtain higher strain energies. Modal strain energy is a useful quantity in identifying candidate elements for design changes to eliminate problem frequencies. These areas (elements) are those which most directly affect the nature of a certain mode.

The locations of the strain intensity for the three modes for a six disc rotor of the first three transverse mode shapes are shown in Figure 4.7- 4.9 (The bolts and the preloads were not modelled for simplicity).

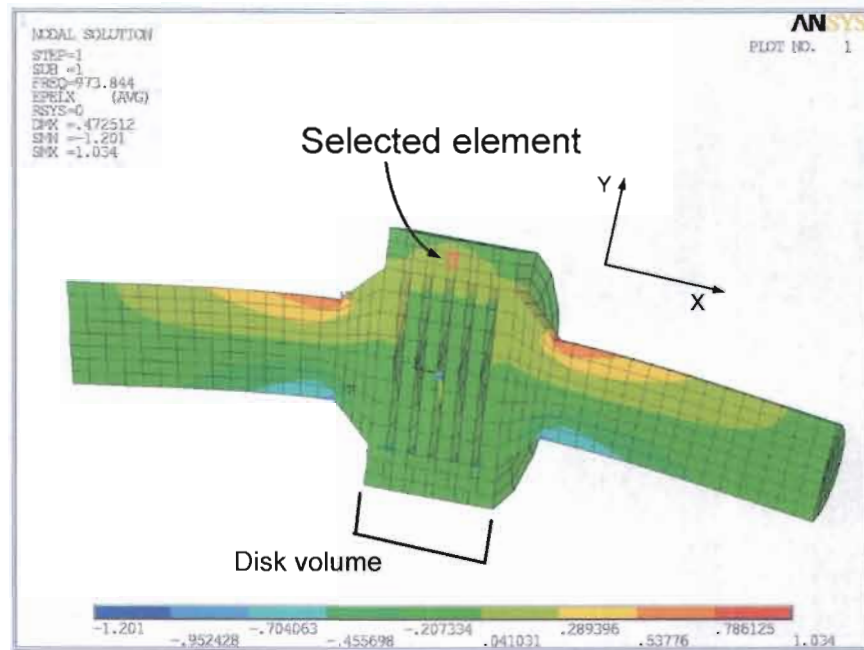


*Fig.4.7 Cross-Sectional Cut of the Elastic Strain Plot along the Axial - direction.  
(Six Discs, No Preload, Mode One. Selected element under tensile : 0.069 strain)*

An element is shown in Figure 4.7 to illustrate the level of strain in the disc-volume during each mode, in the x-direction, the axial direction. During the low frequencies (first two modes) there was very low strain activity in the selected area. Only during mode three did significant strain activity take place in the potential preload zone. The tensile strain in the x-direction for the selected element was 0.069,  $0.120 \times 10^{-10}$  and 0.448 mm/mm for mode one, two and three respectively.

This large bending deformation which occurred in the disc-volume during mode three, and may have caused the significant changes of natural frequency if this is interpreted from the perspective of Adams (1998) who said: "Changing the properties of these elements with large strain energy should have more effect on the natural frequencies and mode shapes than if elements with low strain energy were changed".

The Timoshenko beam theory states that plane sections remain plane for beam elements. In Figure 4.9 the distortion of certain areas of the disc – volume in the axial direction is visible, which make it impossible for this element to model the behaviour correct (Kumar,1995).

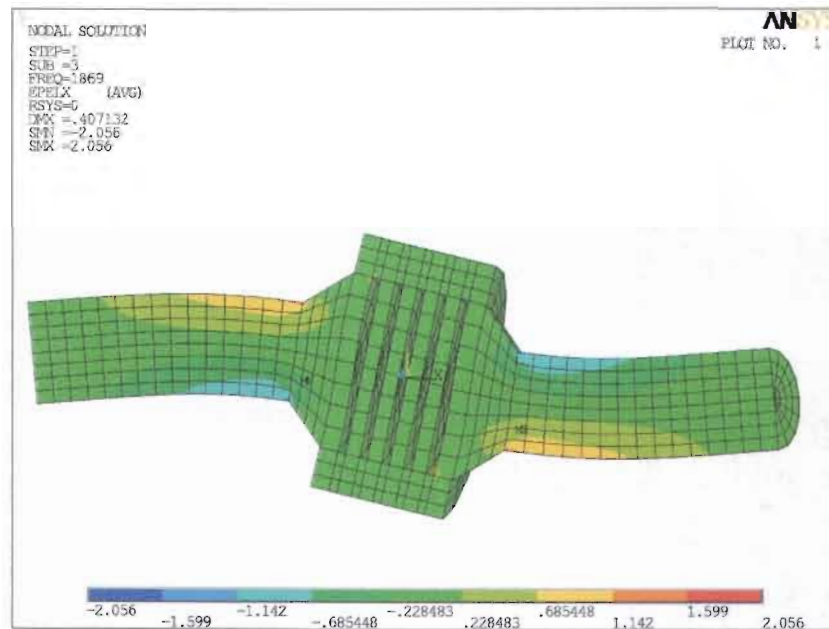


Fig.4.8 Cross-Sectional Cut of the Elastic Strain Plot along the Axial - direction.  
 (Six Discs, No Preload, Mode Two)

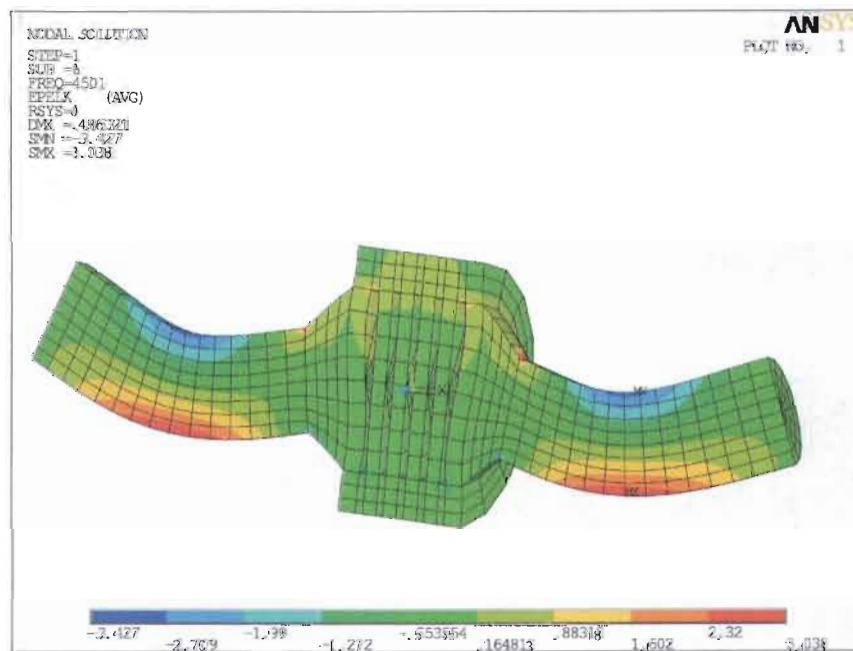


Fig.4.9 Cross-Sectional Cut of the Elastic Strain Plot along the Axial - direction.  
 (Six Discs, No Preload, Mode Three)



To summarise this event, the discs-volume acted as a very stiff spring. In mode three the disc-volume deformed significantly more compared to mode one and two. In this same modes the springback effect make use of the stiffening caused by the pre-tension bolts.

## 4.9 Synthesis

The bending stiffness of a beam is characterised by its cross-sectional moment of inertia  $I$ , and its weight, which is characterised by the cross-sectional area  $A$ . This implies that there is enormous difference in stiffness between discs, cone and hub. The fewer the number of discs, the more the disc volume acts like a rigid mass.

It is always essential to exploit elements with a suitable aspect ratio and refinement in the critical zone. Unfortunately this led to a model with large number of degrees of freedom in this project.

Despite of the generalisation of the FE model (that is: the stiffness of the bolt material, contact assumptions, the mass of the nuts and transducers which were not included, which present an assembled rotor with 12 bolts ), it provided relatively accurate results compared to the experimental model presented in Chapter 3.

**It can be concluded that:** A solid element model, with no contact elements between discs faces, with the same stiffness as the primer structure, and no preload, can be exploited to predict the natural response, allowing for a 3% tolerance on both sides.

In the next chapter, factors which contribute to a possible change in resultant behaviour, like pretension, slenderness and stiffening will be examined in more detail, as well as the verification of the analytical model.

## DISCUSSION

### 5.1 Background

In this chapter the differences and similarities between the experimental results and the valid analytical model are discussed and evaluated.

The most accepted treatment of modal testing is to present a comparison between prediction and measurement of the dynamic behaviour by using the Analytical model and Experimental results. There are different levels of accuracy, the ones that are used here are:

- The natural frequencies should correspond.
- The two models should have similar mode shapes.

The problematic areas that are associated with an analytical model, are:

- Approximation of boundary conditions.
- Discretisation of distributed parameters.
- Estimation of the physical properties of structural materials.
- Inadequate modelling of joints.

And there are potential problems relevant to model reconciliation, including:

- The limited number of mode shapes.
- Complex shapes obtained.
- Unmodelled errors in measurement (noise, nonlinearity etc.)
- Poor modal analysis of the experimental results.

There are a few aspects which should be addressed before advancing to the verification. There are the stiffness, axial preload, and the bolt flange interaction, which are fundamental to the modelling, and necessary when comparing the experimental - and analytical model.

The bolt-flange interaction, which is the focal area, can be regarded as two sub components. The bolt is in tension and the disc volume material surrounding the bolt in compression. During the preload process, the load is transferred from the bolts to the flange material. The contact area is the effective region where the energy is transferred from one component to another. Both the bolt and the disc component will deform to reach an equilibrium configuration that is generally unknown beforehand, so it

is extremely difficult to make an educated guess how large this penetration and deformation will be. Extreme stress concentrations are induced in the threads of the bolt and nut which represent only a small volume in comparison with the overall volume of the test piece. These high stress concentrations are isolated from the bending deformation path. A segment of the disc (*Figure 5.1*) will be examined below to explore the stresses induced between bolt and disc and the possible influence of this induced strain.

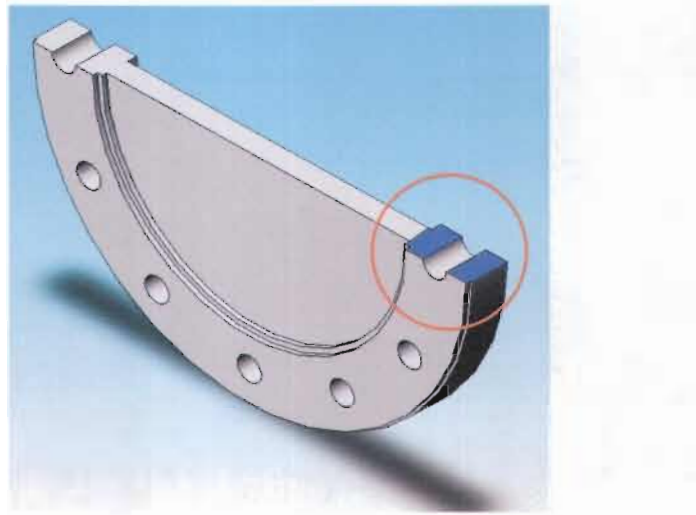


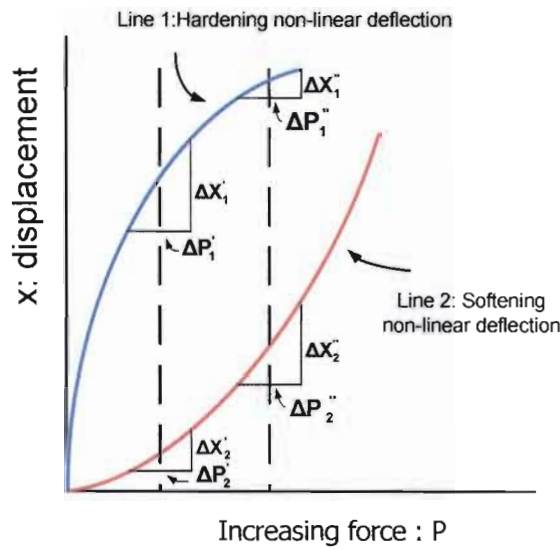
*Fig.5.1 Cross-Sectional Area of Disc.*

*The Circled Area is the Finite Element Analysis Focal Area.*

## **5.2 Stiffness Characterisation**

Structural stiffness is characterised by its elastic modulus  $E$  for tension and compression. In practice, only the two or three of the lowest natural frequencies and modes are important. When the lowest natural frequencies have to be modified, it is important to know which stiffness and inertia components of the structure influence the frequencies and modes of interest to a considerably extent and which ones do not.

Stiffness is the ratio of the force to the displacement caused by the force. Most materials will exhibit a change in modulus before inelastic or plastic behaviour is exposed. There are two types of non-linear load-deflection characteristics, namely; hardening and softening (*Figure 5.2*).



$$\Delta X_1' > \Delta X_1''$$

$$\text{then } K_1' < K_1''$$

$$\Delta P_2' = \Delta P_2'' \text{ and}$$

$$\Delta X_2' > \Delta X_2'' \text{ then}$$

$$K_2' > K_2''$$

$$\Delta P_1' = \Delta P_1''$$

$$\Delta X_1' > \Delta X_1''$$

$$\text{then } K_1' < K_1''$$

Fig.5.2 Hardening and Softening Nonlinear Load Deflections Characteristics.

This diagram represents the stiffness change during an increasing load.

Both types of non-linear load-deflection characteristics allow the actual stiffness to be varied by moving the working point along the characteristic line. This can be achieved by applying a constant preload force that is independent from the actual working load on the system. Line one represents the case when the rate of increase of deflection  $x$  slows down with increasing force  $P$ . If the local (differential) stiffness is defined as the ratio between increments of force  $dP$  and deflection  $dx$ , then  $k = \frac{\Delta P}{\Delta x}$ . The

stiffness along line one increases with the increasing load  $k_1'' = \frac{\Delta P_1''}{\Delta x_1''} > k_1' = \frac{\Delta P_1'}{\Delta x_1'}$  and the same

for  $k_2' > k_2''$ . Line one is called the hardening load-deflection characteristic and line two is called the softening load-deflection characteristic.

In most structures, the structural stiffness depends on both a suitable combination of stiffness and distributed weight, the resultant stiffness can be manipulate using the following:

- Elastic moduli.
- Geometry of the deforming segments (cross sectional area,  $A$ , for: tension, compression, shear,
- cross sectional moment of inertia,  $I$ , for bending, and polar moment of inertia,  $J_p$ , for torsion).
- Linear dimensions (length, width, height).
- The character and magnitude of variation of the above parameters across the structure.
- The character of supporting and loading conditions.

When considering a beam or a shaft, the bending stiffness is characterised by its cross-sectional moment of inertia  $I$ , and its weight, which is related to the cross-sectional area  $A$ . Relating this to the rotor, there is a enormous difference in stiffness between discs, cone and hub.

### 5.3 Analysis of the Preload Region

If a structure experiences large deformations, its changing geometric configuration can cause the structure to respond nonlinearly. Signs of non-linear elastic behaviour will appear long before yield stress is reached, although localised yielding will probably not affect the gross behaviour of the system. As displacement becomes large, the tensile uniaxial or biaxial fields in a material start to induce resistance to further deformation. Therefore, the component stiffens over and above the material properties and as a result, alter the final structural behaviour.

A static finite Element Analysis (FEA) is done to examine the stress distribution in the critical zone (*Figure 5.4*). This is done to examine the magnitude and distribution of strain in this portion. The area surrounding the bolt is modelled (*Figure 5.3*).

A tensile force of 30300 N in the bolt generates a pressure of

$$\sigma = \frac{F}{A} \quad (5.1)$$

= 123.22 MPa exerted on the disc face by each washer.

Contact elements are utilized in this analysis between bolt and washer and between washer and disc to generate a realistic analysis. Note, that when contact elements are involved, the analysis become non-linear. *Figure 5.3* is a schematic description of the analysis. For simplicity all the components are assumed to have the same Young's Modulus ( $E = 200 \times 10^9$  Pa) throughout the analysis.

The volume affected by large stress is relatively small (*Figure 5.4*). The contact pressure plot,

*Figure 5.5*, is an Axial symmetric Contact Area Pressure plot and is included to illustrate the reliability of the analysis and as well the non-linear distribution of stress in the bolt connection. Three elements are selected in *Figure 5.4* to demonstrate the decay in stress from the centre when a preload of 30300 N is modelled in the bolt. The pressure at Node 497 (*Figure 5.5*), in the centre, corresponds with the pressure initiated by the bolt (*Equation 5.1*).



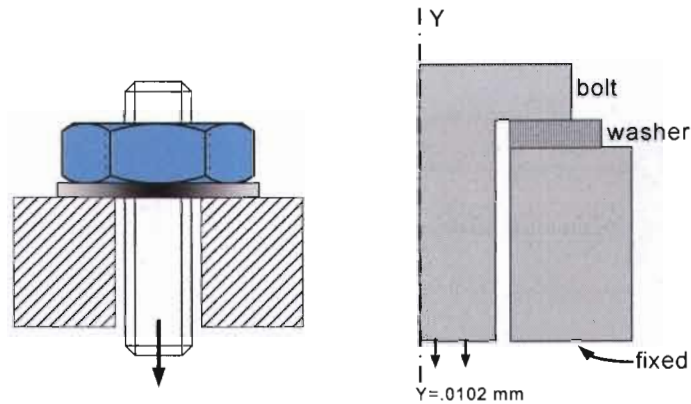


Fig.5.3a and 5.3b Axi-Symmetric Cut of Bolt, Disc and Washer.

Initial displacement of bolt =  $0.102 \times 10^{-4}$  m (equivalent to preload~ 30300 N).

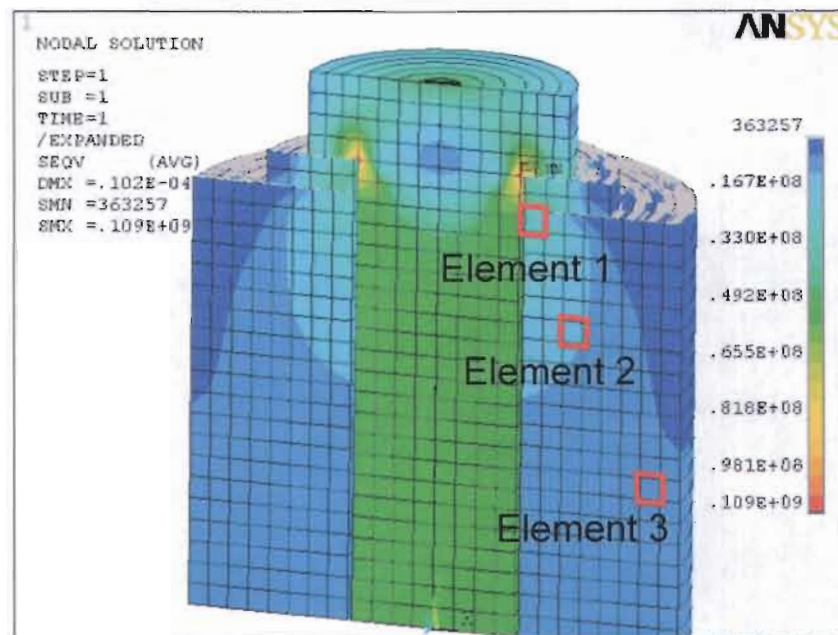


Fig.5.4 Axi-Symmetric Von Misses Stress Plot.

Initial displacement of bolt =  $0.102 \times 10^{-4}$  m (equivalent to preload~ 30300 N)

Contact Elements between Bolt, Washer and Disc. Friction  $\mu = 0.2$  between components.

VonMises stress element 1:  $23.8 \times 10^6$  Pa;

VonMises stress element 2:  $12.9 \times 10^6$  Pa;

VonMises stress element 3:  $6.4 \times 10^6$  Pa

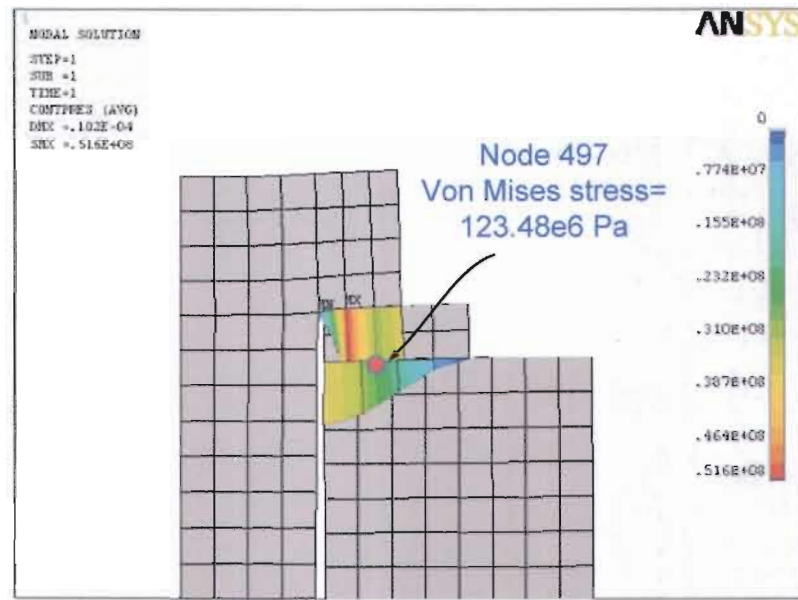


*Fig.5.5 Axi-Symmetric Area Contact Pressure plot.*

*Initial displacement of bolt =  $0.102 \times 10^{-4}$  m (equivalent to preload~ 30300 N).*

*Contact Elements between Bolt, washer and Flange.*

*Mild steel Yield Stress = 310 MPa (Thornton, 1985)*

Little (1967) provided evidence, that the clamping stiffness has been overestimated in the past. The finite element analysis above verifies that he is indeed correct, when considering the small high stress volume. Furthermore, the volume of this high stress region is relatively small compared to the rest of the stress distribution. Stress in the outer region, element three, is 3.7 times smaller than the stress immediately below the washer. It is the bolt which largely experiences extreme stress.

Hammed (2005) refers to 'compression softening' as an effect due to axial compressive preload on a composite beam. Similar conditions are appropriate between the discs of the rotor. This might contribute to a decrease of stiffness.

The contact surfaces respectively between washer and disc and mutually between discs, can be characterized by non-linear hardening due to the increase of effective contact area with an increased load. This might contribute to an increase of stiffness with the effect of an increase in natural frequency, of which the quantity is unknown at this stage.

The pressure cone volume is restricted by the geometry of the disc, namely the web, where there are hardly any stresses induced in the web section of the disc.

The next section examines the overall effect of axial preload applied on sections of the rotor.

## 5.4 Effect of Axial Force

The formula

$$\omega_n = \frac{\pi^2}{l^2} \sqrt{\frac{EI}{\rho A}} \left[ n^4 + \frac{n^2 P l^2}{\pi^2 EI} \right]^{\frac{1}{2}} \quad (5.2)$$

where  $n$  is the mode shape, provides a solution for a simply supported beam subjected to axial forces. The following observation can be made from the above formula: When a tensile force  $P (> 0)$ , is applied to a beam, the beam stiffens and the natural frequency increases. If  $EI = 0$ , the natural frequency reduces to that of a taut string. If this formula is simplified with the dimensions of a shaft it results in:

$$\omega_n = \frac{\pi^2}{l} \left( \frac{r}{2L} \right) \sqrt{\frac{E}{\rho}} \left[ n^4 + \frac{n^2 P l^2}{\pi^2 EI} \right]^{\frac{1}{2}} \quad (5.3)$$

Again factors like slenderness  $\left( \frac{r}{2L} \right)$  and the ratio  $\frac{E}{\rho}$  come forward as parameters that influence  $\omega_n$ .

(Please note that some authors present the slenderness in a different terminology). Table 5.1 contains the solutions of equation 5.3 when using only the disc-ring face section of the disc (*Figure 5.6*) to illustrate the affect of slenderness and preload, when applying the sum of the force of 12 bolts, for the assembling of four and eight discs respectively. The web section and bolts are ignored at this point to simplify and to illustrate the effect of slenderness and preload only on the disc-ring.

The moment of inertia of disc-ring (*Figure 5.6*) :  $I_x = \frac{\pi}{64} (D_{out}^4 - D_{in}^4)$

From Table 5.1, where it is assumed that the total force is applied on the entire disc-ring face, the change in natural frequency for eight discs is larger when increasing the compressive preload. On the actual rotor, the applied forces are much more concentrated. This is done to show how minute the change in natural frequency is due to an applied pressure and a constant Young's moduli, according to the formula.

**Table 5.1 :** Natural Frequencies from Equation (5.3) illustrating the effect of slenderness, when  $\rho = 7800$ ;  $E = 200 \times 10^9$ ;  $n = 1$ .

Compressive Preload P	Mode1 Length = 0.086 m; (Four discs) mean radius = 0.083 m $\frac{2L}{r} = 2.07$	% Decrease in natural Frequency $\frac{\omega_i - \omega_0}{\omega_0} \times 100$	Mode1 Length = 0.136 m; (Eight discs) mean radius = 0.083 m $\frac{2L}{r} = 3.277$	% Decrease in natural Frequency $\frac{\omega_i - \omega_0}{\omega_0} \times 100$
0	645292.3860 Hz	0	161323.0965 Hz	0
240 kN	645284.6710 Hz	0.001196	161319.2390 Hz	0.00239
264 kN	645283.8995 Hz	0.001315	161318.8532 Hz	0.00263
282 kN	645283.1281 Hz	0.001435	161318.4675 Hz	0.00869
312 kN	645282.3566 Hz	0.001554	161318.0817 Hz	0.003108
336 kN	645281.5851 Hz	0.001674	161317.6960 Hz	0.003348
360 kN	645280.8136 Hz	0.001793	161317.3103 Hz	0.003587
384 kN	645280.0421 Hz	0.001913	161316.9245 Hz	0.003826
408 kN	645279.2706 Hz	0.002032	161316.5388 Hz	0.004065

#### 5.4.1 Cross-Sectional Moment of Inertia

According to Rivin (1999), the strength and stiffness of a circular composite beam in bending are determined by the external tubular member, due to the cross-sectional moment of inertia. The external member contributes 85 - 90% to the total stiffness where as the internal member contributes 10 - 15%.

When considering the rotor, the position of the bolts on the disc cross-sectional area is 0.0835 m from the shaft centre where the outer radius of the discs is 0.0975 m.

When considering only the disc face (Figure 5.6), the moment of Inertia of the bolts in their respective positions is:

$$I_x = I_x + Ad_y^2 \quad (5.4)$$

Where

$I_x$  = Moment of Inertia about the x - axis.

A = Cross-sectional area of each bolt.

$d_y^2$  = The parallel y distance of A from x - axis.

$D_{\text{bolt}}$  = 10 mm (diameter of bolt)

$R_{\text{Bc}}$  = 0.0835 mm (Bolt centre from shaft centre)

$$I_{x12bolts} = 12 \frac{\pi}{64} D_{bolt}^4 + \pi \left( \frac{D_{bolt}}{2} \right)^2 R_{Bc} \left[ 4 \left( \left( \sin \left( 30 \frac{\pi}{180} \right) \right)^2 + \left( \sin \left( 60 \frac{\pi}{180} \right) \right)^2 \right) \dots \right. \\ \left. + 2 \left( \left( \cos \left( 30 \frac{\pi}{180} \right) \right)^2 + \left( \cos \left( 60 \frac{\pi}{180} \right) \right)^2 \right) \right] \quad (5.5)$$

$$I_{x12bolts} = 3.22104 \times 10^{-6} \text{ m}^4$$

The moment of Inertia of the disc-ring is (Figure 5.6):

$$I_x = \frac{\pi}{64} (D_{out}^4 - D_{in}^4) \quad (5.6)$$

$$D_{out} = 0.197 \text{ m}$$

$$D_{in} = 0.135 \text{ m}$$

$$I_x = 5.763 \times 10^{-5} \text{ m}^4$$

Then finally the moment of Inertia of the disc-ring with 12 bolt holes is (Figure 5.6):

$$I_{dr} = I_x - I_{x12bolts} \quad (5.7)$$

$$I_{dr} = 5.4 \times 10^{-5} \text{ m}^4$$

Comparing the inertia ratio of the 12 bolts ( $I_{x12bolts}$ ) and the inertia of the disc ring ( $I_{dr}$ ) with the total inertia we have

$$\frac{I_{x12bolts}}{I_x} (100) = 6.298\% \quad \frac{I_{dr}}{I_x} (100) = 93.702\% \quad (5.8)$$

The ratios above give a robust indication of the contribution of both materials to the overall stiffness of the disc-volume in a no-preload state, based on the statement of Rivin (1999). More about this is discussed in Section 5.4.2.

A similar solid FE model, with free-free support, Figure 5.7 is created to explore whether the stiffness are determined by the external tabular member of a composite beam in bending, as proposed by Rivin (1999). The transverse natural frequencies for this complete component are determined after preloading. Tension and compression stresses are respectively generated in the external tabular member through thermal contraction and expansion in the internal core. The two substructures are interconnected through equilibrium with extremely stiff discs on the faces ( $E = 250 \times 10^9 \text{ N/m}^2$ ). Table 5.2 reveals the change in natural frequency. The stress state of the external member, which has the largest mass as well as Inertia, dominates the natural response. A more detailed FE model subjected to preload, presenting the disc-volume, follow in section 5.4.3.



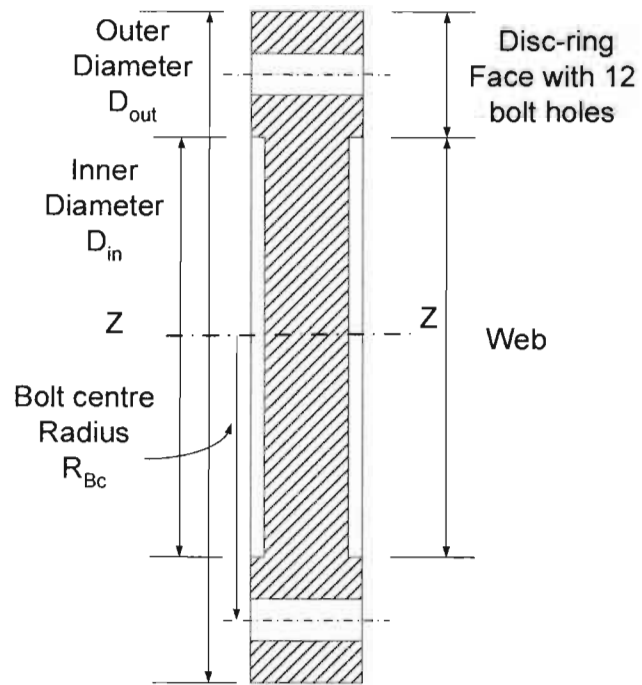


Fig. 5.6 Cross-section Cut of Disc.

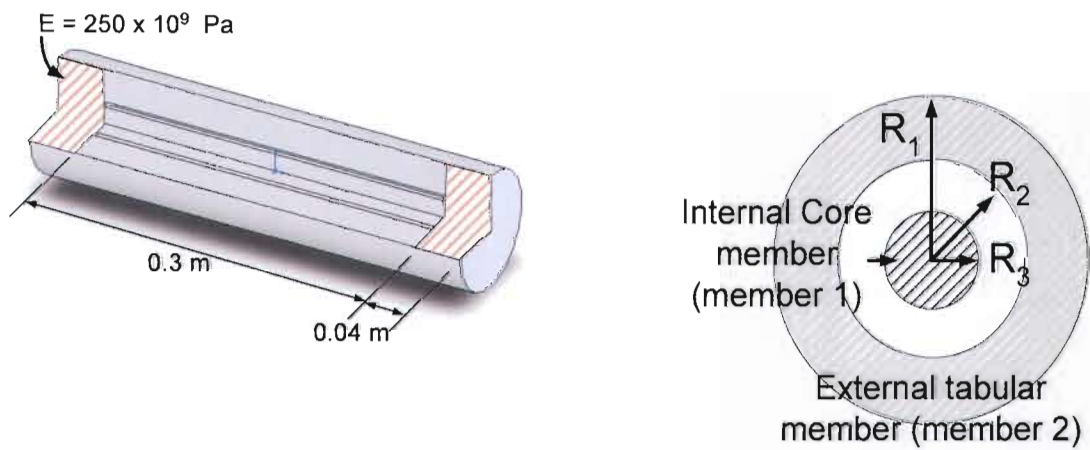


Fig.5.7 a, 3D view and b , Cross-Section of Component.

$$R_1 = 0.05 \text{ m}$$

$$R_2 = 0.02 \text{ m}$$

$$R_3 = 0.015 \text{ m}$$

$$\rho = 7800 \text{ kg/m}^3$$

**Table 5.2:** Natural Frequencies of Compound Component Figure 5.7, Free-Free support.

	No preload		Member 1 in Tension		Member 1 in Compression	
	Member1	Member2	Member1	Member2	Member1	Member2
$T_{ref}$	0	0	20°C	0	20°C	0
$T_{appl}$	0	0	15°C	0	25°C	0
Stress $\sigma_x$ (Pa)	0	0	$0.118 \times 10^9$	$-0.126 \times 10^8$	$-0.118 \times 10^9$	$0.126 \times 10^8$
E (Pa)	$200 \times 10^9$	$200 \times 10^9$	$200 \times 10^9$	$200 \times 10^9$	$200 \times 10^9$	$200 \times 10^9$
I (m <sup>4</sup> )	$3.976 \times 10^{-8}$	$4.909 \times 10^{-6}$	$3.976 \times 10^{-8}$	$4.909 \times 10^{-6}$	$3.976 \times 10^{-8}$	$4.909 \times 10^{-6}$
Mode 1	2707.1 Hz		2707 Hz		2709.2 Hz	
Mode 2	6121.1 Hz		6119.8 Hz		6122.3 Hz	

#### 5.4.2 Geometric Stiffening.

Geometric stiffening (or stress stiffening) results when deformation increases. This is the stiffening of a structure due to the state of stress and the stiffening over and above the inherent stiffness of resulting the component material properties.

As the axial tensile stress in a beam rises, the physical part of the beam will self-stiffen. This is called stress-stiffening. According to Adams (1998) it is a straightforward process to estimate the nonlinearity of a system due to material properties. But it is difficult, if not impossible, to determine whether geometric stiffening will affect the system.

Rivin (1990) presented a formula which defines the stiffening effect of an axial preloaded cylindrical member:

$$\zeta = 4 \frac{L}{D} \sqrt{\frac{\sigma_T}{E}} = 4 \frac{L}{D} \sqrt{\epsilon_T} \quad (5.9)$$

Where

$\zeta$  : Stiffening factor.

$\sigma_T$  : Tensile stress from the tensile force.

$\epsilon_T$  : Relative elongation caused by tensile force.

D : Diameter of member.

L : Length of member.

Notice that in this equation, the slenderness effect appears again. Several important deductions can be made from equation (5.9) :

- A higher stiffening effect can be achieved if higher tensile stress  $\sigma_T$  or strain  $\epsilon_T$  were tolerated. The allowable tensile stress is in many cases determined by the yield stress of the beam material.
- For the same given allowable  $\sigma_T$ , the stiffness effect is more pronounced for lower modulus materials since the deflections for such materials are higher.
- The effectiveness increases linearly with the ratio  $L/D$  .

Table 5.3 illustrates the stiffness effect (Equation 5.9) of a bolt for each disc configuration of the rotor. From these data it can be seen that the stiffness factor significantly increases as the bolts becomes more slender. Where:

Nominal stress area for 10 mm bolt = 58 mm<sup>2</sup> ( $5,8 \times 10^{-5}$  m<sup>2</sup>)

$$\sigma_T = \frac{F}{A_{nominal}} \quad (5.10)$$

Modulus of bolts  $E = 215 \times 10^9$  Pa.

L = length of disc assembly.

D = Diameter of bolt.

F : Tensile Preload (N).

**Table 5.3:** Stiffening effect  $\varsigma$  per bolt for each disc-volume configuration.

Discs	L (mm)	$\frac{L}{D}$ (Bolt)	Preload: F (N)	Tensile stress in bolt : $\sigma_T$ (MPa)	Stiffening Effect In bolt: $\varsigma = 4 \frac{L}{D} \sqrt{\frac{\sigma_T}{E}}$
2	34	3.4	23 500	405.17	0.590391
			30 300	522.41	0.670389
4	68	6.8	23 500	405.17	1.180782
			30 300	522.41	1.340778
6	102	10.2	23 500	405.17	1.771173
			30 300	522.41	2.011168
8	136	13.6	23 500	405.17	2.361563
			30 300	522.41	2.681557

When considering now the rotor, the discs which have the largest inertia are in a state of compression, while the bolts, under tension, have a high stiffening effect, but a smaller inertia.

When considering only the disc-ring section (Figure 5.6) as a simply supported composite shaft without any preload, the bolt and the disc materials are in parallel with each other. The resultant stiffness ( $K_{DR}$ ) of the bolts ( $K_{bolts}$ ) and the discs ( $K_{dr}$ ) can be written as :

$$K_{DR} = K_{dr} + K_{bolts} \quad (5.11)$$

$$\frac{48E_{DR}I_{DR}}{L^3} = \frac{48E_{dr}I_{dr}}{L^3} + \frac{48E_{bolts}I_{x12bolts}}{L^3} \quad (5.12)$$

where

$$E_{dr} = 200 \times 10^9 \text{ N/m}^2$$

$$E_{bolts} = 215 \times 10^9 \text{ N/m}^2$$

$E_{DR}$  : Equivalent Modulus.

$I_{DR}$  : Equivalent Inertia.

$L$  : Length of assembled discs.

$K_{DR}$  : Equivalent stiffness.

$I_{dr}, I_{x12bolts}$  : see above

Then  $E_{DR}$  results in  $200.9 \times 10^9 \text{ N/m}^2$ .

Using this equivalent stiffness to illustrate the contribution made by the bolts :  $\left( \frac{K_{bolts}}{K_{DR}} \right) (100)$

$$\left( \frac{\left( \frac{48E_{bolts} I_{x12bolts}}{L^3} \right)}{K_{DR}} \right) (100) = 6.7\% \quad (\text{no preload}) \quad (5.13)$$

This agrees with the statement of Rivin (1999) section 5.4.1. This fraction will be even smaller if the EI value of the web section is include as well.

### 5.4.3 The stress-stiffening affect of an assembled disc-volume after pretension

A FEM is used to illustrate the effect of stress stiffening on a bolted four disc-volume.

The resulting y-displacement is determined after applying a force on the free end of the assembled discs, (Refer to Appendix E), although a fraction of the applied force (y-direction) is absorbed in the applied location by means of deformation. It will, therefore, not reflect the linear Force/Stiffness ratio, but it is adequate for illustrating the changing stiffness.

Contact areas between discs are assumed solid. The bolt-shafts are separated from the discs, except the nuts. An element in the middle of a bolt is selected to confirm the required stress (Table 5.4).

This analysis was done in two steps.

- Firstly, pre-stress was initiated in the system, using thermal contraction in the bolts,
- Secondly, a static load was applied on the nodes of six adjacent elements.

The resulting y-displacement was measured at a node in the middle of the disc face below the applied force. The nuts were modelled to the same diameter as the washer for simplicity. This enhance the effect of pre-tension from bolts to discs. The mesh below the nuts was refined with elements with a suitable aspect ratio (Appendix E).



The stress stiffness  $[S_i]$  (or geometric stiffness, utilized by the software) contribution can be written symbolically as:

$$[S_i] = \int [G_i]^T [\tau_i] [G_i] d(Vol) \quad (5.14)$$

where  $[G_i]$  is a matrix of shape function derivatives and  $[\tau_i]$  is a matrix of the Cauchy true stresses  $\{\sigma_i\}$  in the global Cartesian system.

The Preconditioned Conjugate Gradient (PCG) solver in the software was used for this analysis. Instead of factoring the global matrix, the PCG solver assembles the full global stiffness matrix and calculates the degrees of freedom solution by iterating to convergence; it is efficient and reliable for all types of analyses.

A stress plot of four discs in Figure 5.8 is included to illustrate the pre-tension effect on four discs before the static load  $F_y$  is applied. Notice again the conical stress area below the washer in the disc.

Table 5.4 presents the resulting transverse y-displacement values after applying a force  $F_y$ . The results point to an overall stress stiffening affect in the structure after axial preload. The reliability of this analysis is confirmed by the last row of data in Table 5.4 which show that the y - displacement is the largest when no preload is initiated.

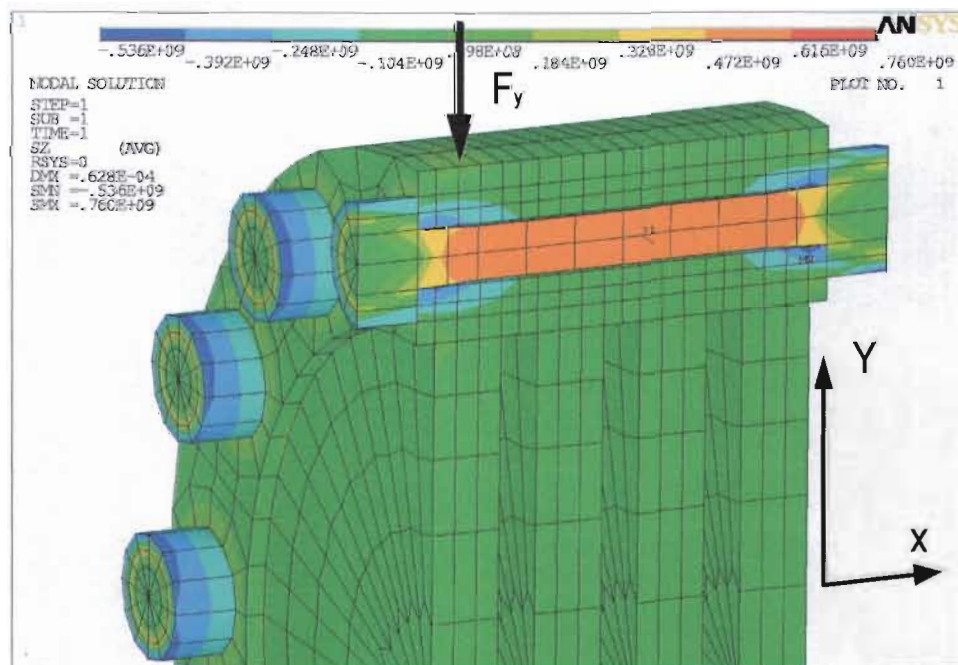


Fig.5.8 A Cross-Sectional Cut of Disc-Volume showing the Main Stresses in x - direction Plot. Stress in Bolts:  $522.4 \times 10^6$  Pa. Thermal Contraction Generates Pre-tension in Bolts before Load  $F_y$  is applied.

**Table 5.4:** *Y - Displacement.*

Force F applied at free end F = 1450 N		Displacement at node in middle of disc. (meter x10 <sup>-6</sup> )
E <sub>bolt</sub> = 215x10 <sup>9</sup> E <sub>disc</sub> = 200x10 <sup>9</sup>	90% preload in bolts $\sigma_z = 522.4 \times 10^6$ Pa	- 0.225
	70% preload in bolts $\sigma_z = 405.08 \times 10^6$ Pa	- 0.22524
E <sub>bolt</sub> = 215x10 <sup>9</sup> E <sub>disc</sub> = 200x10 <sup>9</sup>	No preload in bolts	- 0.2347

#### 5.4.4 Synthesis

The rotor disc-volume consists of two sub-components, the discs and the bolts.

The one component experiences compression softening and the other one tensile stiffening. These two sub-components are interrelated in stability, subject to a preload.

The data in Table 5.1 clearly show that the reduction in natural frequency (stiffness) of discs in pretension is insignificant for the same configurations. However the effect in change is larger when the slenderness is increased.

In contrast with the cylindrical component of Figure 5.7, the pressure of the actual rotor is not applied on the entire cross-sectional area of the discs faces, but it is localised. Stress flow is restricted by the webs of the discs. This means the strain in a large part of the disc, i.e. the web, remains very small if not zero. Stiffening in bolts is indicated by an increasing factor ( $\zeta$ ) when subjected to increasing tensile preload and slenderness. Section 5.4.2 shows that there is a significant increase in stiffness ( $\zeta$ ) when tensioning the bolts, although the bolts contribution to the resultant stiffness is relative small due to their moment of inertia.

The additional FEA of a disc assembly (Figure 5.8) indicates that the resultant behaviour leads to stiffening. The resulting stiffness of the disc-volume is a combination of the bolt stiffnesses in series which are in parallel with the stiffness of the discs. Since the moment of inertia of a round beam is proportional to the fourth power of its diameter, the location and the stiffening affect of the bolt elements contributes a measurable fraction towards the global stiffness of the disc-volume during bending, larger than the minute reduction in stiffness of the discs due to their state of compression.

## 5.5 Slenderness of Structure

The importance of slenderness is shown by the formulas in the previous sections.

The bar graphs below (Figure 5.9), where the frequency of each configuration is plotted against mode shape, demonstrates the slenderness effect,  $r = \frac{2L}{R}$ . (5.15)

where

R: Radius of disc.

L: Disc length.

It is noticeable that the more slender the disc-volume becomes, the more perceptible the effect of preload turns out to be. The slenderness ratios depicted in the graphs in Figure 5.10 - 5.12 are expressed as a function only of the disc-volume. The FEA results were taken from Chapter 4.

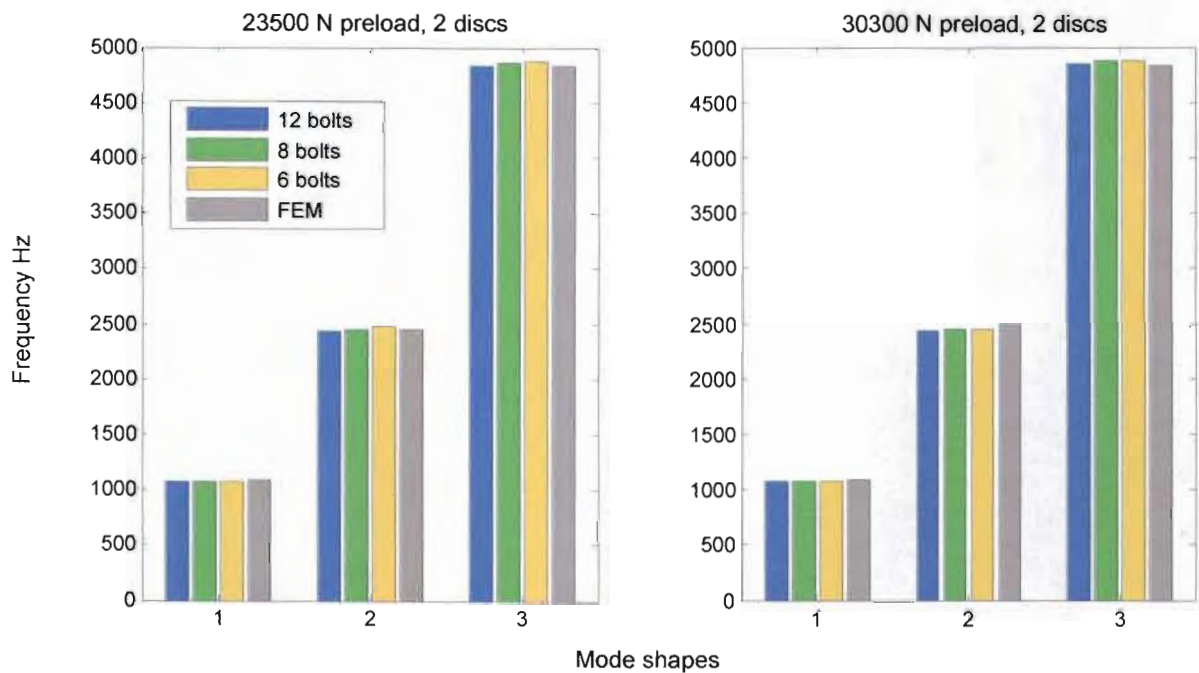


Fig.5.9 Bar Graphs comparing Different Number of Bolts for each Mode Shapes, for Two Disc Assembly.  
Slenderness Ratio of Two Discs = 0.348

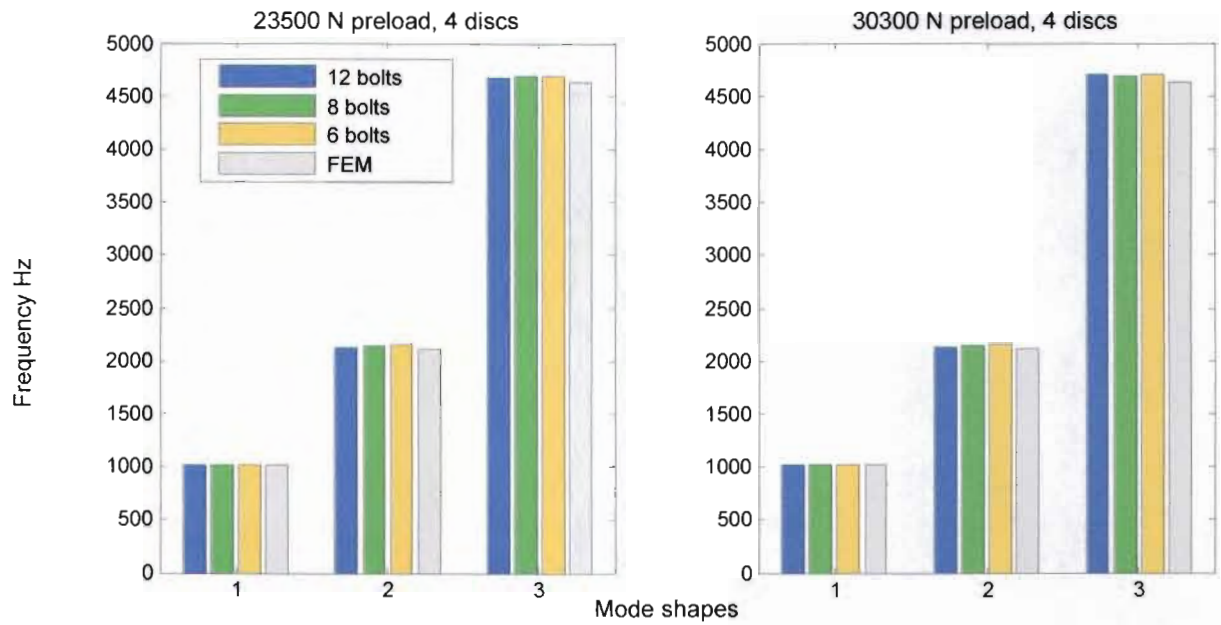


Fig.5.10 Bar Graphs comparing Different Number of Bolts for each Mode Shapes, for Four Disc Assembly.  
Slenderness Ratio Four Discs = 0.697

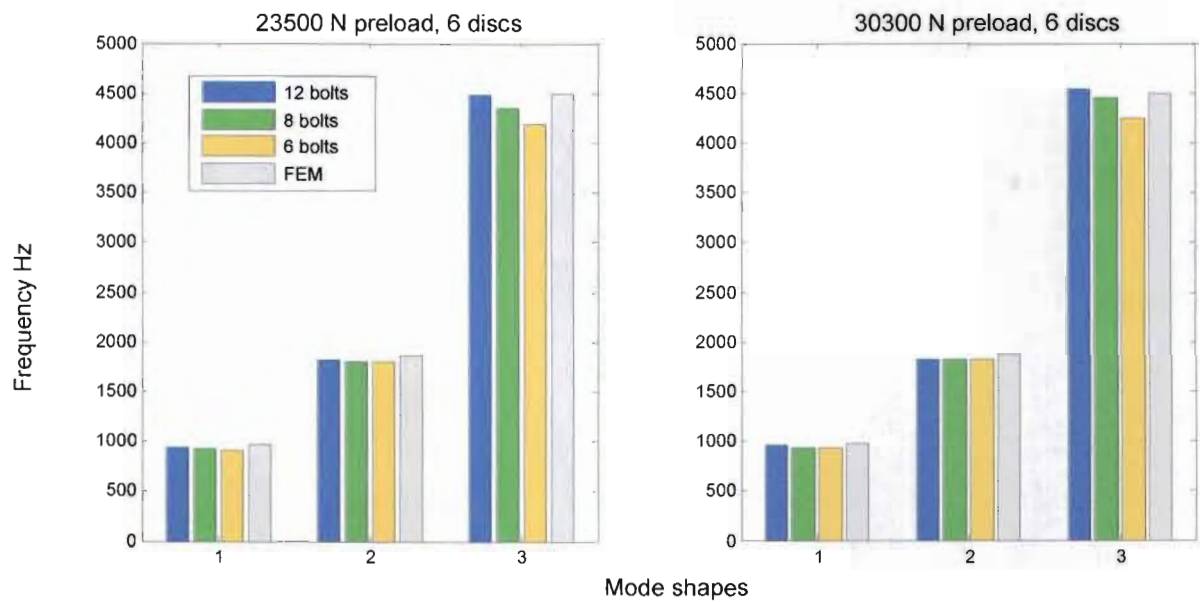


Fig.5.11 Bar Graphs comparing Different Number of Bolts for each Mode Shapes, for Six Disc Assembly.  
Slenderness Ratio Six Discs = 1.046



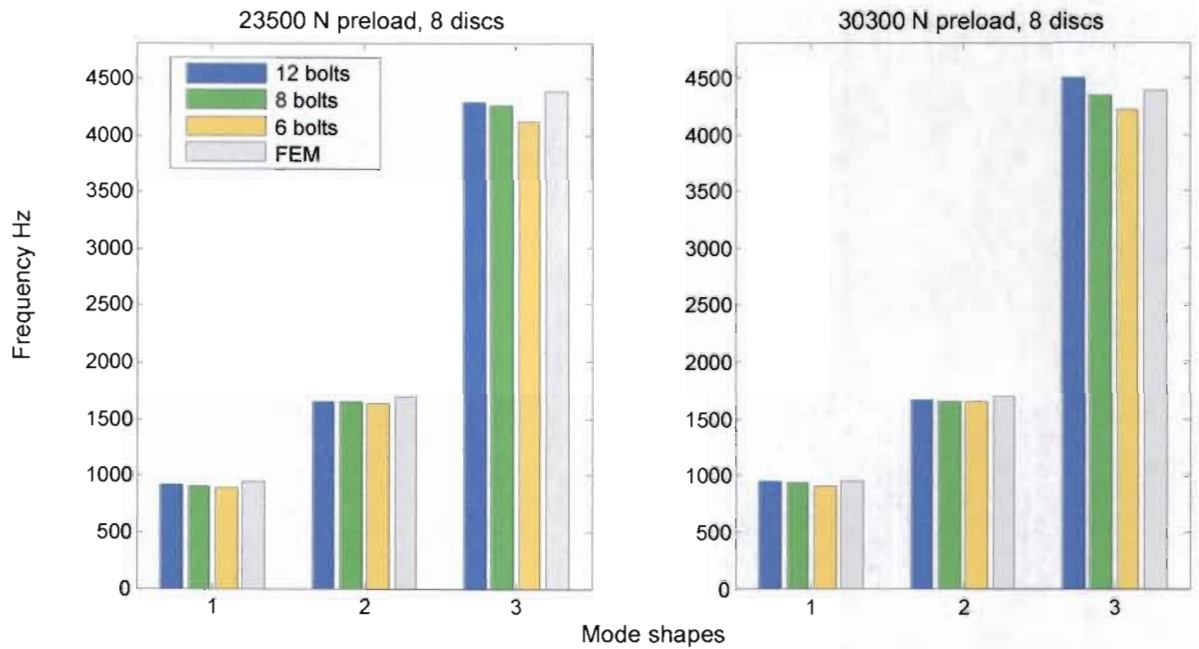


Fig.5.12 Bar Graphs comparing Different Number of Bolts for each Mode Shapes, for Eight Disc Assembly.  
Slenderness ratio Eight Discs = 1.394

When considering the slenderness of the disc-volume, there is no significant change in natural frequency for four and fewer discs, for similar configurations. It is only when the length of the disc-volume increases that the effect of pre-tension becomes more obvious. A slenderness transition occurs between four and six discs.

## 5.6 Verification of Models

Normally during modal analysis the aim is to update the analytical model continually. In this section the preliminary assessment of compatibility of the solid FE and experimental model and the differences which exist between the two models will be discussed. This will clarify why it is not crucial for the experimental model not to have the same number of degrees of freedom as the analytical model.

### 5.6.1 Comparison and Correlation Between Prediction and Experimental Results

The finite element solid model as discussed and presented in Chapter 4 is the analytical model. The results are displayed in Tables 5.5 to 5.8. Figure 3.10 illustrates the first three transverse mode shapes at resonance using the Imaginary Component. These shapes are similar to the shape of the structure predicted by the FE model in Chapter 4.



In Figures 5.13 to 5.20 the natural frequencies of the experimental results are plotted against the predicted FE values. This approach makes it possible to note the degree of correlation and the discrepancies. The correctly paired points of a mode should lie on or close to a straight line of slope = 1. Although the FE model in Chapter 4 characterizes a 12 bolt rotor system, the rest of the bolt configurations are also compared here. These points deviate slightly from the ideal line in a systematic fashion. There is very good correspondence between the lower modes of experimental and analytical values, even with fewer than 12 bolts. When the disc-volume develops into a slender structure the higher frequencies of the models deviate perceptibly, but systematically.

### Graphical Comparison of Frequencies

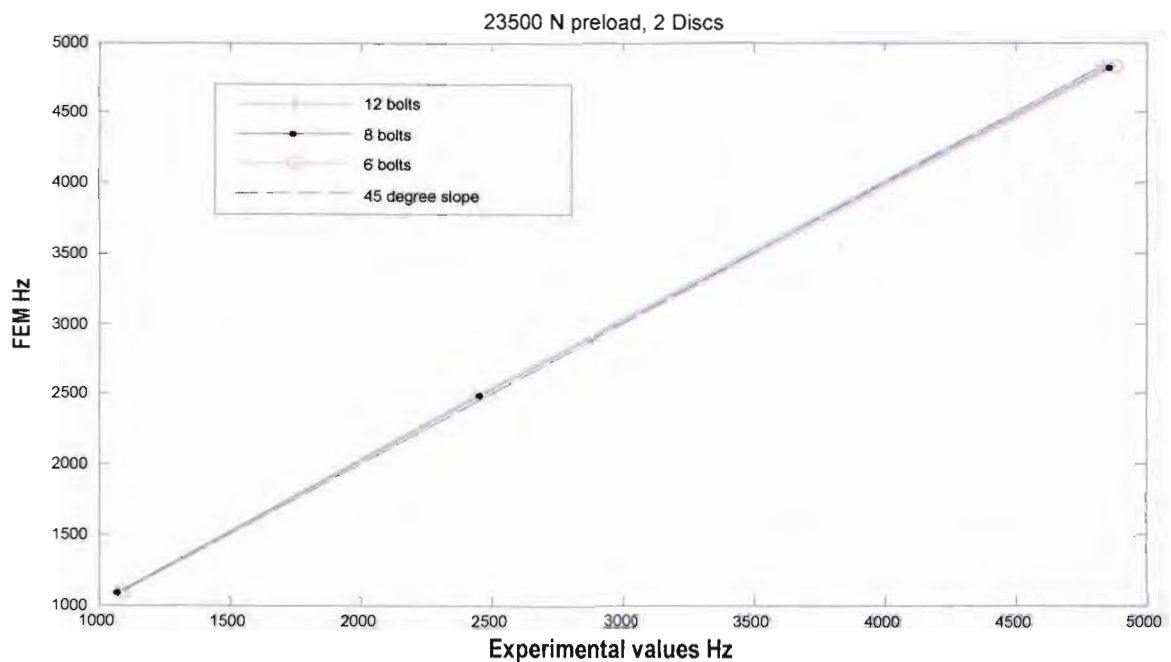


Fig.5.13

*Frequency results FE model vs Frequency results Experimental model  
for 23 500 N preload on a Two Disc Rotor.*

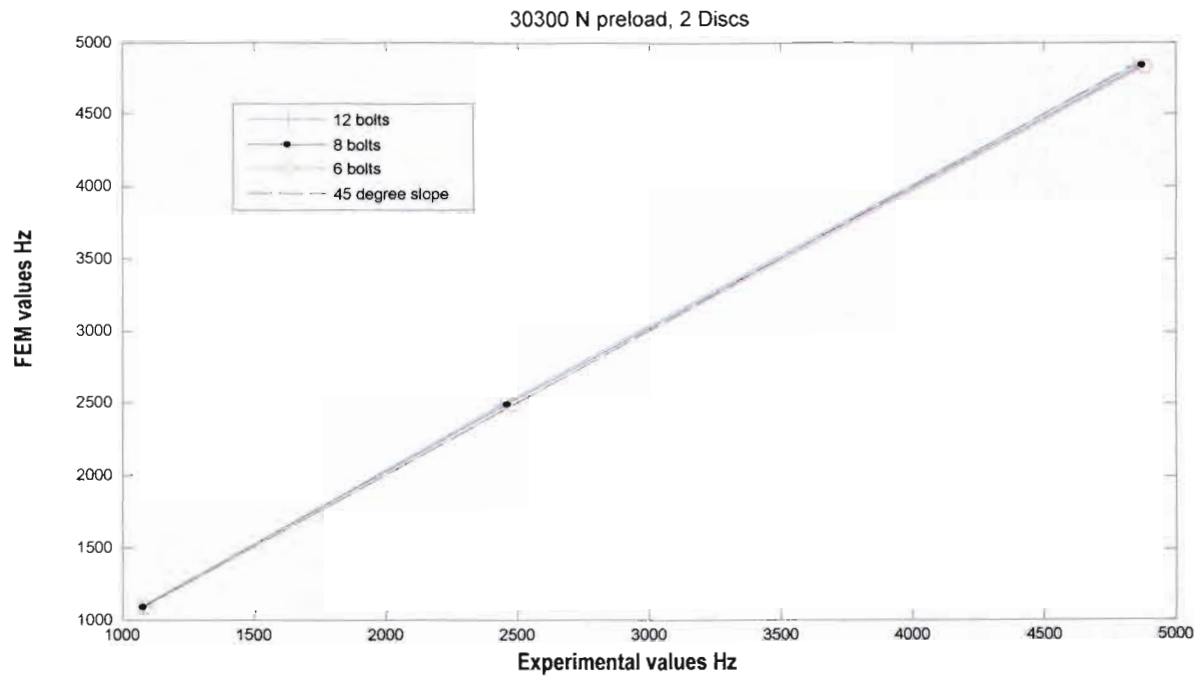


Fig.5.14

Frequency results FE model vs Frequency results Experimental model  
for 30 300 N preload on a Two Disc Rotor.

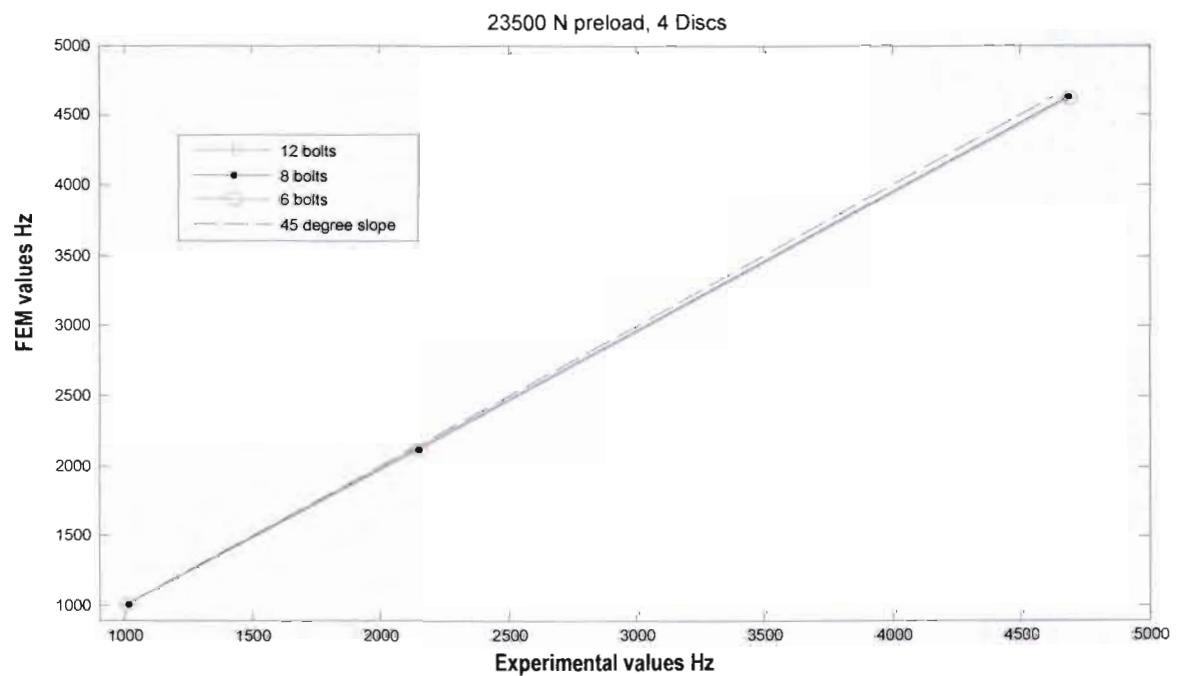


Fig.5.15

Frequency results FE model vs Frequency results Experimental model  
for 23 500 N preload on a Four Discs Rotor.

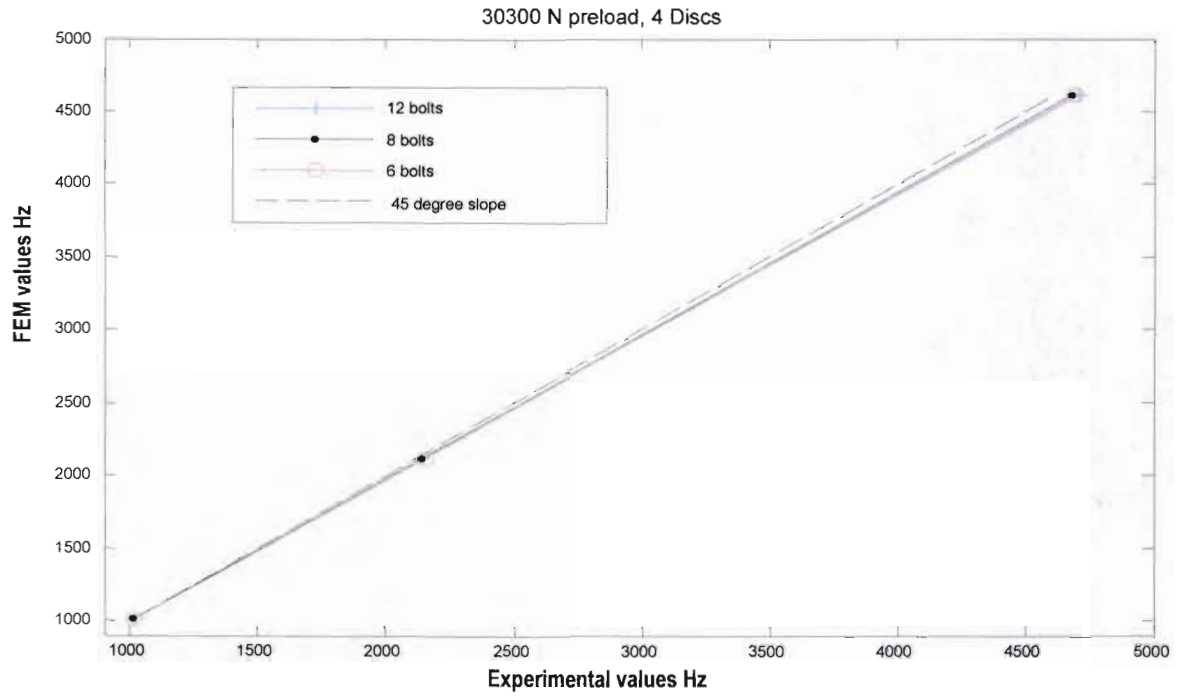


Fig.5.16

Frequency results FE model vs Frequency results Experimental model  
for 30 300 N preload on a Four Disc Rotor.

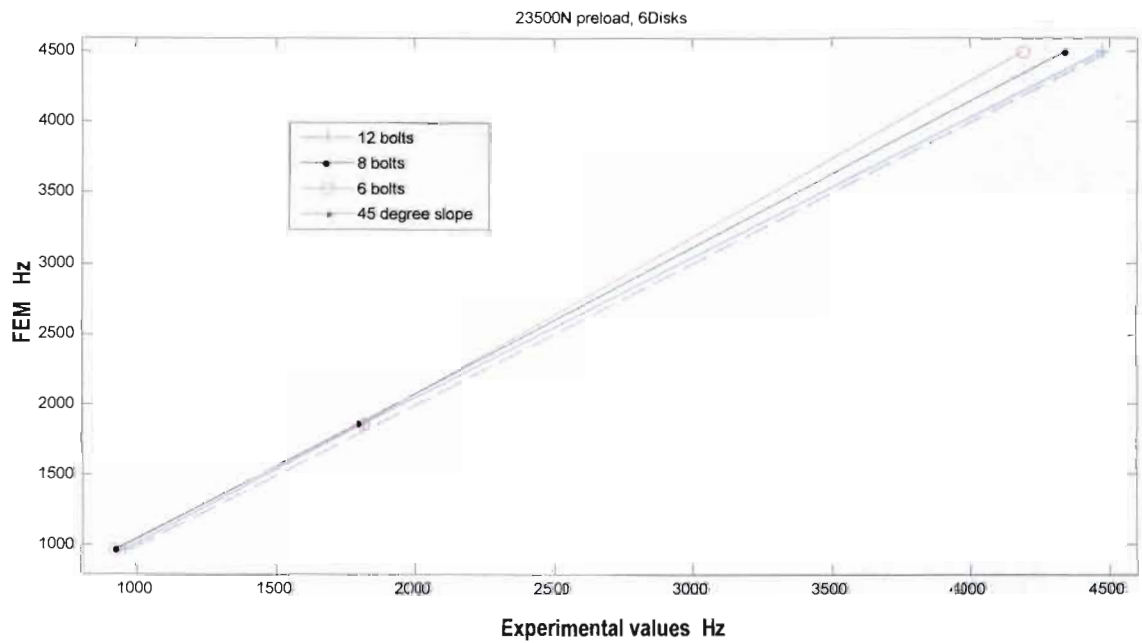


Fig.5.17

Frequency Results FE model vs Frequency results Experimental model  
for 23 500 N preload on a Six Disc Rotor.

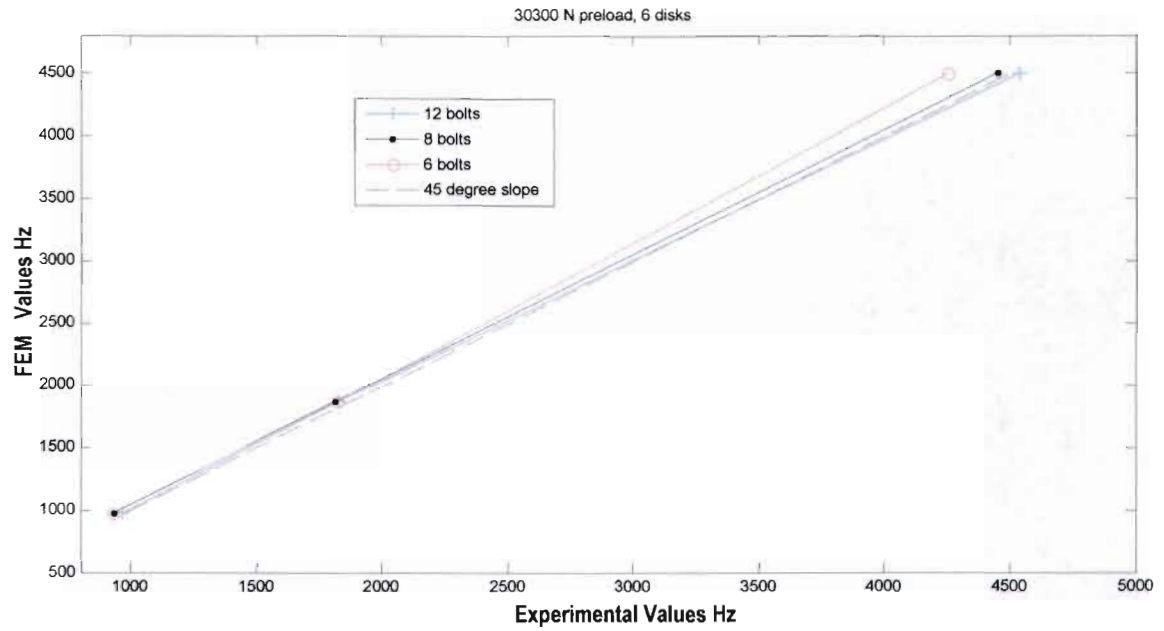


Fig.5.18

Frequency results FE model vs Frequency results Experimental model  
for 30 300 N preload on a Six Disc Rotor.

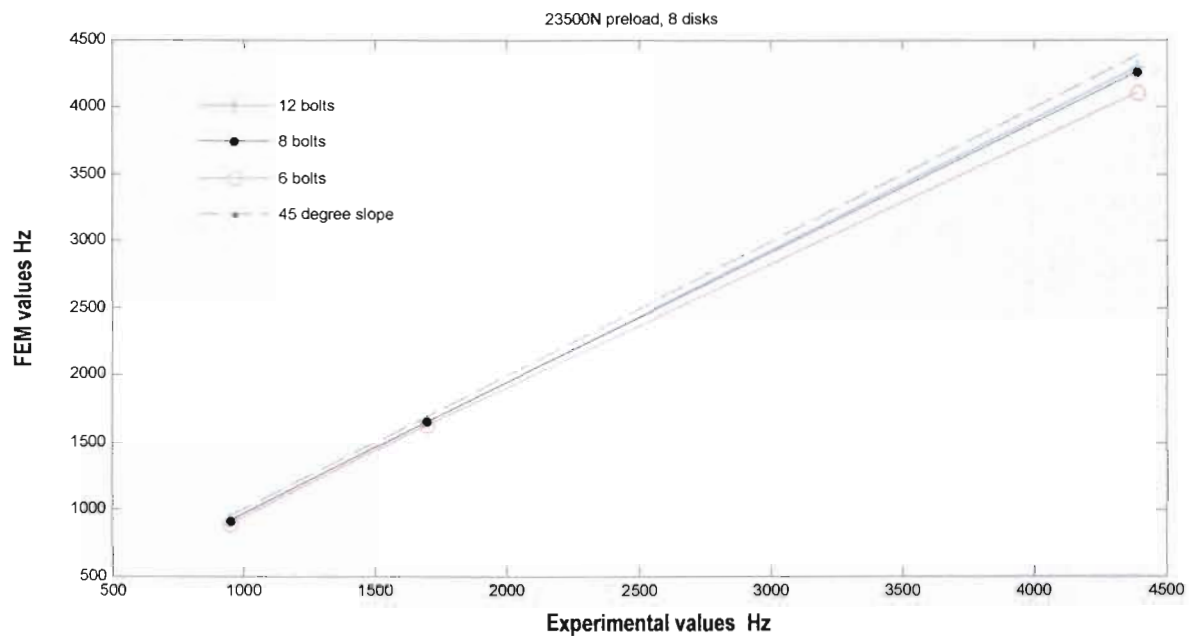


Fig.5.19

Frequency results FE model vs Frequency results Experimental model  
for 23 500 N preload on a Eight Disc Rotor.

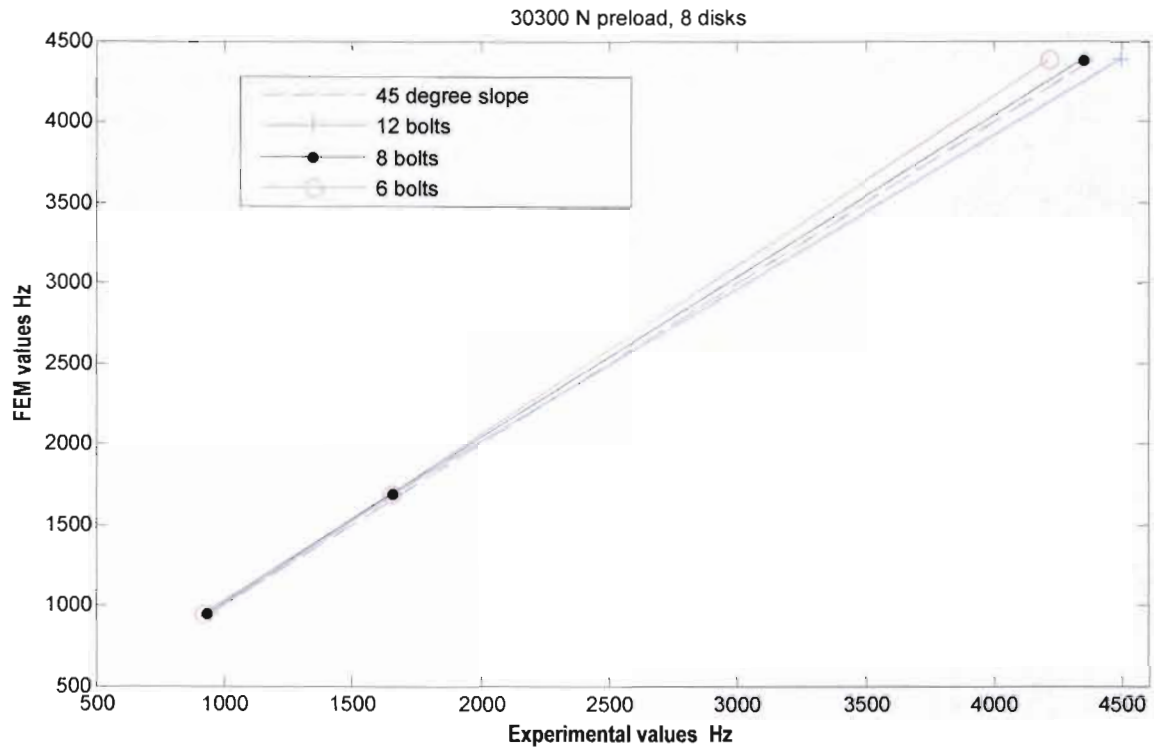


Fig.5.20

*Frequency Results FE Model vs Frequency Results Experimental Model  
for 30 300 N Preload on a Eight Disc Rotor.*

Tabular comparisons between FE model and Experimental results, and the percentage difference for each case are provided in Tables 5.5 to 5.8.

**Table 5.5:** Natural frequencies (Hz), Two Discs, 12 Bolts, 70% and 90% Preload.

2 discs 12 bolts	FEA	23 500 N (Exp.)	% $\Delta$	30 300 N (Exp.)	% $\Delta$
mode 1	1084	1075	0.83	1075	0.83
mode 2	2486	2438	1.93	2438	1.93
mode 3	4835	4838	-0.06	4844	-0.186



**Table 5.6:** Natural frequencies (Hz) Four Discs, 12 Bolts, 70% and 90% Preload.

4 discs 12 bolts	FEA	23 500 N (Exp.)	% $\Delta$	30 300 N (Exp.)	% $\Delta$
mode 1	1013	1013	0	1013	0
mode 2	2117	2125	-0.377	2131	-0.66
mode 3	4620	4669	-1.06	4706	-1.86

**Table 5.7:** Natural frequencies (Hz), Six Discs, 12 Bolts, 70% and 90% Preload.

6 discs 12 bolts	FEA	23 500 N (Exp.)	% $\Delta$	30 300 N (Exp.)	% $\Delta$
mode 1	973	950	2.36	962	1.13
mode 2	1869	1813	2.99	1825	2.35
mode 3	4496	4475	0.46	4538	-0.93

**Table 5.8.** Natural frequencies (Hz) Eight discs, 12 Bolts, 70% and 90% Preload.

8 discs 12 bolts	FEA	23 500 N (Exp.)	% $\Delta$	30 300 N (Exp.)	% $\Delta$
mode 1	947	925	2.32	943	0.42
mode 2	1689	1656	1.95	1663	1.53
mode 3	4386	4294	2.08	4494	-2.46

## 5.6.2 Localisation

**Table 5.9:** Differences between the two models.

Experimental Test rig	Finite Element Model
<ul style="list-style-type: none"> <li>- Pre-tensioned.</li> <li>- Supported by two ropes.</li> <li>- Extra mass of transducers, nuts, extended studs.</li> <li>- Cyclic pre-tensioning.</li> </ul>	<ul style="list-style-type: none"> <li>- No Pre-Tension.</li> <li>- Theoretically Free-Free.</li> <li>- Mass of transducers, nuts, extended studs were not modelled.</li> <li>- No possible creep.</li> </ul>

**Table 5.10:** *Mass differences between Experimental (12 bolts) and FEM.*

Configuration	Total Mass of Experimental Rotor (kg)	Total Mass of FEA Rotor (kg)	Difference (kg)	$\Delta\%$
Two discs	28.051	26.39	1.661	5.92
Four discs	34.045	32.91	1.135	3.33
Six discs	40.316	39.428	0.888	2.20
Eight discs	46.625	45.947	0.678	1.45

### 5.6.3 Reconciliation

Minor deviations between dissimilar preloads of the same configuration indicate that there is indeed a change in stiffness in the structure. A good correlation between the experimental and the solid FE model results for the two- to four disc configurations, suggesting that the physical rotor-structure behaves in an extremely linear fashion (The FE model is linear).

The small systematic deviation from the ideal line for high frequencies indicates a discrepancy which is due to erroneous material property modelling in the predictions, which suggests that there is a specific characteristic responsible for the deviation, not attributable to experimental errors. If the points lie on a straight line other than one, then the problem may be a mass loading problem, or an incorrect material property, such as elastic modulus or material density in the finite element model (Section 5.4.2 argued that the stiffness in the disc-volume increased slightly after preload). The mass difference decrease, the more slender the rotor become.

For the configuration of four discs and lower the mass difference should have an effect.

During higher frequencies more strain energy is involved when the bolts are already close to their elastic limit. In the experimental model the rotor discs and the bolts consist of two types of material with different physical properties, for example rate of strain ( $\dot{\epsilon}$ ), which stiffens and softens during preload as well as the contribution of the position of the sub-components on the cross-section of the disc.

### 5.6.4 Conclusion

Even with the dissimilarity between the FEM and the experimental test rig, like the support, mass and pre-tension, the natural frequencies do not mutually differ very much between the models (similar configurations). It also shown the more slender the rotor become, the more perceptible the affect of preload

turn out to be. As a result the FE solid model of the rotor (Chapter 4), with the simplifications, without any preload, produced acceptable results.

## **5.7 Synthesis**

The bolts are the primary path of energy transfer in this structure; moreover this is one of the areas which possesses the highest strain energy during bending in the transverse vibrating modes. From the theory it is expected that the compression stress induced in the discs would reduce the natural frequency, but the opposite effects arises.

Due to small deviations caused by pre-tension and material properties, certain assumptions can be made, which makes the common solid FE model a good predictor of the real structure when considering the mode shapes and the natural frequencies.

In the next chapter, Chapter 6, an attempt is made to synthesize the experimental results, literature study and the analytical results.

## CONCLUSIONS AND RECOMMENDATIONS

In this chapter the main research question raised in Chapter 1 will be discussed. Guidelines for designing an assembled rotor-system and the overall synthesis of the findings of this work will be provided.

### 6.1 Analytical Models

There may exist more complex mathematical models which will describe the rotor behaviour under investigation sufficiently. The aim of this research was to locate a method which is straightforward to use, simple to interpret and applicable to similar structures. It appears this is not attainable. The geometry of the discs, the sharp transfer from the hub to the disc-volume, large diameter steps and positions of the bolts comprise a complicated problem which cannot be described sufficiently by low order finite elements or the Transfer Matrix Method. The only method which describes the natural response of the rotor sufficiently is the solid FE model. The solid model utilized in Chapter 4 is not capable of simulating changing dynamic characteristics due to external physical modifications in the current capacity.

### 6.2 Reconciliation Between Literature, Test Results and Analytical Model

Both Sabuncu and Kacar (1990) and Tomski (1994) noted that an applied preload on a structure has a significant effect on the natural frequency when the beam-like structure becomes slender. This was confirmed in this project on increasing the number of discs on the rotor-structure, although the magnitude of these changes were very small. The experimental results also verified the findings of Rivin (1999), who stated that stiffness adjustment would not be possible for very inflexible components by preloading. The disc-volume rotor acted as a very inflexible mass with very little effect on the natural frequencies when using four or fewer discs.

Results obtained from the rotor structure during testing oppose some findings of Tomski (1994). His evidence indicated that the natural frequencies of a composite structure will decrease with an axial preload, tensile or compressive, but the opposite occurred in this project.

The bolts are one of the dominating mediums through which force or energy is transferred during vibration. The stiffness of the rotor is affected by the number of bolts, in that fewer bolts lowers the stiffness. This becomes more noticeable when the rotor becomes more slender (more discs).

Therefore, the mechanical properties of the bolts are seen to be one of the essential parameters, besides the slenderness, which will affect the natural vibration behaviour.

The clamping stiffness ( $K_c$ ) of clamped flanges depends mainly on the ratio  $D/d$  (Figure 2.5). Changing the  $D/d$  ratio is the most effective way to increase  $K_c$ . The large diameter hardened washers used during this experimentation on both sides of the force transducer were responsible for a good pressure distribution in the discs. In a real situation the contact area would be smaller when the discs are clamped together with normal size washers, which will probably reduce the volume of the high stress zone.

By increasing the preload during experimentation, the natural frequency increased a tiny amount while the mass of the structure remains constant, indicated that an increase in stiffness took place. There was a clear improved shift in natural frequency in the higher modes between different preloads. Although non-linear systems are characterized by stiffness varying with the loading conditions, the majority of the results deviate in a systematic fashion, which points to the stress stiffening phenomenon.

## 6.3 Design Methodology for an Assembled Rotor-Disc System

### 6.3.1 Concepts of modelling

The modelling and analysis of a complicated rotor assembly involves several different phases. Discretion needs to be used as to the required complexity of a system. In general it is advisable to utilize a simple model as far as possible to provide reasonable estimates of the desired system's dynamic characteristics. Simplicity keeps one closer to the physical process and may give an insight that leads to improvements. Several steps are required in the development of the equation of motion in modelling the dynamic characteristic of a rotor dynamic system. The key components of the rotor system must be identified and a set of simplifying assumptions must be made regarding the nature of each component and how they interact with relating components. Nonlinearity must be taken into consideration for FFT based dynamic experimental techniques during measurement, since it might initiate undesirable effects. In this case a linear FEA simulating the rotor produced good results.

### 6.3.2 Preliminary design

Analytical techniques play an important role in virtually all phases of preliminary design, detailed design and development of a rotor structure.

An important key design factor in the preliminary design stage is the determination of the critical speeds with respect to the operating conditions of the machine. During the preliminary design phase, system damping is not well established. The general practice is to consider only undamped system models. The effect of damping must be considered in the detailed design stage. In the preliminary design phase, the system parameters need to be adjusted so as to change the systems natural frequencies of whirl and



thereby locate the critical speeds required. The parameters which should have the most influence in this regard, are the support stiffness (bearings and support structure), support locations and the mass and stiffness distribution of rotating assemblies.

It is often useful to plot the system's critical speed versus a particular design parameter to obtain a graphical description of the sensitivity of the critical speeds to this parameter, i.e. a critical speed-map. Another useful procedure is to generate energy maps of the system which display the kinetic and /or the potential energy distribution associated with a natural mode, when damping is neglected.

### **6.3.3 Important key factors for an assembled structure**

- Enhanced surface finishing results in higher contact stiffness, damping decreases with improved surface finish.
- Proper orientation of machining traces on the contacting surfaces is important.
- Damping increases slightly with increasing width of the contact area.
- Optimization of contact areas and loads to take advantages of hardening Nonlinearity should be done.
- Modal quantities can be used to identify problem areas by indicating the more highly stressed elements. Elements that are consistently highly stressed across many or all modes will probably be highly stressed when dynamic loads are applied.
- Stiffness can be modified by proper selection of the component geometry (shape) and its interaction with other components.
- Changes in temperature during operation may enhance stresses in flange materials.
- The stresses in the material depends on how large the applied pressure area is (stress concentrations). A small stress concentration area will not influence the global behaviour.

## **6.4 Final Conclusions**

The most suitable analytical model for describing the natural response of a complex rotor structure turns out to be the solid FE model, due to its capability to model distortion in the axial direction. Even when modelled without a preload, the largest differences between model prediction and experimentation results were still below 3%.

The Impact method produced very good results concerning this specific structure. Although this method was not able to indicate nonlinearities, repeating the tests on similar configurations gave an indication of tendencies.

The complex geometry of the discs needed a refined analytical model to simulate the preload. There was a clear indication that the pre-tension in the bolts used to clamp an assembled discs system, influenced the natural frequencies of the rotor. However it is insignificant.

The FE analysis revealed there is a relatively small volume that is subjected to high stresses induced in the disc material during clamping caused by the bolts.

The results in this project show that natural frequency rises when the preload increases, but that it is also subject to the slenderness of the structure, in this instance the disc-volume. In addition, the material properties of some of the involved components, in this case, the bolts, influenced the natural response as well due to their position on the cross-section. Fewer bolts decreased the stiffness of the rotor. This became noticeable when the rotor was slender.

Therefore stiffness can be modified (enhanced) by identification of the dominant parameters, proper selection of the components geometry (shape and size) and the mutual interaction between components. A solid FE rotor model, where the contact areas are considered as solid and neglecting the bolts mechanical properties can generate acceptable predictions of the natural frequencies of the stationary rotor. Therefore, in any analytical model the rotor can be modelled as a solid continuous shaft, when taking into account the correct representative moment of inertia and equivalent stiffness.

## **6.5 Recommendations**

The article, Vibrations of a pre-stressed compound beam with a concentrated mass, Journal of Sound and Vibration., Tomsaki, L., Przybylski, J., et al 1994, should be investigated. Materials with different diameters and physical properties should be used.

# APPENDIX A

## Formulae

$r = 2L/R$ .....	Slenderness ratio	Yamamoto (2001)
$K_c = \beta.E.d$ .....	Clamping Stiffness	Robert (1967)
$\phi_y = \frac{12EI_z k_y}{AGL^2}$ .....	Characterization of shear force	Cook et al. (2001)
$H(\omega) = \frac{X(\omega)}{F(\omega)}$ .....	Frequency Response Function	Ewins(2000)
$F = \sigma.A_{no \ min \ al}$		
$k = \frac{\Delta P}{\Delta x}$ .....	Stiffness ratio	Rivin, E.(1999)
$\omega_n = \frac{\pi^2}{l^2} \sqrt{\frac{EI}{\rho A}} \left[ n^4 - \frac{n^2 P l^2}{\pi^2 EI} \right]^{\frac{1}{2}}$ .....	Natural frequencies of preload on beam n: modes	Rao, (1995)
$\beta = \frac{F_x}{kAG}$ .....	Shear factor	Yamamoto (2001)
$\{v_n\}^R = [P_n][F_n][P_{n-1}][F_{n-1}] \dots [P_1][F_1]\{v_0\}^L$	Transfer Matrix	Fertis (1995)
$\phi = \frac{12EI}{L^2 K_s AG}$ .....	Characterization of shear	Lalanne(1998)
$I_x = \underline{I}_x + Ar_y^2$ .....	Moment of Inertia	Hibbler(1978)
$A = \pi(R_2^2 - R_1^2) - \pi(\frac{d}{2})^2 (12holes)$ .....	Area of disc-ring	
$\zeta = 4 \frac{L}{D} \sqrt{\frac{\sigma_T}{E}} = 4 \frac{L}{D} \sqrt{\varepsilon_T}$ .....	Stiffness affect	Rivin(1990)

$$[S_i] = \int [G_i]^T [\tau_i] [G_i] d.Vol \dots\dots\dots \text{Stiffening Matrix}$$

ANSYS  
Notes

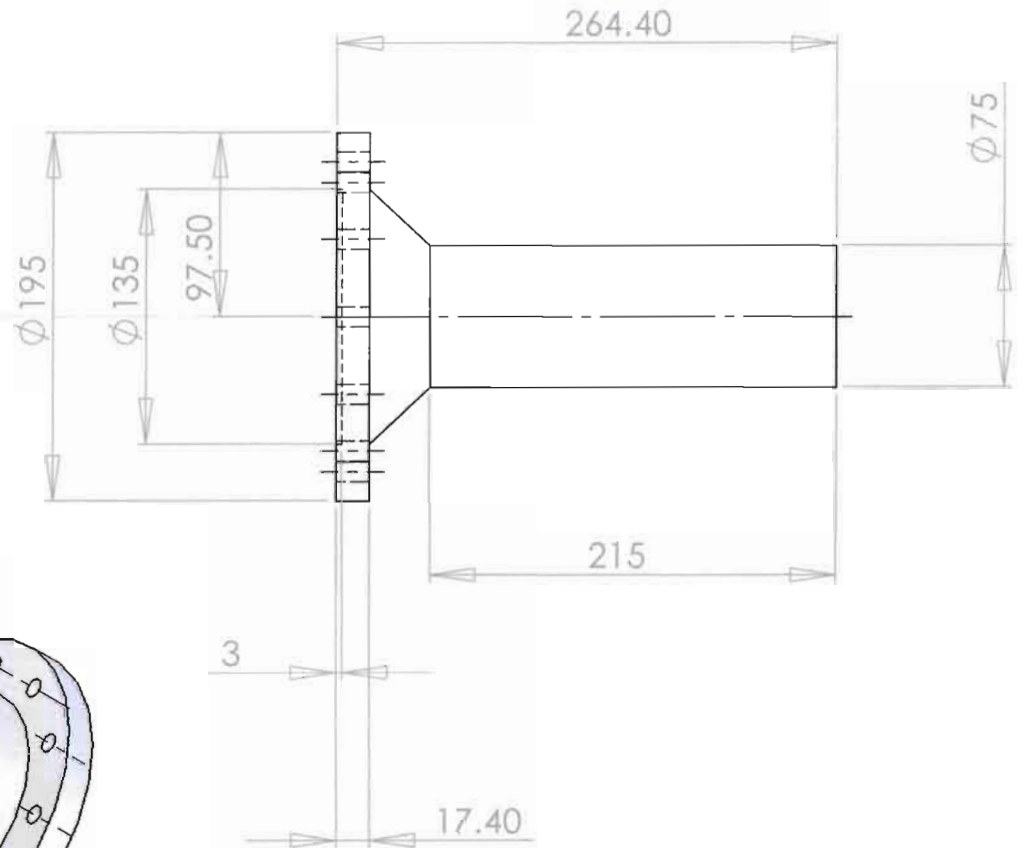
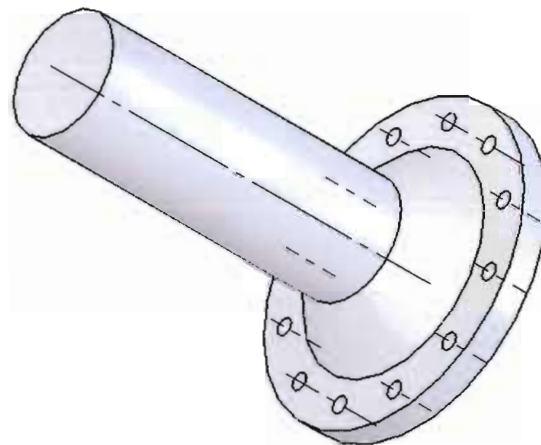
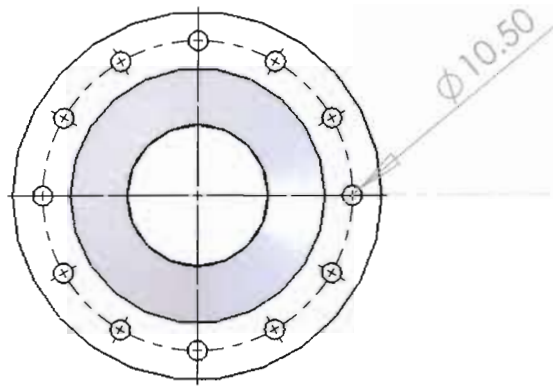
$$K = \frac{48E I}{L^3} \dots\dots\dots \text{Stiffness}$$

Inman(1996)

## **APPENDIX B**

### **Drawings**





UNLESS OTHERWISE SPECIFIED: DIMENSIONS ARE IN MILLIMETERS				FINISH:		DEBUR AND BREAK SHARP EDGES		DO NOT SCALE DRAWING		REVISION	
DRAWN <b>G Blignaut</b>				SIGNATURE		DATE		TITLE:			
CHK'D											
APPV'D											
MFG											
Q.A											
MATERIAL: <b>Mildsteel</b>						DWG NO. <b>Rotor hub 2tek</b>					
WEIGHT:						SCALE:1:5					
						SHEET 1 OF 1					

Ø75

264.40

3

17.40

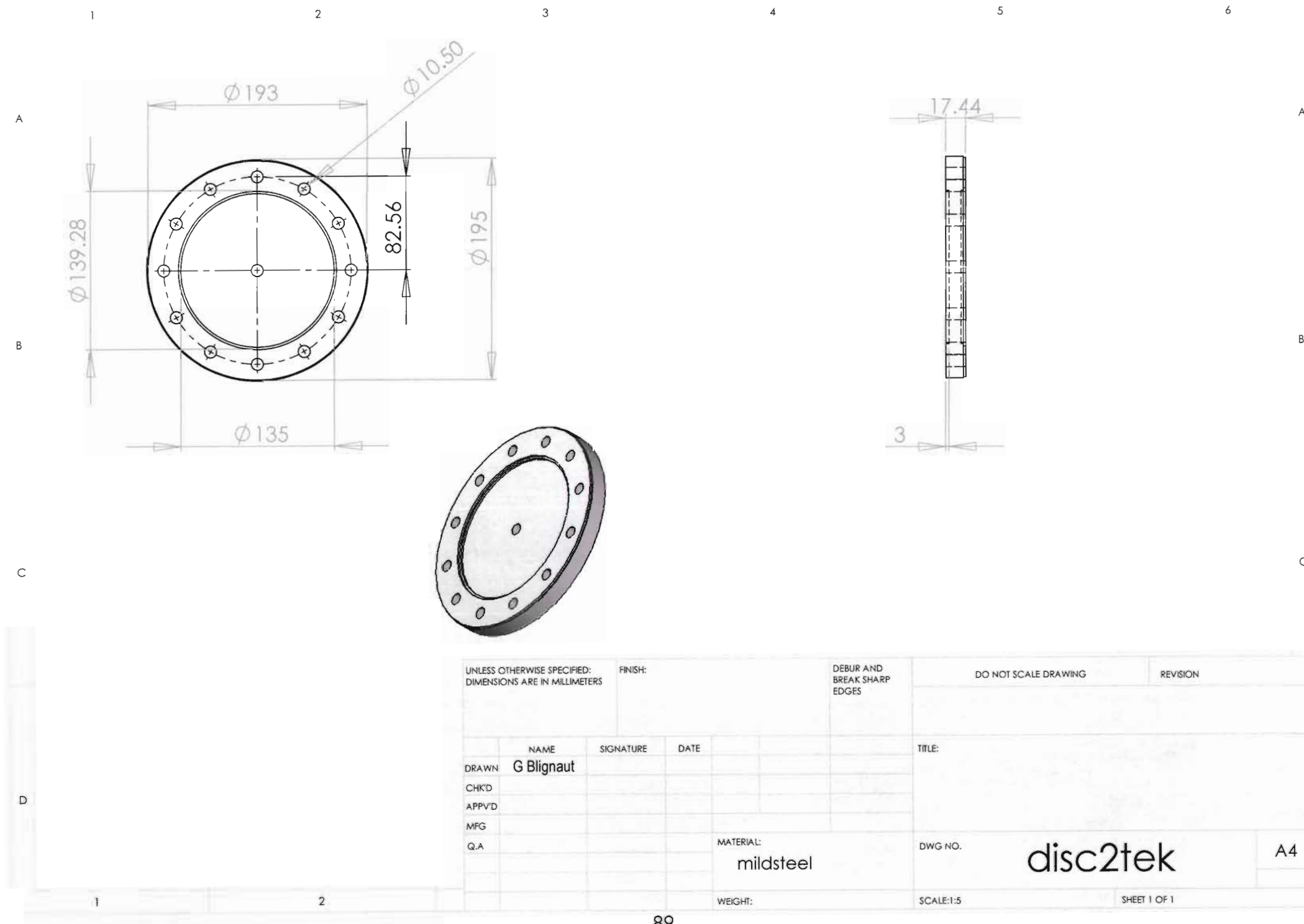
215

Ø135

Ø195

97.50

Ø10.50



UNLESS OTHERWISE SPECIFIED: DIMENSIONS ARE IN MILLIMETERS				FINISH:		DEBUR AND BREAK SHARP EDGES		DO NOT SCALE DRAWING		REVISION	
DRAWN		NAME		SIGNATURE		DATE		TITLE:			
CHK'D		G Blignaut									
APPV'D											
MFG											
Q.A											
MATERIAL:						DWG NO.		disc2tek		A4	
mildsteel											
WEIGHT:						SCALE:1:5		SHEET 1 OF 1			

## **APPENDIX C**

### **Frequency Response Function Graphs**

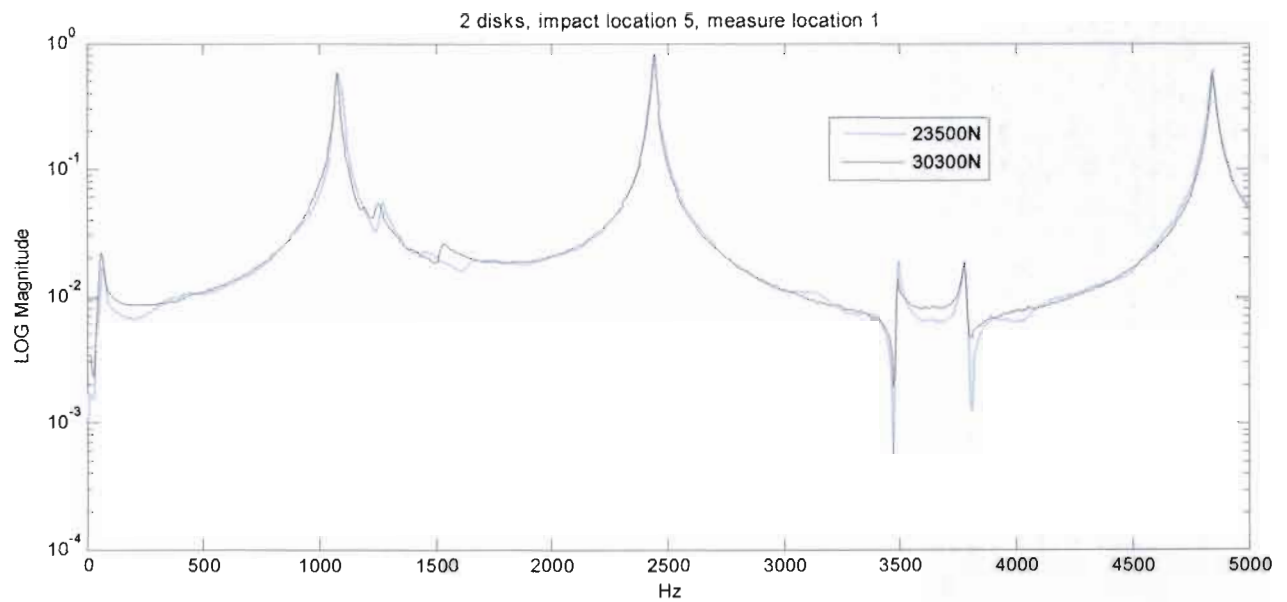


Fig. C.1, Plot of Logarithmic Magnitude of Accelerance vs Frequency Data for Two Discs, 12 Bolts, 23500N, 30300N Preload in bolts.

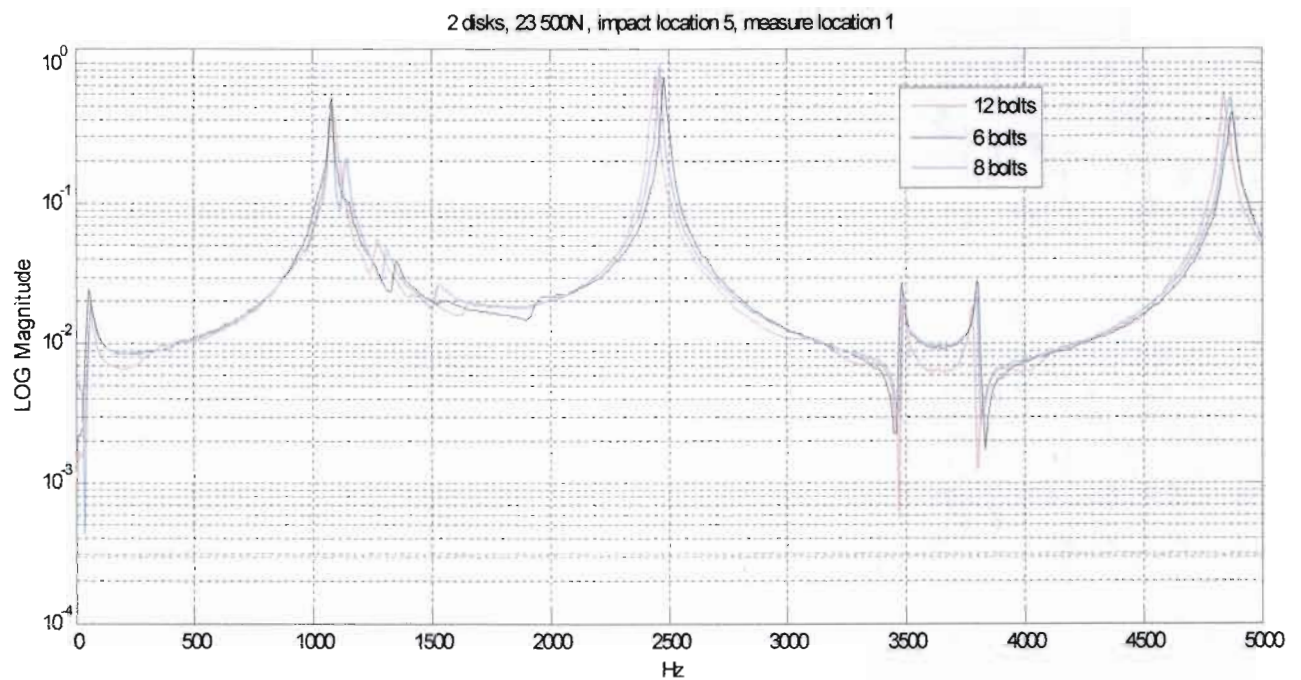
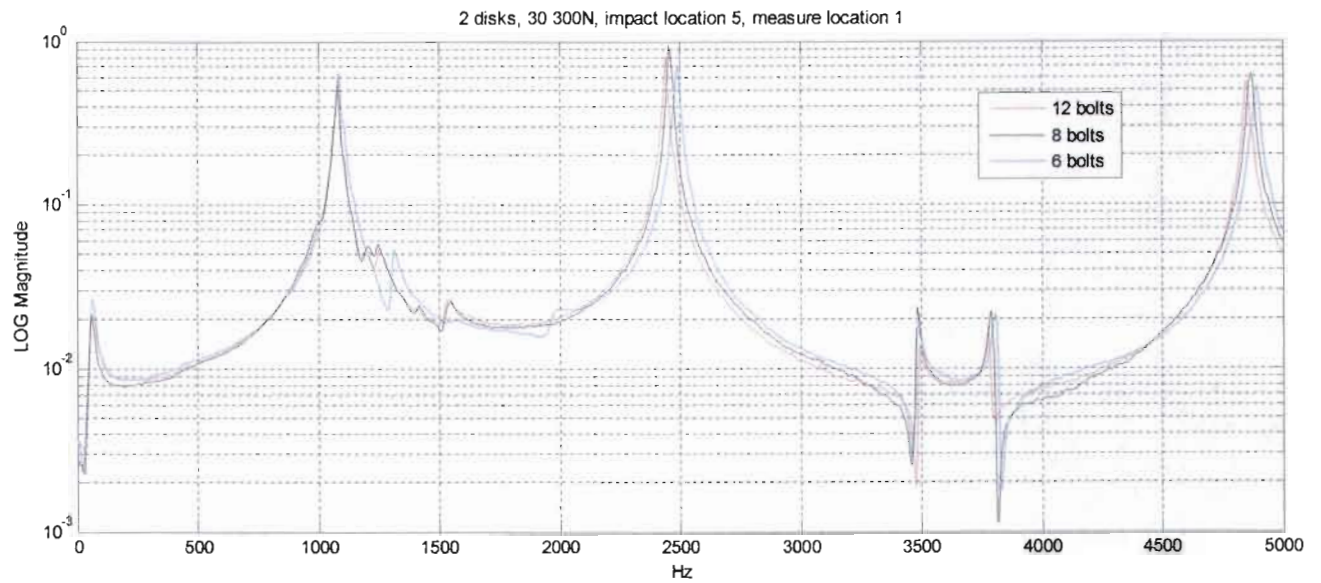
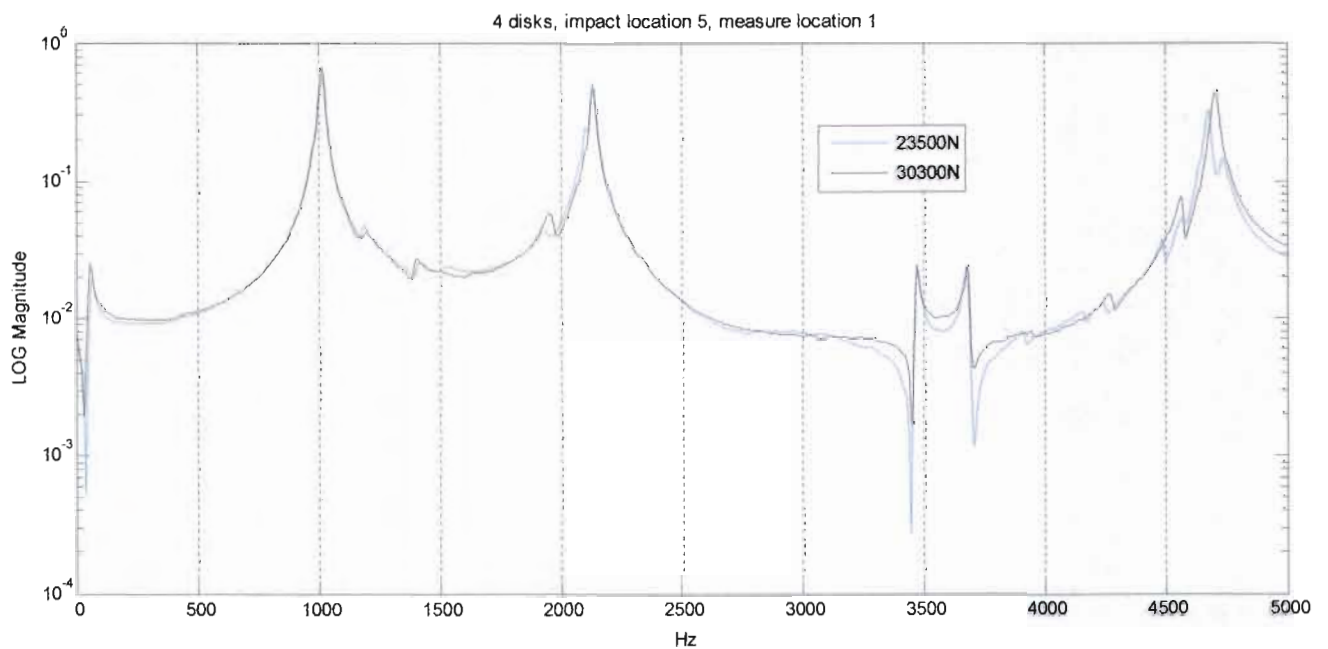


Fig. C.2, Plot of Logarithmic Magnitude of Accelerance vs Frequency Data for Two Discs, 6,8,12 Bolts, 23500N Preload in Bolts.



*Fig. C.3, Plot of Logarithmic Magnitude of Accelerance vs Frequency Data for Two Discs, 6,8,12 Bolts, 30300N Preload in Bolts.*



*Fig. C.4, Plot of Logarithmic Magnitude of Accelerance vs Frequency Data for Four Discs, 12 Bolts, 23500N, 30300N Preload in bolts.*



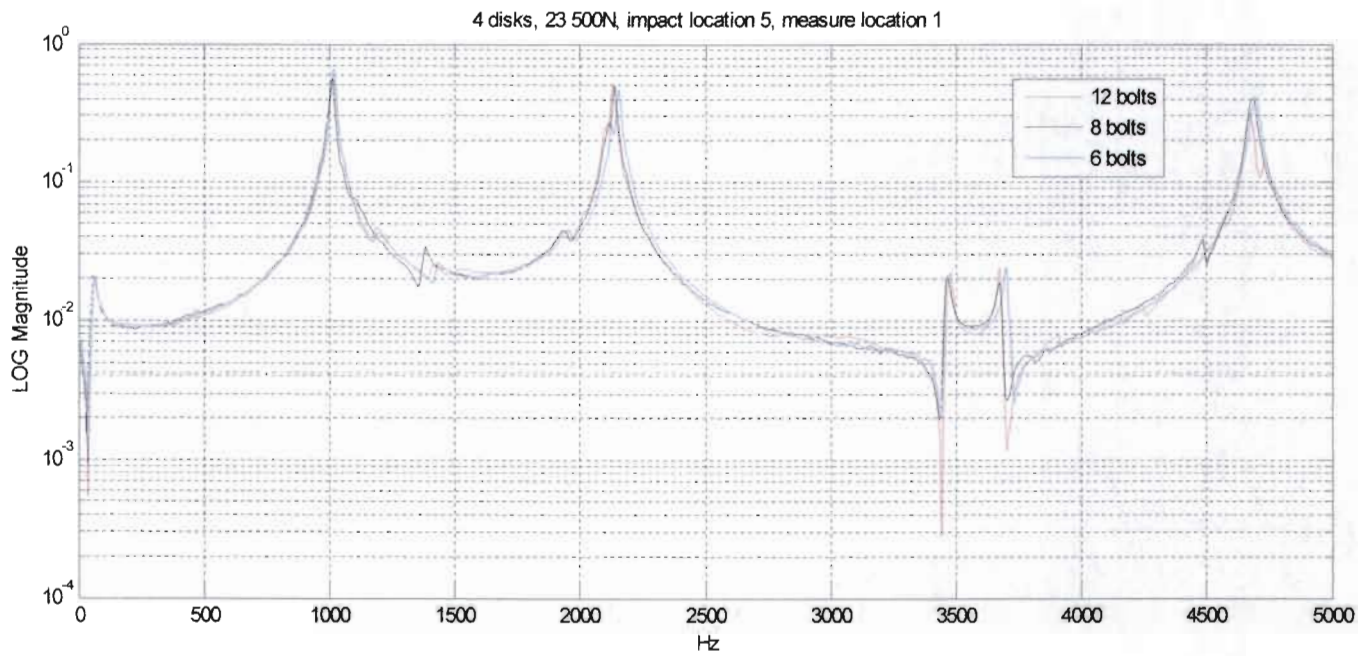


Fig. C.5, Plot of Logarithmic Magnitude of Accelerance vs Frequency Data for Four Discs, 6,8,12 Bolts, 23500N Preload in Bolts.

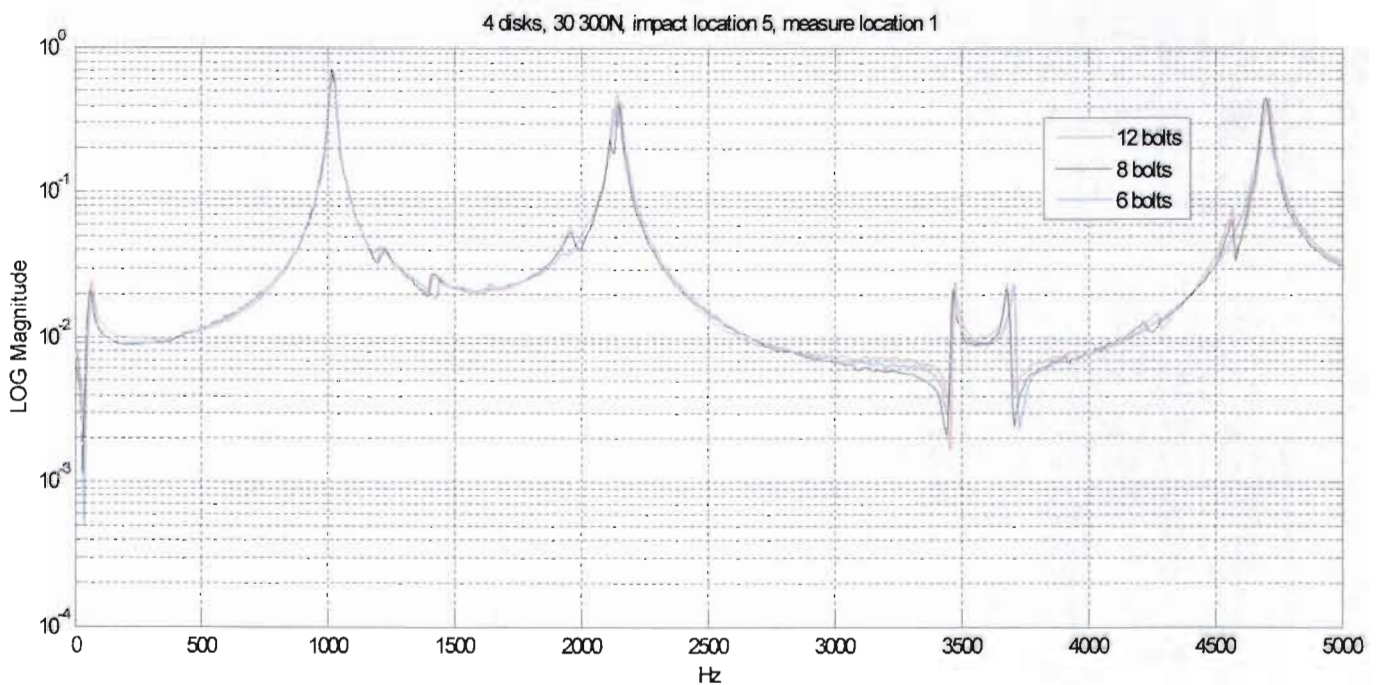


Fig. C.6, Plot of Logarithmic Magnitude of Accelerance vs Frequency Data for Four Discs, 6,8,12 Bolts, 30300N Preload in Bolts.

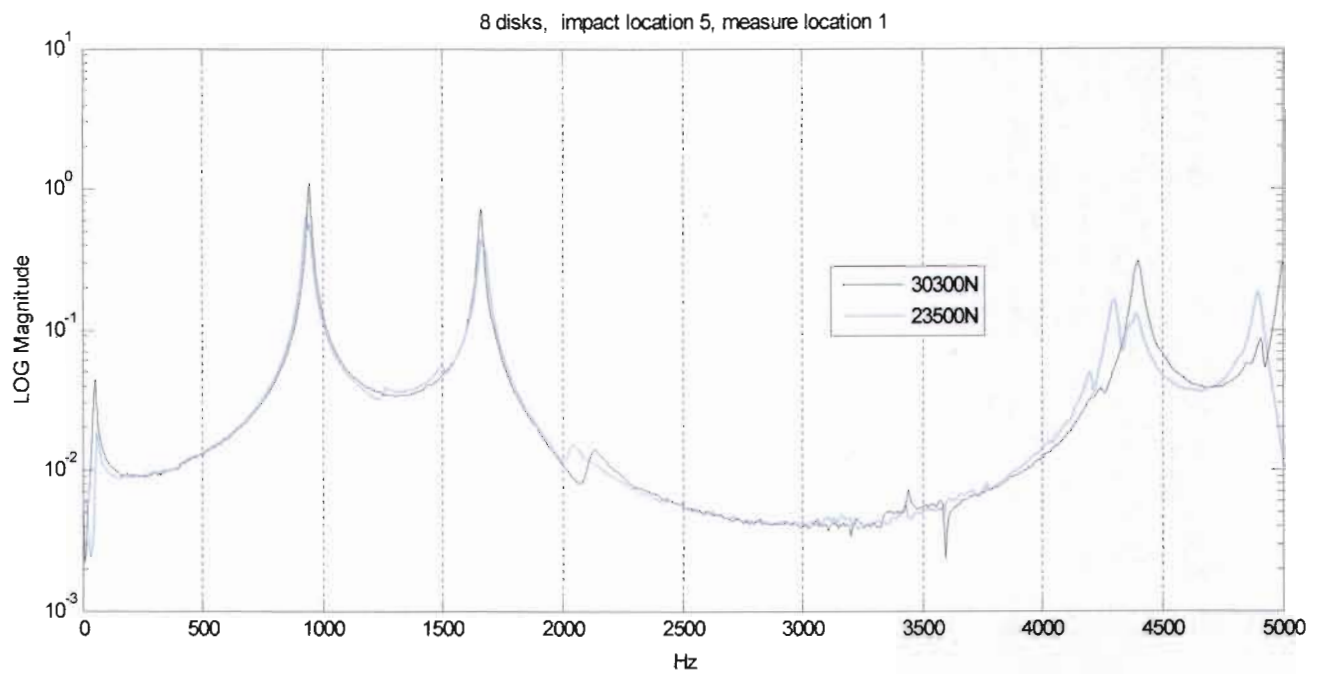


Fig. C.7, Plot of Logarithmic Magnitude of Accelerance vs Frequency Data for  
Eight Discs, 12 Bolts, 23500N, 30300N Preload in bolts.

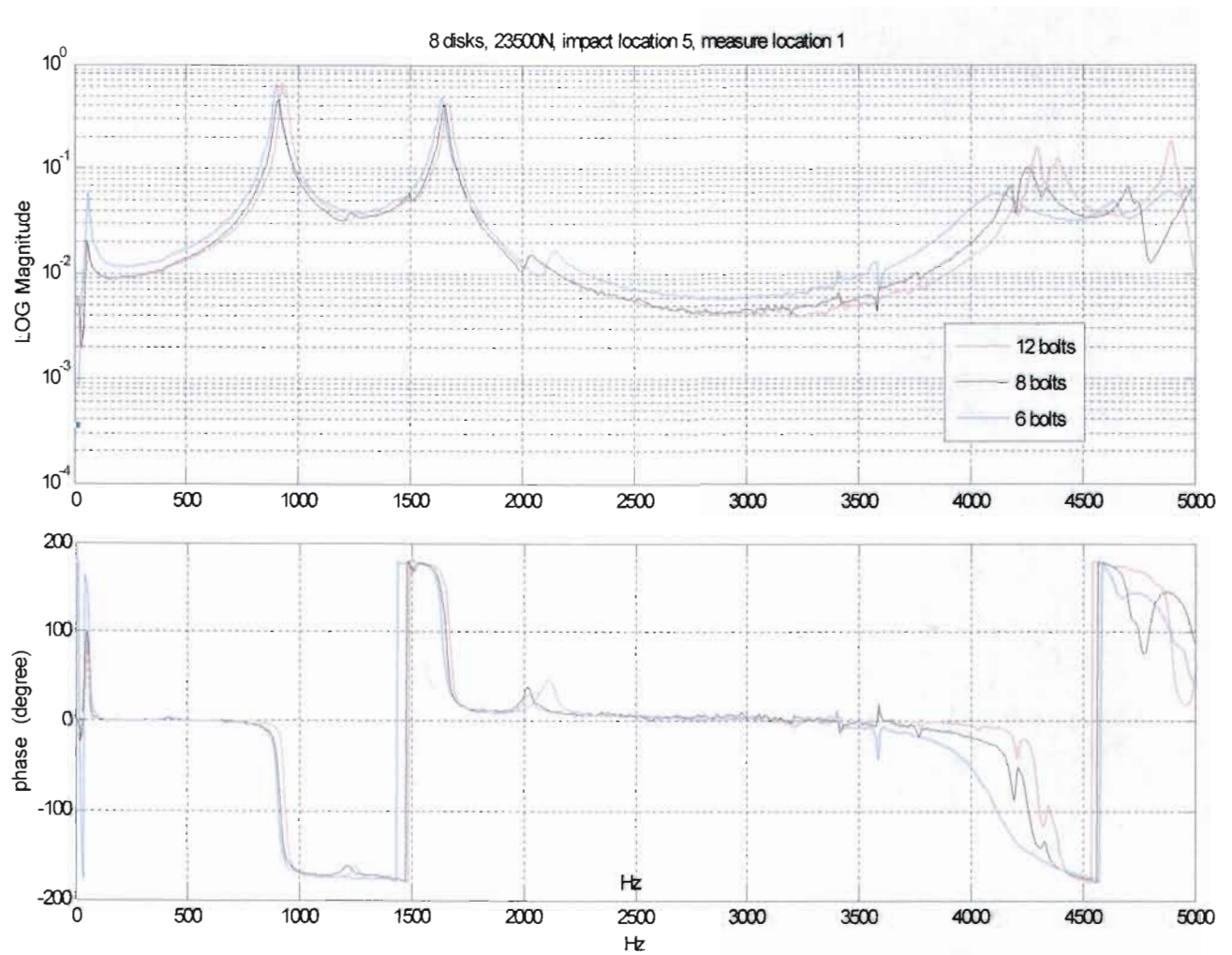


Fig. C.8, Plot of Logarithmic Magnitude of Accelerance and Phase vs Frequency Data for Eight Discs, 6,8,12 Bolts, 23500N Preload in Bolts.

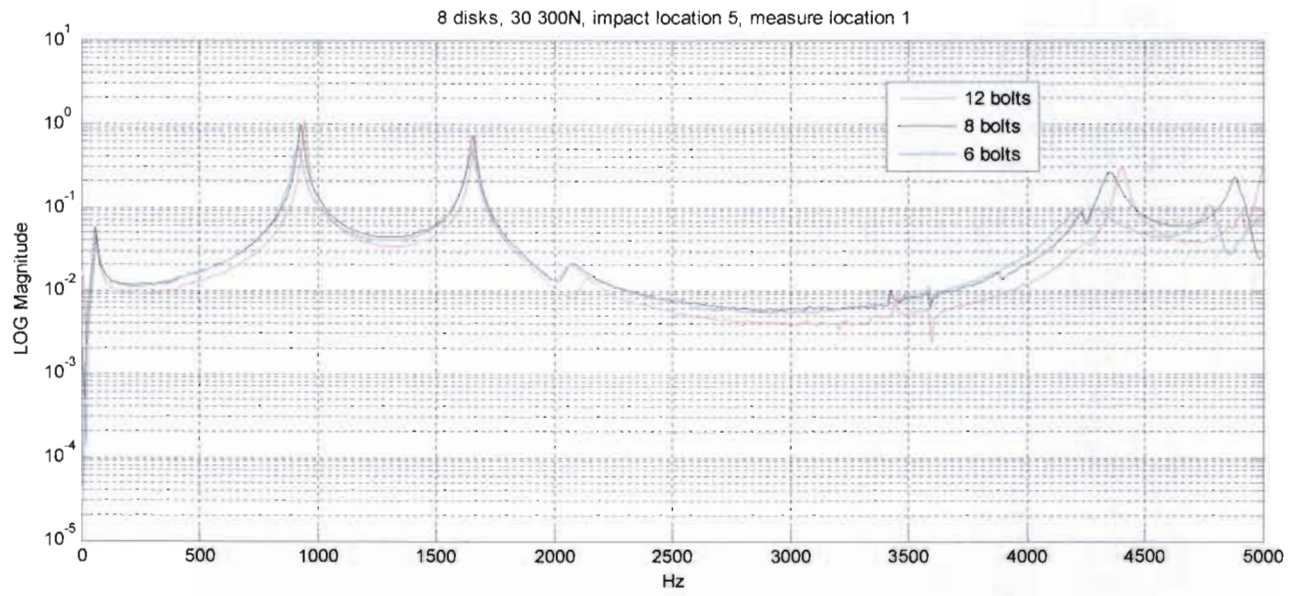


Fig. C.9, Plot of Logarithmic Magnitude of Accelerance vs Frequency Data for  
Eight Discs, 6,8,12 Bolts, 30300N Preload in Bolts.

## **APPENDIX D**

### **Equipment**



### 1. Accelerometer Model 352C68

High sensitivity, miniature (2 gm), ceramic shear ICP® accel., 100 mV/g, 0.5 to 10k Hz, 10-32 pin connection.

- Sensitivity: ( $\pm 10\%$ ) 100 mV/g (10.2 mV/(m/s<sup>2</sup>))
- Measurement Range:  $\pm 50$  g pk ( $\pm 491$  m/s<sup>2</sup> pk)
- Broadband Resolution: (10000 to 1 Hz) 0.00016 g rms (0.0015 m/s<sup>2</sup> rms)
- Frequency Range: ( $\pm 5\%$ ) 0.5 to 10000 Hz
- Weight: 0.070 oz (2.0 gm)

### 2. Modally Tuned Impulse Hammer.

Model no.	086B01
Linear error	<1.0 %
Sensitivity	9.54 mV/g
Frequency range	10 kHz

### 3. Flat Force Washer (Transducer) KMR



Max. operating force [%]	150
Nominal temp. range [°C]	-10 ... +70
Protection system	IP 67
Material	stainless steel
Direction of force	compressive
Nominal force	100kN
Nominal sensitivity [mV/V]	1.7...2.3

## **APPENDIX E**

### Finite Element Information

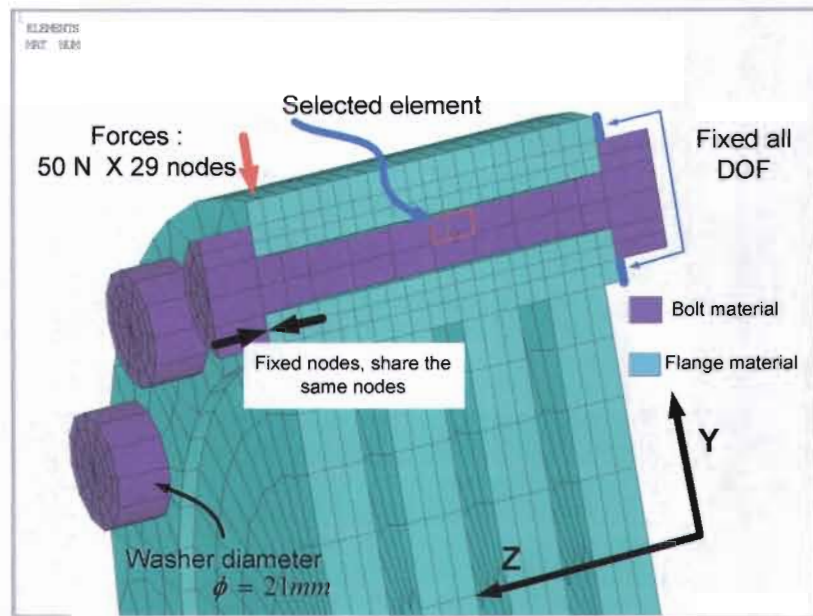


Fig. E 1. Geometry of Four Discs during Analysis illustrating the Constraints,  
(Bolts and Disk Material, Position of Point-Load, Axis Direction and Selected Element)

#### Comments on the model

- Body constraints: Fixed in all degrees of freedom at the right face.
- Flange and nuts share the same nodes on the faces of disks. The rest of the bolt is separated from the disk.
- Static force is applied to the nodes of three elements. (50N x 29 nodes =1450 N)
- 20-Node brick elements were used.

# **Appendix F**

## **Tensile Test: Bolt**

TEST CERTIFICATE  
TECHNOLOGY  
PRODUCT TESTING

MITTAL

ISCOR 6mm Round GI-30mm Lo-36mm

Test type: Tensile  
Operator name: A Faurie  
Sample Identification: 2005070  
Interface Type: 8500/8800

Instron Corporation  
Series IX Automated Materials Testing System 8.15.00  
Test Date: 19 July 2005

Sample Rate (pts/secs): 10.0000  
Ramp Rate: 0.3300 %/min  
Ramp Rate 2: 10.0000 mm/min  
Ramp Rate 3: 0.0000 mm/min  
Full Scale Load Range: 100.0000 kN

Humidity ( % ): 35  
Temperature: 18 C

Sample comments:

	Yield Stress 0.2% (MPa)	Stress at Max Load (MPa)	Maximum Percent Strain (%)	Modulus (AufYoung) (MPa)
1 No. 2	660.152	905.923	7.850	214908.953
Median	0.000	0.000	0.000	0.000



# Bibliography

- Adams, V. & Askenazi, A. 1998. Building better products with finite element analysis. Onward press.
- ANSYS. 2004. Release 9.0. Documentation for ANSYS. In ANSYS 9.0. [CD – ROM].
- Avitabile, Peter. 2001. Experimental Modal Analysis, A simple non-mathematical presentation. Sound and Vibration. January.
- Bruel & Kjaer. 1999. Modal Analysis. [Online]. Available at : < <http://www.bksv.com/17.asp> >. 2004.
- Cook, R.D. & Malkus, D.S. 2001. Concepts and applications of finite element analysis. Fourth edition. Wiley.
- Diagnostic Instruments. 2003. Users manual. [Online]. Available at : < [http://www.icats.co.uk/downloads/DI\\_notes.PDF](http://www.icats.co.uk/downloads/DI_notes.PDF) > . 2003.
- Dimarogonas, A. 1996. Vibration for Engineers. 2nd edition. Prentice Hall International INC.
- Ewins, D.J. 2000. Modal Testing theory , practice and application. England: Research studies Press LTD.
- Ehrich, F. F. 1992. Handbook of Rotordynamics. McGraw-Hill.
- Fertis, G.D. 1995. Mechanical and Structural Vibrations. John Wiley & Sons, Inc.
- Law, S.S. & Lu, Z.R. 2005. Time domain responses of a pre-stressed beam and pre-stress identification. Journal of Sound and Vibration, 288: 1011 – 1025.
- Hamed, E. & Frostig, Y. 2006. Natural frequencies of bonded and unbonded pre-stressed Beams – pre-stress force effects. Journal of Sound and Vibration, 295: 28 – 39.
- Hibler, R.C. 1978. Engineering Mechanics: Statics. Macmillan Publishing Co., Inc.
- Inman. J.D. 1996. Engineering Vibration. Prentice Hall, Inc.
- Ito, Y. & Toyoda, J. & Nagata, S. 1979. Interface Pressure Distribution in a Bolt-Flange Assembly. Transactions of the ASME. Vol. 101, April.
- Kerr, A.D. 1979. Journal of Sound and Vibration, 49(4): 569 - 573.
- Kumar, D.S. & Sujatha, C. 1995. A modified Semi-Analytical Approach towards the modelling of a shaft-disc system. Computers and structures, Vol. 6(1).
- Lalanne, M. & Ferraris, G. 1997. Rotordynamics Prediction in Engineering. 2nd edition. John Wiley and Sons.
- Li, Q. S. et al. 2000. Free vibration analysis of cantilevered tall structures under various axial loads. Engineering Structures, 22: 525 - 534.
- Little, R.E. 1967. Bolted joints. Machine Design, Nov. 9.

- Maia, N. M. et al. 1997. Theoretical and Experimental Modal Analysis. England: Research Studies Press LTD.
- Majid, K.I. 1972. Non-linear Structures. Butterworth & Co.
- Rivin, E. & Karlic, P. et al. 1990. Improvement of Machining Conditions for Turning of Slender Bars by Application of Tensile Force. ASME PED, Vol. 43.
- Rivin, E. 1999. Stiffness and Damping in Mechanical Design. New York: Marcel Dekker, Inc.
- Rao, S.S. 1995. Mechanical Vibrations. 3rd edition. Addison-Wesley Publishing Company.
- Sabuncu, M. & Kaçar, A. 1990. Critical speeds of continuous shaft disks systems. Vibration and wear in High Speed Rotating Machinery: 241 - 251.
- Storck, H. & Sumali, H. 1999. Characterising of a vibration damping mount. SAE Technical paper series.
- Thornton, P. A. 1985. Fundamentals of Engineering Materials. Prentice Hall.
- Tomski, L. & Przybylski, J. et al. 1994. Vibrations of a pre-stressed compound beam with a concentrated mass, Journal of Sound and Vibration, 174(3):315 - 321.
- Van Nostrand, D. 1952. Metallurgy for Engineers. New Jersey: Van Nostrand Company.
- Yamamoto, T. & Ishida, Y. 2001. Linear and nonlinear rotordynamics. USA: John Wiley & Sons, INC.